nature neuroscience

# Amygdala inputs to prefrontal cortex guide behavior amid conflicting cues of reward and punishment

Anthony Burgos-Robles[1,3], Eyal Y Kimchi[1–3], Ehsan M Izadmehr[1], Mary Jane Porzenheim[1], William A Ramos-Guasp[1], Edward H Nieh[1], Ada C Felix-Ortiz[1], Praneeth Namburi[1], Christopher A Leppla[1], Kara N Presbrey[1], Kavitha K Anandalingam[1], Pablo A Pagan-Rivera[1], Melodi Anahtar[1], Anna Beyeler[1] & Kay M Tye[1]

**Orchestrating appropriate behavioral responses in the face of competing signals that predict either rewards or threats in the environment is crucial for survival. The basolateral nucleus of the amygdala (BLA) and prelimbic (PL) medial prefrontal cortex have been implicated in reward-seeking and fear-related responses, but how information flows between these reciprocally connected structures to coordinate behavior is unknown. We recorded neuronal activity from the BLA and PL while rats performed a task wherein competing shock- and sucrose-predictive cues were simultaneously presented. The correlated firing primarily displayed a BLA→PL directionality during the shock-associated cue. Furthermore, BLA neurons optogenetically identified as projecting to PL more accurately predicted behavioral responses during competition than unidentified BLA neurons. Finally photostimulation of the BLA→PL projection increased freezing, whereas both chemogenetic and optogenetic inhibition reduced freezing. Therefore, the BLA→PL circuit is critical in governing the selection of behavioral responses in the face of competing signals.**



When animals engage in reward-seeking behaviors such as foraging or hunting, they often expose themselves to potential threats, and they must assess competing signals that may trigger conflicting motivational drives. The ability to appropriately weigh competing environmental cues and execute appropriate behavioral responses is paramount for survival and a key feature of mental health, yet little is known about the neural circuits that underpin this ability.

For decades, the amygdala has been identified as a focal point in emotional processing and is thought to be a hub for translating sensory information into motivated behaviors[1,2]. The BLA is important for the acquisition, encoding and retrieval of both positive and negative associations, and plasticity occurs in BLA neurons upon the encoding of cues that predict either positive or negative outcomes[3–8]. The BLA also shows prominent neuronal correlates of reward-seeking and fear-related responses in seminaturalistic tasks in which animals need to forage and retrieve food in the presence of imminent predator-like threats[9,10].

An important target of the BLA thought to be crucial for the coordination of reward-seeking and fear-related behaviors is the medial prefrontal cortex (mPFC)[11–13], which receives robust monosynaptic glutamatergic inputs from the BLA[14,15] and sends a reciprocal connection in return[16]. Like the BLA, the mPFC has been widely implicated in the regulation of both reward-seeking[17,18] and fear-related behavior[19–21], and pharmacological inactivation of the mPFC produces deficits in the coordination of these behaviors[22,23]. Furthermore, the mPFC shows prominent neuronal responses that are highly correlated with the time course of behavioral manifestations of reward-seeking and fear-related behavior[11,18]. While some studies have examined the necessity of BLA activity for fear-related signaling in the mPFC[24,25], little is known about how dynamic interactions between these structures may govern the coordination of reward-seeking and fear-related behavior upon presentation of competing signals. In this study, we focus on the PL subregion of the mPFC, though some experiments may also influence BLA projections to other subregions of mPFC.

In this study, we used electrophysiological recordings, optogenetically mediated photoidentification of BLA→PL neurons and supervised machine learning algorithms to decode behavior during competition, along with circuit-specific manipulations during a modified Pavlovian cue discrimination task in which conditioned stimuli predicting either sucrose or shock were presented separately on some trials and simultaneously in others. We address several questions. Is correlated firing between the BLA and PL dynamic upon presentations of cues associated with positive (rewards) or negative (punishments) outcomes? What is the directionality of information flow? Can we use neural activity and behavior during Pavlovian discrimination to accurately decode the behavior of an animal during the presentation of conflicting signals? And finally, is the BLA→PL projection necessary for and sufficient to promote fear-related behavior?

We also examined whether either brain region was particularly sensitive to the sucrose-predictive or the shock-predictive cue. We found that predominantly excitatory cross-correlations (CCs) between the BLA and PL developed a BLA→PL directionality during the shock-predictive but not the sucrose-predictive cue. On the basis of this finding, we hypothesized that this projection supplies information

[1]Picower Institute for Learning and Memory, Department of Brain and Cognitive Sciences, Massachusetts Institute of Technology, Cambridge, Massachusetts, USA. [2]Department of Neurology, Massachusetts General Hospital, Boston, Massachusetts, USA. [3]These authors contributed equally to this work. Correspondence should be addressed to K.M.T. (kaytye@mit.edu).

Received 18 January; accepted 22 March; published online 24 April 2017; doi:10.1038/nn.4553

critical for driving fear responses. To further test this, we used channelrhodopsin-2 (ChR2) to activate BLA inputs to PL. This produced a selective enhancement of conditioned fear but not reward-seeking responses. Conversely, we used both optogenetic and chemogenetic approaches to inhibit BLA inputs to PL and observed suppression of freezing.

## RESULTS

To investigate the neural dynamics that occur when an animal is challenged with competing environmental signals, we developed a variation of a Pavlovian discrimination task wherein one conditioned stimulus (CS) was paired with a sucrose reward (CS-Suc) whereas a second CS was paired with shock (CS-Shock). We used CSs of different sensory modalities (auditory and visual) to subsequently allow us to simultaneously present these stimuli during 'competition' trials without perceptual interference (**Fig. 1a** and **Supplementary Fig. 1a**).

Rats first learned a reward association in which a cue (for example, a light) was associated with the delivery of a palatable sucrose solution. Rats rapidly learned to explore the sucrose port during the cue presentation as compared to the inter-trial intervals (ITI; **Supplementary Fig. 1c**). Rats then learned to discriminate a second cue (for example, a tone) with an electrical shock, while still being exposed to the sucrose-predictive cue. Rats responded to the cue that predicted shock by freezing, which is a robust and consistent behavioral manifestation thought to be related to fear. By the third discrimination session, rats exhibited differential behavioral responses during the sucrose-predictive and shock-predictive cues. For simplicity, we used the terms reward and fear epochs to describe the time during which the cues associated with either sucrose or shock, respectively, were presented. Rats spent more time exploring the sucrose port than freezing during the reward epochs, whereas they spent more time freezing than exploring the sucrose port during the fear epochs (**Fig. 1b**,**c** and **Supplementary Fig. 1d**).

During subsequent competition sessions, the CS-Suc and CS-Shock associations were simultaneously presented to induce motivational conflict and competition of reward-seeking and fear-related behavior. Pairing of these associations produced a mean performance that was between the behaviors produced when the CS-Suc and CS-Shock were presented independently (**Fig. 1d**,**e** and **Supplementary Fig. 1d**). Throughout training, while the sucrose- and shock-predictive cues were of different sensory modalities, these cues were counterbalanced across animals, and differences in the cue modalities did not introduce significant differences in behavioral performance (**Supplementary Fig. 1e–g**).

### BLA led more excitatory correlations with PL during the shock-predictive cue

To explore the potential contribution of interactions between the BLA and PL in governing behavioral selection in the face of conflicting cues signaling competing motivational drives, we first investigated the correlated activity across these two brain regions during distinct behavioral epochs during a discrimination session wherein the CS-Suc and CS-Shock were presented independently (**Fig. 2**). Recording sites are shown in **Supplementary Figure 2a–d**. Details on the detection of correlated activity are provided in the Online Methods (section "Cross-correlations") and in **Supplementary Figure 3a**. Of 3,037 total possible pairs of BLA and PL neurons, we observed 639 pairs with positively correlated activity, which we termed "excitatory BLA/PL CCs" (**Fig. 2a**), and 107 pairs with negatively correlated activity, which we termed "inhibitory BLA/PL CCs" (**Fig. 2b**). Although excitatory CCs were more common during all task epochs (ITI, CS-Suc and CS-Shock; **Fig. 2c**,**e**), inhibitory CCs were also observed albeit less frequently and with more variability in the number of significantly correlated pairs across each epoch (**Fig. 2d**,**f**).

We wondered whether the directionality of information flow might be dynamic, depending on environmental cues predicting unconditioned stimuli of positive or negative valence. To begin exploring this question, we examined the proportion of pairs during each epoch wherein spiking of neurons in the BLA or PL preceded spiking of neurons in the other structure. We observed that a significantly greater proportion of BLA/PL neural pairs showing excitatory CCs were putatively led by neurons in the BLA during the CS-Shock, but not during either the CS-Suc or ITI epochs (**Fig. 2g**). Conversely, among inhibitory CCs, the BLA putatively led a greater proportion of cell pairs during the CS-Suc (**Fig. 2h**), though there was a smaller sample size among inhibitory CCs. Smaller bin widths showed more variable CCs, primarily due to sparse firing (**Supplementary Fig. 4**).

To control for stimulus generalization, we found that rats displayed neither reward-seeking nor fear-related behaviors during a habituation phase before any training or during the discrimination of a neutral cue (CS–) that was never paired with sucrose or shock (**Supplementary Fig. 5a–c**). Notably, significantly smaller proportions of BLA/PL cell pairs exhibited correlated activity during the CS– and during habituation (**Supplementary Fig. 5d**), suggesting that BLA/PL correlations developed over the course of training. We also confirmed that cue modality did not influence the BLA/PL lead and lag dynamics (**Supplementary Fig. 6a**,**b**). Furthermore, the lead and lag dynamics were consistent across distinct pairwise BLA/PL populations that exhibited correlated activity during different task events (**Supplementary Fig. 6c**,**d**). Of note, these dynamics were also strong in a BLA/PL population that exhibited excitatory correlations during all task events but that showed significant shifts in BLA and PL leading across task events (**Supplementary Fig. 6c**). Finally, these lead and lag dynamics were also maintained across multiple combinations of putative projection cells and interneurons (**Supplementary Fig. 6e–i**).

### Populations of BLA cells encoding sucrose and shock cues exhibited similar levels of correlated activity with PL

Preferential encoding of the sucrose and shock associations by the BLA cells could potentially contribute to differential patterns of BLA/PL correlations. We examined this possibility by assessing CS-elicited changes in BLA activity and then quantifying correlations with PL for the reward- and fear-encoding BLA cells (**Fig. 3a–d**). Details on CS-evoked responses are provided in the Online Methods. While many BLA cells responded to either of the CSs or to both (**Fig. 3a**,**b** and **Supplementary Fig. 7a**,**c**,**e**), no significant differences were observed between the proportions of BLA cells that exhibited biased responses to either the CS-Suc or CS-Shock (**Fig. 3c**). Furthermore, the reward- and fear-biased populations showed similar levels of cross-correlated activity with PL (**Fig. 3d**). In addition, the patterns of lead and lag in the CCs were preserved across multiple combinations of BLA and PL cells that responded to either the reward- or fear-associated cues (**Supplementary Fig. 7g–j**). Therefore, the differential dynamics we observed in the BLA/PL CCs across reward and fear epochs could not solely be attributed to preferential encoding of the BLA cells of the reward and fear associations.

### More PL cells encoded shock cues, and they exhibited stronger correlations with BLA than PL cells encoding sucrose cues

We next examined whether the PL cells that encoded the reward and fear associations exhibited distinct degrees of cross-correlated

activity with the BLA. Representative PL cells exhibiting significant responses to the reward- and fear-associated cues are shown in **Supplementary Figure 7b**. In contrast to the BLA, PL exhibited a larger proportion of cells that encoded the fear-associated cue (**Fig. 3e**,**f** and **Supplementary Fig. 7d**). Furthermore, a significantly greater overall population of PL cells exhibited biased responses to the fear-associated cue (**Fig. 3g**), and this population showed more CCs with the BLA than the population of PL cells that exhibited biased responses

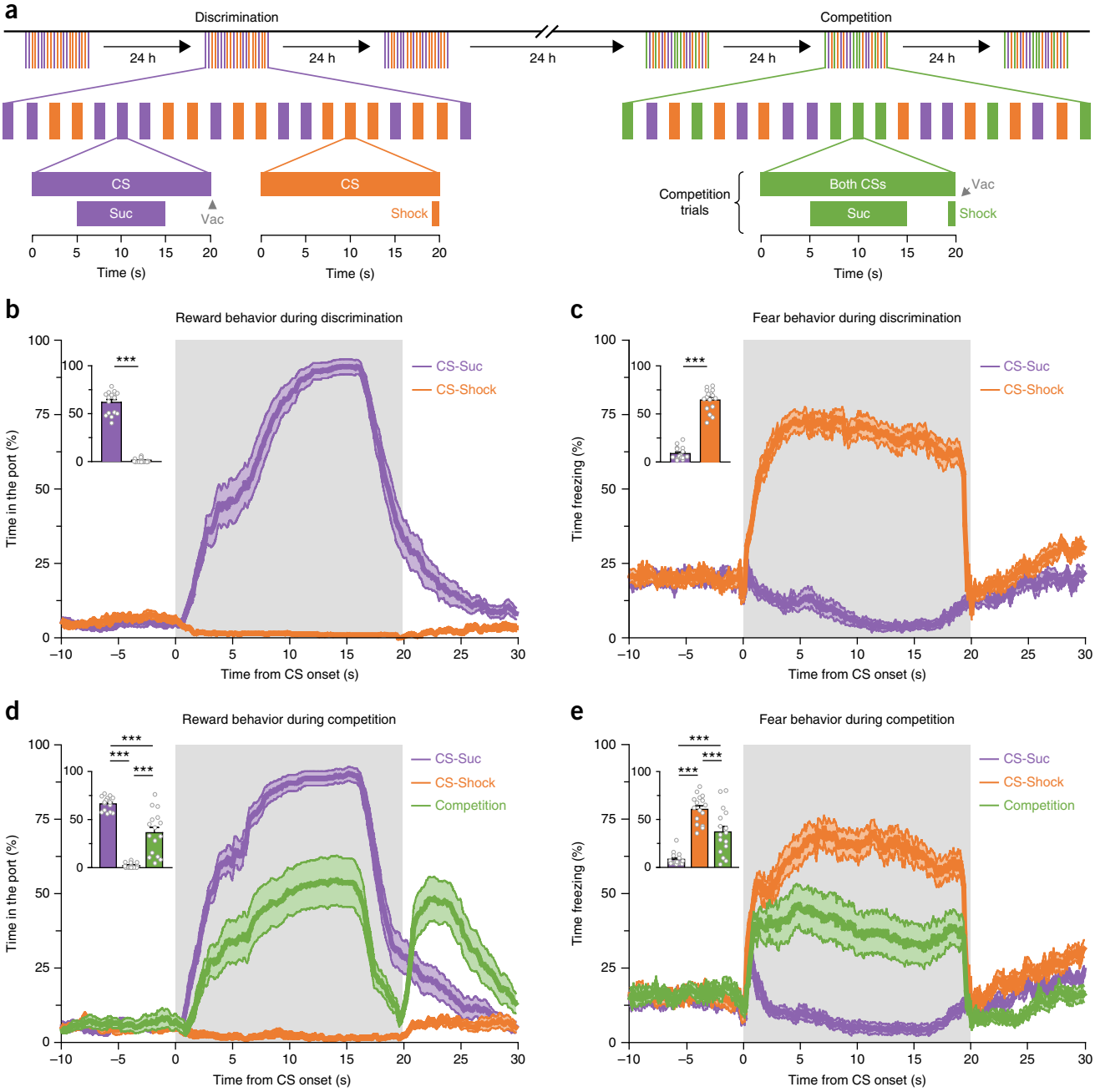


**Figure 1** Behavioral tasks to examine the discrimination and competition of reward and fear memories. (**a**) During discrimination, discrete CS-Suc and CS-Shock cues predicted sucrose or shocks, respectively. Their sensory modalities (light versus tone) were counterbalanced across animals. Sucrose was removed from the port by vacuum (Vac) if animals did not collect it by the end of the CS. During competition, in addition to the individual CS-Suc and CS-Shock, animals were challenged by the co-presentation of these associations to induce conflicting motivational drives and competition between them. (**b**,**c**) We operationalize "reward" to refer to port entry and "fear" to refer to freezing. (**b**) Port entry responses per CS during the last discrimination session. Inset show the average time that animals spent in the port per CS (paired *t*-test: $t_{15} = 20.3$, $^{***}P < 0.001$, $n = 16$ animals). (**c**) Freezing responses per CS during the last discrimination session. Inset shows the average time that animals spent freezing per CS (paired *t*-test: $t_{15} = 20.6$, $^{***}P < 0.001$, $n = 16$ animals). (**d**) Port entry responses during the last competition session. Inset shows the average time in the port per CS (repeated measures one-way ANOVA: $F_{2,30} = 107.6$, $P < 0.001$, $n = 16$ animals; Bonferroni *post hoc* tests: $t_{15} > 6.85$ and $^{***}P < 0.001$ for all comparisons). (**e**) Freezing responses during the last competition session. Inset shows the average time that animals spent freezing per CS (repeated measures one-way ANOVA: $F_{2,30} = 89.0$, $P < 0.001$, $n = 16$ animals; Bonferroni *post hoc* tests: $t_{15} > 6.01$ and $^{***}P < 0.001$ for all comparisons). Error bands in line plots and error bars in insets represent s.e.m.

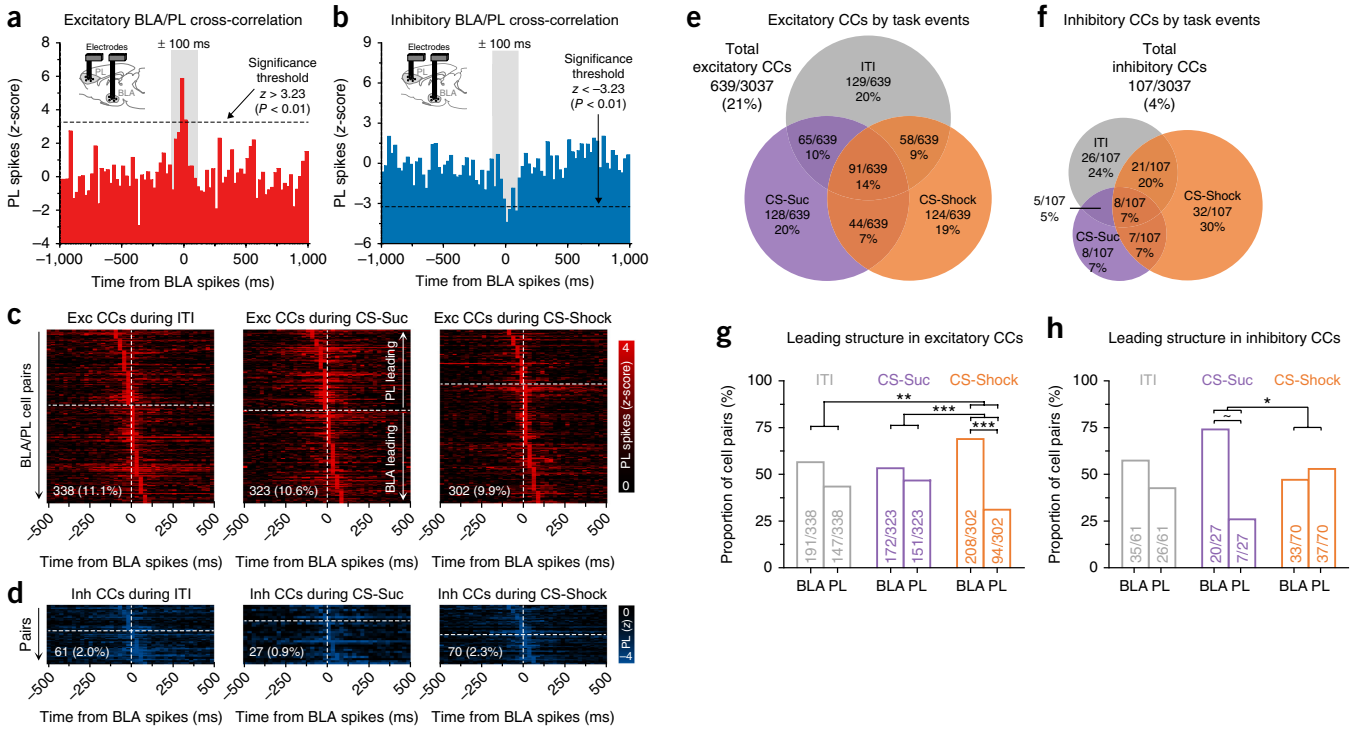


**Figure 2** Correlated activity between the BLA and PL varied between the retrieval of reward- and fear-related memories. (**a**,**b**) Neural activity was simultaneously recorded in the BLA and PL ($n = 12$ animals). Representative CCs between BLA/PL neural pairs (25-ms bins) exhibit either excitatory correlations (the target cell showed increased firing when the reference cell fired) or inhibitory correlations (the target cell showed reduced firing when the reference cell fired). Significant peaks or troughs were detected within ±100 ms of the reference spikes. Correlations due to common input (those with zero lag) were excluded by examining CCs generated with smaller bin widths (5-ms bins; see **Supplementary Fig. 3**). Only a small fraction of cell pairs showed zero lag (**Supplementary Fig. 6c,d**). (**c**,**d**) Excitatory (Exc) correlations predominated over inhibitory (Inh) correlations in all task epochs (Bonferroni-corrected chi-square tests: $\chi^2 > 136.5$, $P < 0.001$ in all task epochs). In the heat maps, cell pairs were ordered based on the latency of peaks and troughs. Mean latency ± s.e.m. of peaks for excitatory CCs: ITI, 3.9 ± 2.4 ms; CS-Suc, 5.9 ± 2.5 ms; and CS-Shock, 13.0 ± 2.4 ms. Mean latency of troughs for inhibitory CCs: ITI, 12.5 ± 5.3 ms; CS-Suc, 17.1 ± 7.6 ms; CS-Shock, –1.4 ± 5.2 ms. Numbers at the bottom of the heat maps indicate the overall proportion of correlated cell pairs per epoch. Vertical dashed lines represent the time of the reference spikes and horizontal dashed lines represent the separation between putative BLA-led and PL-led correlations. (**e**,**f**) Distinct populations of BLA/PL neural pairs exhibited correlated activity during different epochs. (**g**) Putative leading structure in the excitatory CCs, based on the latency of peaks. Cell pairs were deemed BLA-led if the peak occurred within +2.5 to +100 ms of the reference, whereas they were deemed PL-led if the peak occurred within –100 to –2.5 ms of the reference ($n$ values reported within each bar). BLA leading was significantly greater than PL leading only during CS-Shock (ITI, $\chi^2 = 3.83$, $P = 0.14$; CS-Suc, $\chi^2 = 0.91$, $P = 0.71$; CS-Shock, $\chi^2 = 29.2$, $^{***}P < 0.001$). The leading ratio during CS-Shock was also significantly different than during other epochs (ITI versus CS-Suc, $\chi^2 = 0.71$, $P = 0.78$; ITI versus CS-Shock, $\chi^2 = 10.4$, $^{**}P = 0.004$; CS-Suc versus CS-Shock, $\chi^2 = 16.0$, $^{***}P < 0.001$). (**h**) Putative leading structure in the inhibitory CCs. There was a trend toward higher BLA than PL leading during CS-Suc (ITI, $\chi^2 = 0.89$, $P = 0.72$; CS-Suc, $\chi^2 = 4.28$, $^{\sim}P = 0.11$; CS-Shock, $\chi^2 = 0.15$, $P = 0.97$). The leading ratio during CS-Suc was significantly different than during CS-Shock (ITI versus CS-Suc, $\chi^2 = 2.33$, $P = 0.35$; ITI versus CS-Shock, $\chi^2 = 1.37$, $P = 0.56$; CS-Suc versus CS-Shock, $\chi^2 = 5.70$, $^{*}P = 0.05$).

to the reward-associated cue (**Fig. 3h**). This suggested that fear-biased cells in PL have greater functional connections with the BLA.

Taken together, these observations raised the possibility that information was flowing from the BLA to the PL during fear-related cues. However, these experiments did not allow us to differentiate between direct information flow, indirect connectivity or activity driven by a common upstream site. These findings ultimately prompted us to perform optogenetically mediated photoidentification of BLA→PL neurons.

### Most photoidentified BLA→PL neurons recorded were excited by the shock-predictive cue

Given that the BLA, rather than PL, led more excitatory correlations during the CS-Shock, we wondered whether this might be related to monosynaptic input from the BLA to PL. To test this hypothesis, we used a dual virus approach as performed by Nieh *et al.*[26], wherein a retrograde viral vector injected into PL (canine adenovirus, CAV2) resulted in expression of Cre recombinase, while an anterograde viral vector injected into the BLA allowed Cre-dependent expression of ChR2 fused to enhanced yellow fluorescent protein (eYFP; **Fig. 4a**). We first confirmed in an *ex vivo* preparation that this viral approach produced reliable ChR2 expression and selective photoresponses in BLA→PL neurons (**Fig. 4b,c**). We also determined in the *ex vivo* preparation the photoresponse latency threshold in these cells (**Fig. 4d,e**). For *in vivo* recordings, we implanted into the BLA an optrode (probe that combined an optical fiber with recording wires) to allow photoidentification of the BLA→PL cells shortly after the recording session during the behavioral task (**Fig. 4f**). Photoidentification parameters are provided in the Online Methods (section "*In vivo* photoidentification of the BLA→PL population").

Among the BLA neurons recorded *in vivo*, 11 of 60 (18%) were identified as BLA→PL neurons, based on short-latency photoresponses

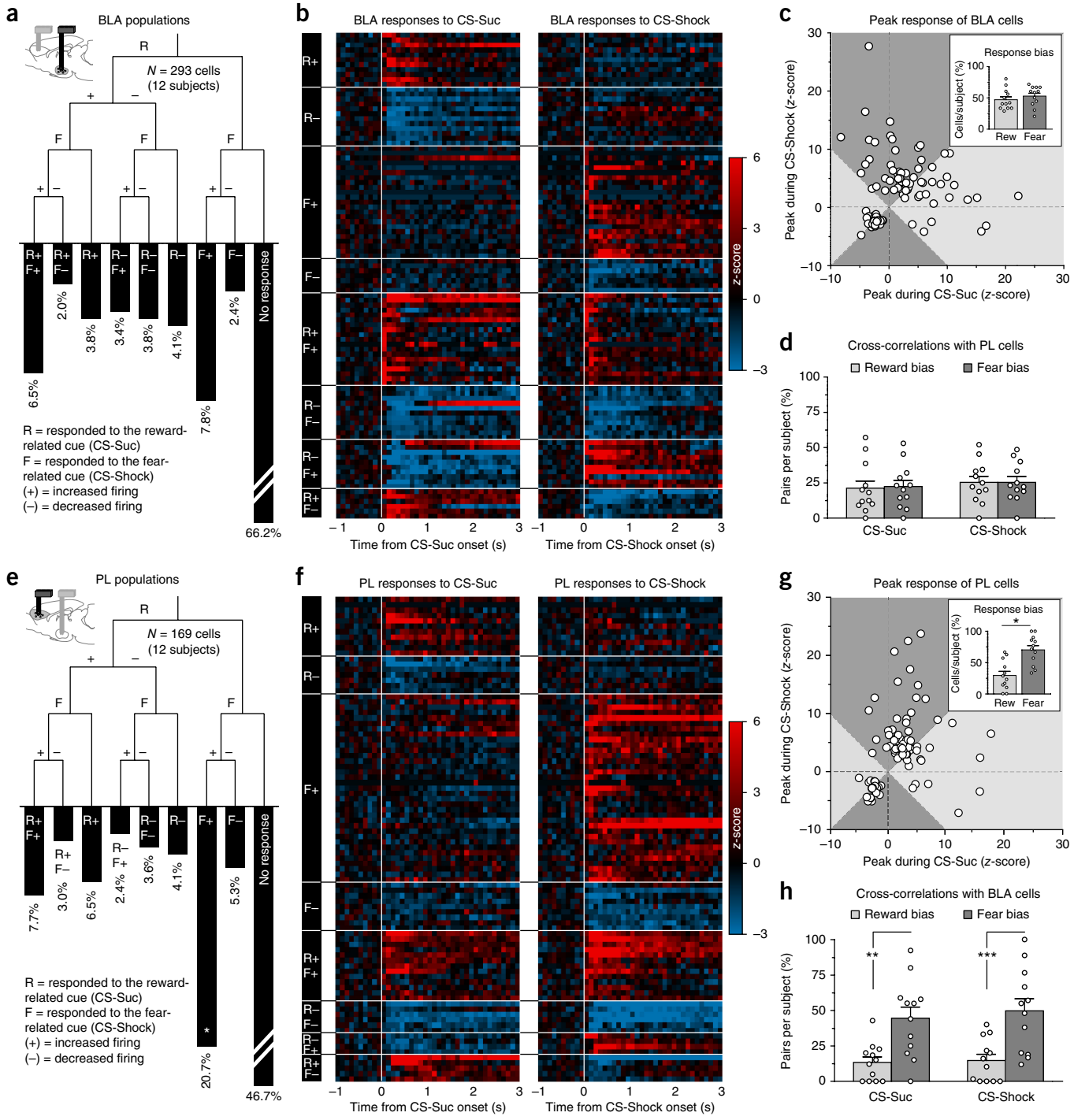




**Figure 3** BLA neurons biased toward encoding CS-Suc or CS-Shock exhibited similar proportions of correlated activity with PL, whereas a greater proportion of fear-biased PL cells exhibited correlated activity with BLA. (**a**,**b**) BLA populations based on the response to CS-Suc (R), CS-Shock (F) or both cues (R and F combinations). There were no significant differences in proportions across these populations (Bonferroni-corrected chi-square tests: $\chi^2 < 9.50$ and $P > 0.056$ for all comparisons). (**c**) Separation of reward- and fear-biased BLA cells, based on the peak response to each cue. Cells in the light gray zones exhibited larger responses to the reward-related cue and were deemed reward-biased. Cells in the dark gray zones exhibited larger responses to the fear-related cue and were deemed fear-biased. Inset shows the average proportion of reward- and fear-biased cells in the BLA per subject (paired *t*-test: $t_{11} = 0.61$, $P = 0.56$, $n = 12$ animals). (**d**) Reward- and fear-biased BLA cells showed similar proportions of cross-correlated activity with simultaneously recorded PL cells. These values were normalized to the total number of correlated neural pairs per subject per cue (repeated measures two-way ANOVA: cells, $F_{1,22} = 0.01$, $P = 0.91$; cue, $F_{1,22} = 1.48$, $P = 0.24$; interaction, $F_{1,22} = 0.04$, $P = 0.85$; $n = 12$ animals). (**e**,**f**) PL populations based on the response to the cues. The F+ population was significantly larger than most other populations ($\chi^2 = 8.86$ and $P = 0.079$ compared to R+F+; $\chi^2 > 11.06$ and $^*P < 0.024$ compared to all other populations). (**g**) Separation of reward and fear biased PL cells, based on the peak response to each cue. A greater proportion of PL cells exhibited fear bias than reward bias ($t_{11} = 3.03$, $^*P = 0.011$, $n = 12$ animals). (**h**) A greater proportion of fear-biased PL cells showed CCs with simultaneously recorded BLA cells (cells, $F_{1,22} = 13.5$, $P = 0.0013$; cue, $F_{1,22} = 3.66$, $P = 0.069$; interaction, $F_{1,22} = 1.23$, $P = 0.28$; CS-Suc, $t_{11} = 3.32$, $^{**}P = 0.0026$; CS-Shock, $t_{11} = 3.73$, $^{***}P < 0.001$; $n = 12$ animals). Error bars represent s.e.m.

that were below the 12-ms threshold (**Fig. 4g,h**), which was determined in our visually guided *ex vivo* recordings (**Fig. 4e**). In addition, we observed a subpopulation of BLA cells (8 of 60, 13%) exhibiting inhibition in response to the photostimulation of BLA→PL neurons. We termed this subpopulation "network-inhibited cells," though the precise number of synapses and distribution of the neurons in this network are not known.

We found that a greater proportion of the photoidentified BLA→PL neurons showed excitatory responses to the fear-associated

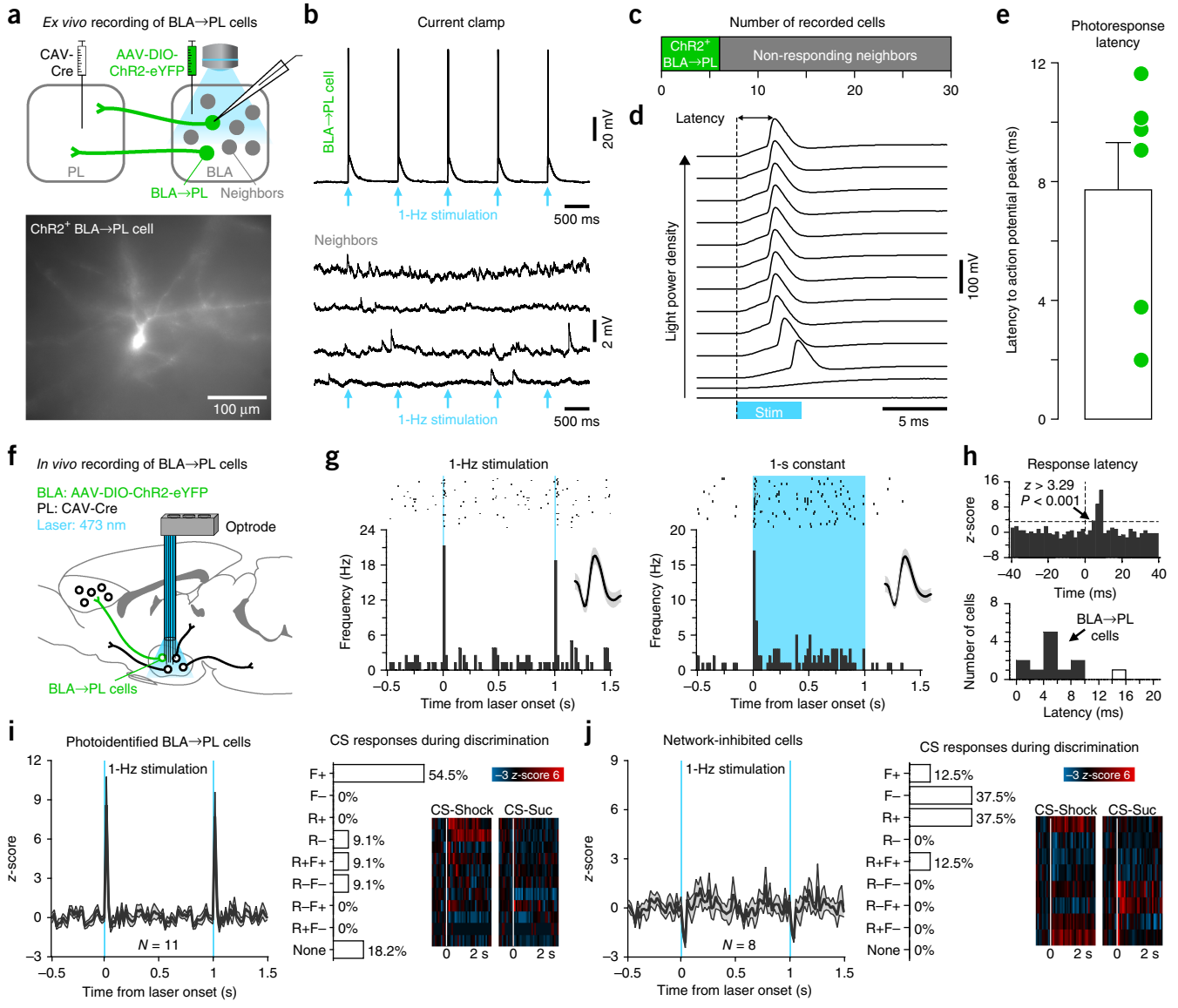


**Figure 4** Most BLA→PL cells recorded showed selective excitation to the shock-predictive cue. An optogenetic approach was used to photoidentify these cells ("BLA→PL population"). (**a**–**e**) Assessment of photoresponse latencies in slices. (**a**) *Ex vivo* whole-cell patch-clamp recordings were performed after selectively expressing ChR2 in BLA→PL cells using a Cre-dependent viral system ($n = 7$ animals). Expressing cells ($n = 6$ cells) and nonexpressing neighbors ($n = 24$ cells) were recorded while stimulating with blue light (5-ms pulses at 1 Hz). (**b**) Representative traces from a ChR2$^+$ BLA→PL cell and four nonexpressing neighbors. (**c**) Distribution of all cells sampled with whole-cell patch-clamp recording. (**d**) Representative traces show the latency of photoresponses at various light power densities (power range, 0.5–84 mW/mm$^2$). Latencies were calculated from light onset to action potential peaks. (**e**) Distribution of photoresponse latencies for the BLA→PL cells. Dots represent individual cells and error bar represents s.e.m. (**f**–**h**) Photoidentification of BLA→PL cells in behaving animals. (**f**) Optrodes were chronically implanted in the BLA for neural recordings after selectively expressing ChR2 in BLA→PL cells. Optimal ChR2 expression and detection of photoresponses was achieved in a subset of animals ($n = 2$ of 6 animals, 33%). (**g**) BLA→PL cell displaying photoresponses *in vivo* (bin width, 20 ms). (**h**) Assessment of photoresponse latencies *in vivo*. Latencies were calculated from laser onset to the time at which cells exhibited a significant increase in firing frequency. Eleven of 60 cells (18%) were deemed BLA→PL cells, as they displayed photoresponse latencies shorter than 12 ms, which was the longest latency observed in slices. One cell displayed latencies greater than 12 ms (white-filled bin) and was excluded from further analyses. (**i**,**j**) Response profiles of photoidentified BLA populations, and peri-event heat maps reflecting *z*-scores for neurons referenced to the CS-Shock and CS-Suc. Error bands in line plots represent s.e.m. (**i**) BLA→PL population. A greater proportion of the BLA→PL cells sampled displayed selective excitatory responses to the fear-associated cue (F+, $n = 6$ of 11 cells, 55%). (**j**) An additional BLA population that exhibited significant inhibition during ChR2 stimulation. These cells thus did not terminate in PL, and they perhaps received inhibitory influence from the BLA→PL network. These cells were deemed network-inhibited cells ($n = 8$ of 60 cells, 13%). During the discrimination task, most of these cells exhibited either inhibitory responses to the fear cue (F–, 3 of 8, 38%) or excitatory responses to the reward cue (R+, 3 of 8, 38%).

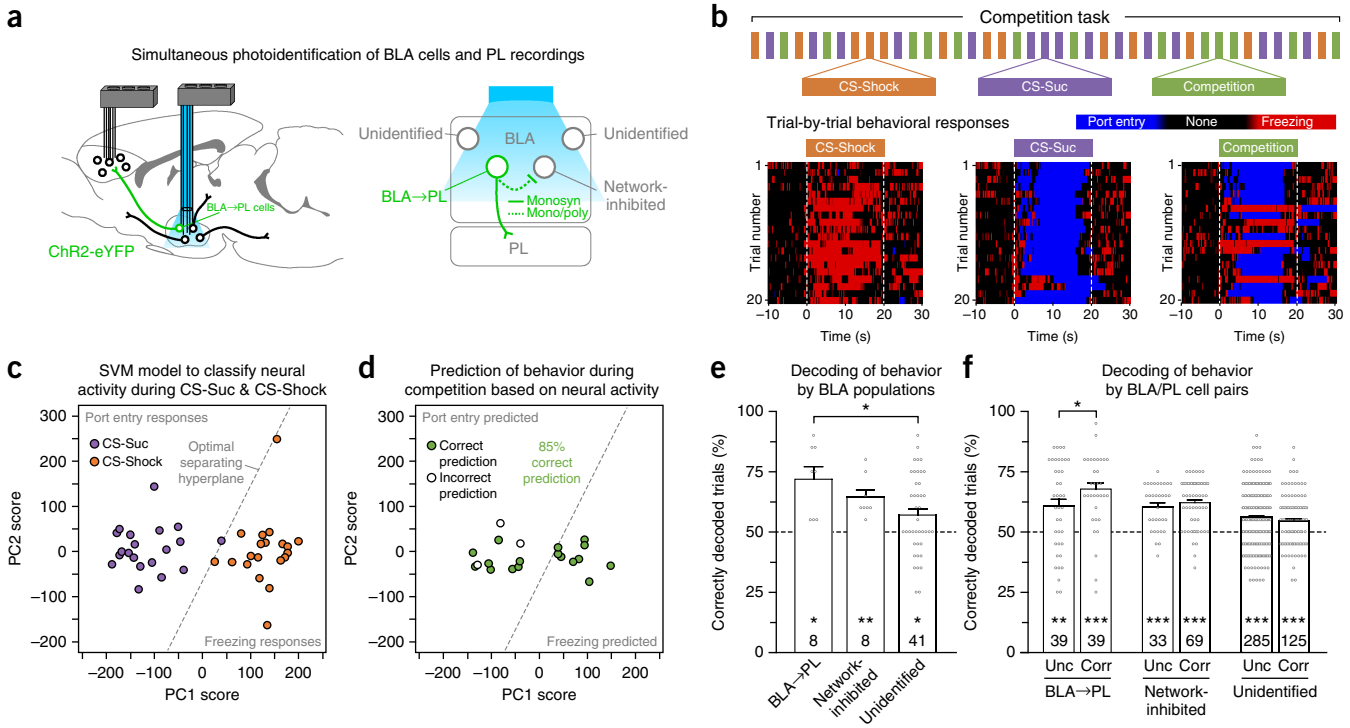


**Figure 5** BLA cells terminating in PL more accurately predicted the animal's behavioral response during competition. (**a**) Photoidentification of the distinct BLA populations: BLA→PL (8 of 57, 14%), population terminating in PL; network-inhibited (8 of 57, 14%), population that showed inhibition during photostimulation; and unidentified (41 of 57, 72%), population that did not respond to light stimulation. Monosyn, monosynaptic; mono/poly, mono- or polysynaptic. (**b**) Schematic of the competition task, in which, in addition to CS-Suc and CS-Shock trials, animals were challenged by the co-presentation of these associations to induce behavioral competition. Below, trial-by-trial behavioral output for a representative animal during each trial type. (**c**,**d**) SVM model to predict behavioral responses during 20 competition trials. The SVM model was trained using neural activity during the CS-Suc and CS-Shock trials. Data for the entire 20 s of CS presentation were used to classify neural activity. The model was then tested during competition trials to predict behavioral responses based on neural activity. For this example, this BLA→PL cell accurately predicted behavioral responses on 85% of the competition trials. PC, principal component. (**e**) Mean decoding accuracy for the distinct BLA populations. Superimposed dots represent individual cells (*n* values per population are reported in the bars). All BLA populations showed averaged decoding accuracies that were significantly higher than chance (Bonferroni-corrected paired *t*-test comparisons against scrambled data are represented by the asterisks above the number of cells per population: BLA→PL, $t_7 = 3.31$, $^*P = 0.013$; network-inhibited, $t_7 = 3.74$, $^{**}P = 0.007$; unidentified, $t_{40} = 2.29$, $^*P = 0.028$). Furthermore, the BLA→PL population but not the network-inhibited population showed significantly higher decoding accuracy than unidentified cells (one-way ANOVA: $F_{2,54} = 3.36$, $P = 0.042$; Bonferroni *post hoc* tests: BLA→PL versus unidentified, $t_{47} = 2.74$, $^*P = 0.017$; network-inhibited versus unidentified, $t_{47} = 1.22$, $P = 0.23$). (**f**) Mean decoding accuracy for the BLA populations, when their activity was paired with the activity of simultaneously recorded PL cells with which they showed either uncorrelated activity (Unc) or significantly correlated activity (Corr). Superimposed dots represent BLA/PL neural pairs (number of cell pairs per population are reported within the bars). All populations showed decoding accuracies that were significantly higher than chance (BLA→PL Unc, $t_{38} = 2.91$, $^{**}P = 0.006$; BLA→PL Corr, $t_{38} = 6.76$, $^{***}P < 0.001$; network-inhibited Unc, $t_{32} = 5.87$, $^{***}P < 0.001$; network-inhibited Corr, $t_{68} = 10.5$, $^{***}P < 0.001$; unidentified Unc, $t_{284} = 8.36$, $^{***}P < 0.001$; unidentified Corr, $t_{124} = 4.24$, $^{***}P < 0.001$). Furthermore, the BLA→PL cells showed significantly higher decoding accuracy when their activity was paired with correlated PL activity (one-way ANOVA: $F_{5,584} = 11.1$, $P < 0.001$; Bonferroni *post hoc* tests: BLA→PL, Unc versus Corr, $t_{76} = 2.64$, $^*P = 0.011$; network-inhibited, Unc versus Corr, $t_{100} = 0.68$, $P = 0.50$; unidentified, Unc versus Corr, $t_{408} = 1.18$, $P = 0.24$). Error bars represent s.e.m.

cue ("F+"; **Fig. 4i**). This was in contrast to the network-inhibited cells, among which only one cell showed selective excitatory responses to the fear-associated cue (**Fig. 4j**), while most cells recorded showed inhibitory responses to the fear cue ("F–") or excitatory responses to the reward-associated cue ("R+").

### Activity of BLA→PL neurons decoded behavior in moments of conflict more accurately than unidentified BLA neurons

On the basis of the above findings taken together, we hypothesized that the neural activity of photoidentified BLA→PL neurons during independent presentations of the fear- and reward-related cues would allow us to decode the behavior of animals challenged with competing signals, specifically the simultaneous presentation of CS-Suc and CS-Shock (**Fig. 5**). The selection of a behavioral output during competition trials varied between animals and even between trials within a single animal (**Fig. 5b**), as competition trials could produce behaviors related to either reward-seeking (port entry) or fear (freezing).

To test this, we used a support vector machine (SVM) algorithm to compare the decoding accuracy of individual neurons in the BLA. CS-Suc trials, which reliably induced port entry, and CS-Shock trials, which reliably induced freezing, were used as training data for the SVM (**Fig. 5c**; see "Machine learning to decode neuronal activity and predict behavior" in the Online Methods). The SVM algorithm was then tested on competition trials to determine the percentage of trials for which the activity of each individual BLA neuron accurately predicted behavioral selection (port entry or freezing; **Fig. 5d**). A representative BLA→PL neuron is shown that had 85% decoding accuracy (**Fig. 5d**).

Photoidentified BLA→PL neurons indeed showed a significantly higher mean decoding accuracy than unidentified BLA neurons (**Fig. 5e**).

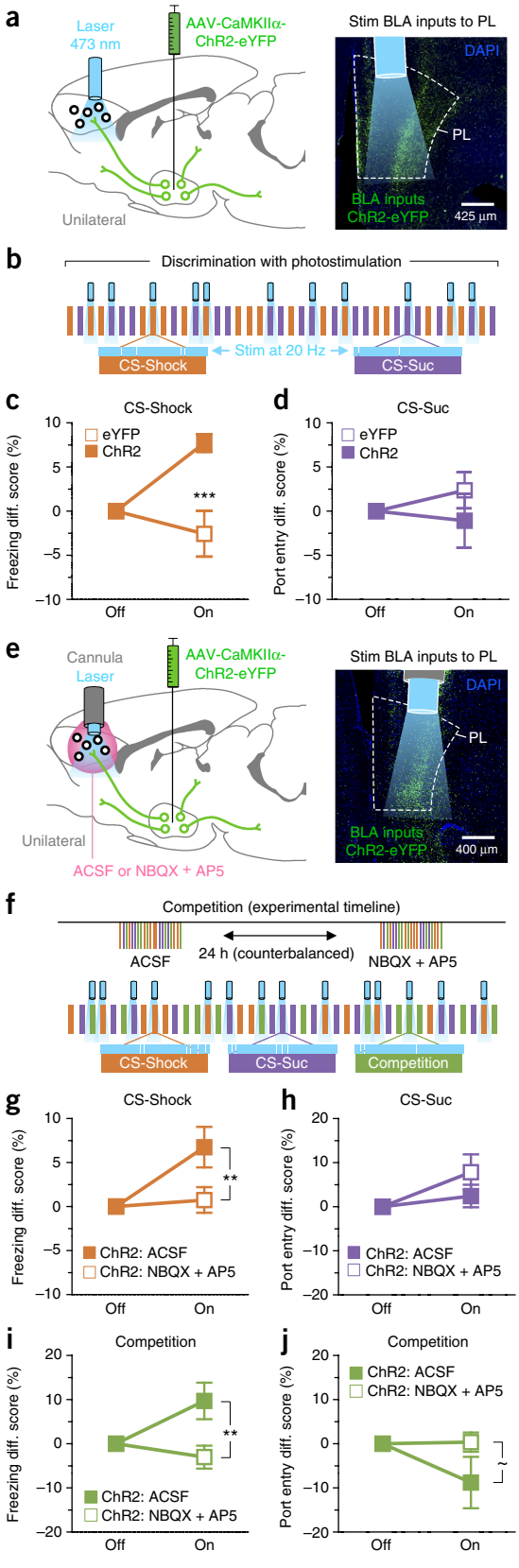


**Figure 6** Stimulation of BLA inputs to PL was sufficient to promote fear-related behavior and bias behavioral responses toward fear during competition. (**a**) Optogenetic strategy to stimulate (Stim) BLA inputs to PL. Illumination may have also reached other subregions of mPFC. The BLA was unilaterally transduced with either eYFP ($n = 10$ animals) or ChR2 ($n = 8$ animals), and an optical fiber was chronically implanted in dorsal PL to locally stimulate BLA inputs. (**b**) Schematic of the discrimination task, in which half of the trials were paired with 20-Hz blue light stimulation. The trial and laser sequences were pseudorandom. (**c**) Freezing behavior during CS-Shock trial, illustrated as the difference score in the percentage of time spent freezing in laser-on relative to laser-off. Stimulation of BLA inputs to PL significantly enhanced freezing responses (repeated measures two-way ANOVA: group, $F_{1,16} = 11.4$, $P = 0.004$; laser, $F_{1,16} = 2.88$, $P = 0.11$; interaction, $F_{1,16} = 11.4$, $P = 0.004$; eYFP versus ChR2 during laser-on: $t_{16} = 4.78$, $^{***}P = 0.0002$). (**d**) Port entry behavior during CS-Suc trials, illustrated as the difference score in the percentage of time spent in the sucrose port, relative to laser-off. No significant differences were detected for port entry responses (group, $F_{1,16} = 0.95$, $P = 0.34$; laser, $F_{1,16} = 0.13$, $P = 0.72$; interaction, $F_{1,16} = 0.95$, $P = 0.34$). (**e**) Pharmacology experiment to rule out a contribution from stimulation of fibers of passage or BLA terminals beyond PL. After unilateral transduction of the BLA with ChR2 ($n = 8$ animals), a cannula was chronically implanted above PL to allow the infusion of either ACSF or a combination of NBQX and AP5 ~10–15 min before inserting an optical fiber for optical stimulation and behavioral testing. (**f**) Experimental design for drug treatment and schematic of the competition task, in which half of the trials were paired with light stimulation. The trial and laser sequences were pseudorandom. (**g**) Freezing behavior during CS-Shock trials. Ruling out the possibility of stimulation of fibers of passage, the NBQX + AP5 treatment abolished the stimulation effect on freezing observed after the ACSF treatment (drug, $F_{1,14} = 4.88$, $P = 0.044$; laser, $F_{1,14} = 7.64$, $P = 0.015$; interaction, $F_{1,14} = 4.88$, $P = 0.044$; ACSF versus NBQX + AP5 during laser-on: $t_7 = 3.12$, $^{**}P = 0.0075$). (**h**) Port entry behavior during CS-Suc trials. No significant differences were detected (drug, $F_{1,14} = 1.27$, $P = 0.28$; laser, $F_{1,14} = 4.58$, $P = 0.0504$; interaction, $F_{1,14} = 1.27$, $P = 0.28$). (**i**) Freezing during competition trials. Stimulation of BLA inputs to PL also enhanced freezing during competition trials under the ACSF treatment, and this effect was abolished by the NBQX + AP5 treatment (drug, $F_{1,14} = 6.79$, $P = 0.02$; laser, $F_{1,14} = 1.89$, $P = 0.19$; interaction, $F_{1,14} = 6.79$, $P = 0.02$; ACSF versus NBQX + AP5 during laser-on: $t_7 = 3.69$, $^{**}P = 0.0024$). (**j**) Port entry behavior during competition. There was a trend toward reduced port entry responses during competition (drug, $F_{1,14} = 2.18$, $P = 0.16$; laser, $F_{1,14} = 1.83$, $P = 0.20$; interaction, $F_{1,14} = 2.18$, $P = 0.16$; ACSF versus NBQX + AP5 during laser-on: $t_7 = 2.09$, $^{\sim}P = 0.056$). Error bars represent s.e.m.

Additionally, cross-regional neuronal pairs containing a photoidentified BLA→PL neuron had greater decoding accuracy if the PL neuron showed correlated firing with the PL-projecting BLA neuron (**Fig. 5f**). The significantly greater accuracy in predicting action selection during competition trials suggests that the BLA→PL projection encodes information that can guide behavior.

### Photostimulation of BLA inputs to PL were sufficient to promote freezing

To test whether the BLA→mPFC projection was sufficient to promote fear-related behavior such as freezing, we photostimulated ChR2-expressing BLA terminals in the mPFC (**Fig. 6a–d** and **Supplementary Fig. 8a**). During the Pavlovian discrimination session, rats expressing ChR2 displayed significantly more freezing during laser-on than laser-off epochs relative to eYFP-expressing controls (**Fig. 6c**).

To control for the potential contribution of vesicle release from BLA terminals at targets other than PL, which may be induced by backpropagating action potentials or stimulation of axons of passage, in a separate experiment (**Fig. 6e–j** and **Supplementary Fig. 8b,c**) we used a standard pharmacological control for projection-specific optogenetic manipulation[27]. In ChR2-expressing animals, we either infused a glutamate receptor antagonist cocktail (NBQX plus AP5; see Online Methods) or artificial cerebrospinal fluid (ACSF) unilaterally into the PL, counterbalanced for order across two different sessions

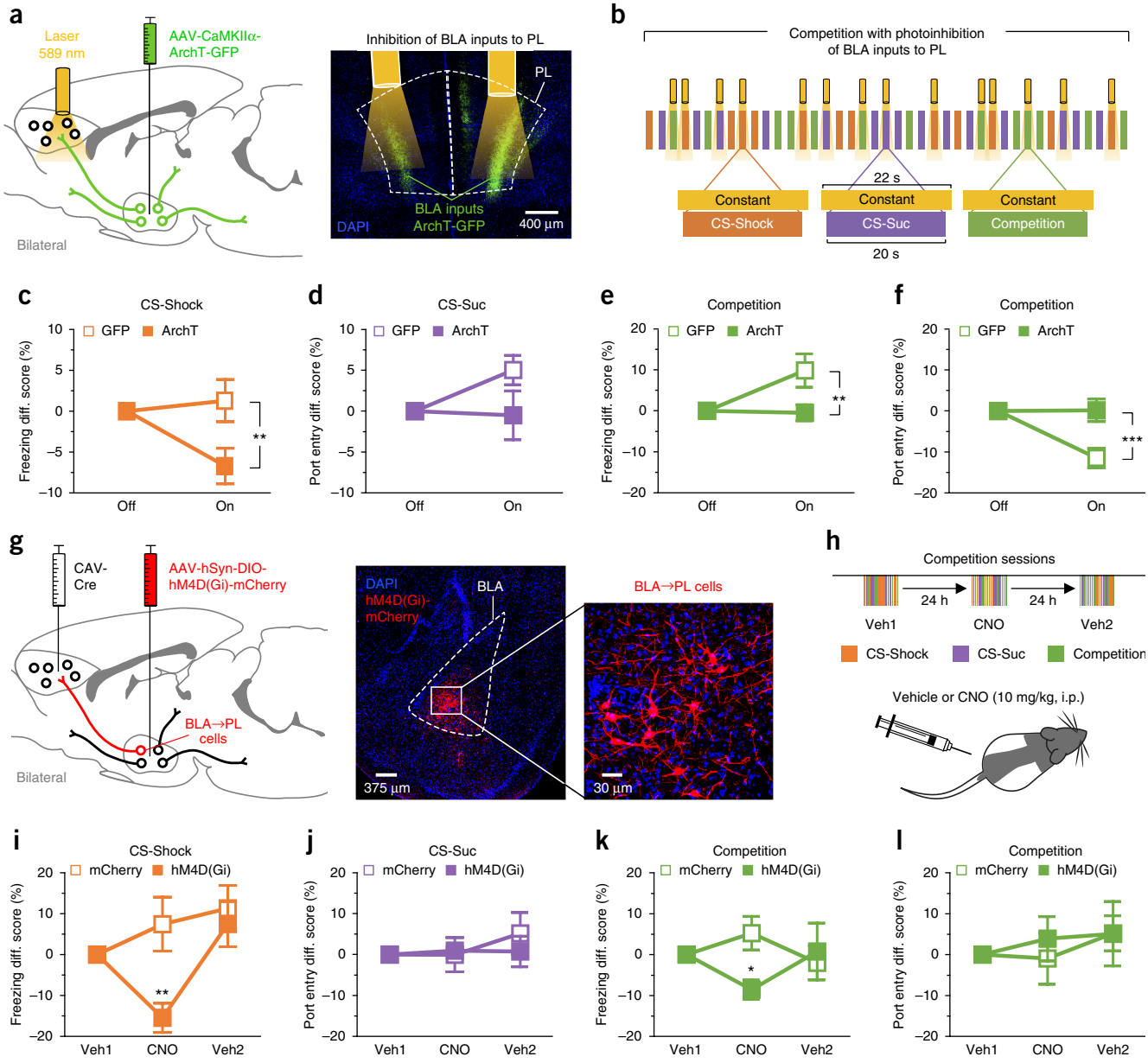


**Figure 7** The BLA→PL pathway is necessary for expression of the fear-associated memory, but not for reward-seeking behavior. (**a**) Optogenetic strategy to inhibit BLA inputs to PL. Illumination may have also affected BLA terminals in other subregions of mPFC. The BLA was bilaterally transfected to express either GFP ($n = 6$ animals) or the opsin ArchT ($n = 6$ animals), and optical fibers were chronically implanted just above PL to silence BLA inputs locally. (**b**) Competition model, in which half of the trials were paired with constant yellow light to silence BLA inputs to mPFC. The trial and laser sequences were pseudorandomized. (**c**) Silencing of BLA inputs to mPFC significantly impaired freezing responses during CS-Shock trials (repeated measures two-way ANOVA: group, $F_{1,10} = 5.64$, $P = 0.039$; laser, $F_{1,10} = 2.75$, $P = 0.14$; interaction, $F_{1,10} = 5.64$, $P = 0.039$; GFP versus ArchT during laser-on: $t_{10} = 3.36$, $^{**}P = 0.0072$). (**d**) No statistically significant differences were detected on port entry responses during CS-Suc trials (group, $F_{1,10} = 2.53$, $P = 0.14$; laser, $F_{1,10} = 1.70$, $P = 0.22$; interaction, $F_{1,10} = 2.53$, $P = 0.14$). (**e**) Significant group differences were detected for freezing during competition (group, $F_{1,10} = 5.20$, $P = 0.046$; laser, $F_{1,10} = 4.37$, $P = 0.063$; interaction, $F_{1,10} = 5.20$, $P = 0.046$; GFP versus ArchT during laser-on: $t_{10} = 3.23$, $^{**}P = 0.0091$). (**f**) Significant group differences were also detected for port entries during competition (group, $F_{1,10} = 10.5$, $P = 0.009$; laser, $F_{1,10} = 9.73$, $P = 0.011$; interaction, $F_{1,10} = 10.5$, $P = 0.009$; GFP versus ArchT during laser-on: $t_{10} = 4.58$, $^{***}P = 0.001$). (**g**) Chemogenetic strategy to selectively silence BLA→PL cells. Using a Cre-dependent dual-virus method, BLA→PL cells were bilaterally transduced with either mCherry ($n = 7$ animals) or hM4D(Gi) ($n = 7$ animals). (**h**) Experimental design to treat animals with either vehicle (5% DMSO in 0.9% saline, i.p.; Veh) or CNO (10 mg/kg, i.p.) ~15–20 min before behavioral testing. (**i**) Silencing the BLA→PL cell population significantly impaired freezing responses during CS-Shock trials (group, $F_{1,12} = 3.41$, $P = 0.09$; drug, $F_{2,24} = 7.96$, $P = 0.0022$; interaction, $F_{2,24} = 6.31$, $P = 0.006$; mCherry versus hM4D(Gi) during CNO: $t_{12} = 3.66$, $^{**}P = 0.0033$). (**j**) No significant differences were detected in port entry behavior during CS-Suc trials (group, $F_{1,12} = 0.13$, $P = 0.72$; drug, $F_{2,24} = 0.69$, $P = 0.51$; interaction, $F_{2,24} = 0.57$, $P = 0.58$). (**k**) Silencing the BLA→PL cell population impaired freezing responses during competition trials (group, $F_{1,12} = 1.45$, $P = 0.25$; drug, $F_{2,24} = 0.09$, $P = 0.91$; interaction, $F_{2,24} = 2.67$, $P = 0.09$; mCherry versus hM4D(Gi) during CNO: $t_{12} = 2.56$, $^{*}P = 0.025$). (**l**) No significant differences were detected in port entry behavior during competition trials (group, $F_{1,12} = 0.13$, $P = 0.72$; drug, $F_{2,24} = 0.60$, $P = 0.55$; interaction, $F_{2,24} = 0.17$, $P = 0.84$). Error bars represent s.e.m.

wherein a subset of trials were paired with photostimulation. If off-site vesicle release contributed to the behavioral change in ChR2-expressing animals relative to eYFP animals, then we would expect those contributions to persist after the NBQX plus AP5 treatment. We found that infusion of NBQX plus AP5 abolished the light-induced increase in freezing observed in CS-Shock trials (**Fig. 6g**), as well as during competition trials (**Fig. 6i**), confirming that transmission from BLA terminals in the PL was sufficient to promote cue-induced freezing.

### Inhibition of the BLA→PL pathway suppressed cue-induced fear-related behavior

Although our photostimulation experiments demonstrated that the BLA→PL projection is sufficient to augment freezing, fear-related behavior is likely governed by parallel, redundant circuits. We next tested the necessity of the BLA→mPFC pathway with optogenetic inhibition and the necessity of BLA→PL cells with chemogenetic inhibition during discrimination and competition (**Fig. 7** and **Supplementary Figs. 9** and **10**).

For optogenetic inhibition, we bilaterally expressed the inhibitory opsin ArchT[28,29] in BLA neurons and photoinhibited BLA terminals in the mPFC during the presentation of a subset of CS-Suc, CS-Shock and competition trials (**Fig. 7a**,**b**). We found that ArchT-expressing animals showed a significant reduction in freezing during the laser-on versus laser-off trials relative to GFP-expressing controls during CS-Shock trials (**Fig. 7c**) and competition trials (**Fig. 7e**).

Given the caveats associated with optogenetic inhibition, including the possibility of photoinhibition of adjacent mPFC subregions, effects of heating or sensory detection of the light stimulation, we also performed chemogenetic inhibition. We selectively expressed an inhibitory chemogenetic tool, hM4D(Gi) DREADDs (designer receptors exclusively activated by designer drugs)[30], which are activated by clozapine-*N*-oxide (CNO), in BLA→PL neurons using the CAV2-Cre virus strategy (**Fig. 7g**). We then systemically injected either vehicle or CNO into animals before sessions wherein CS-Suc, CS-Shock and competition trials were presented in a pseudorandom order (**Fig. 7h**). As in our optogenetic inhibition experiment, we observed that selective inhibition of the BLA→PL neurons reduced freezing relative to mCherry-expressing controls during CS-Shock trials (**Fig. 7i**) and competition trials (**Fig. 7k**).

## DISCUSSION

In this study, we developed a new model for studying the orchestration of competing mechanisms elicited by simultaneous presentation of cues associated with conflicting motivational drives. By presenting these stimuli in a trial structure, we enabled systematic observation of neural correlates (**Fig. 1**). Electrophysiological recordings revealed correlated neural activity in the BLA and PL that was predominantly excitatory during the entire task. However, the direction of information flow changed depending on the specific behavioral epoch: the BLA was more likely to lead excitatory correlations with PL during fear-related behavior (**Fig. 2**), and PL neurons encoding the fear-associated cue were more likely to be correlated with BLA activity (**Fig. 3**). This result was bolstered by our finding that most photoidentified BLA→PL neurons recorded showed excitations in response to the fear-associated cue and more accurately decoded behavior in the face of competing signals (**Figs. 4** and **5**), showing that this effect was at least in part due to direct input from BLA to PL. Conversely, inhibitory CCs were more often led by the BLA upon presentation of the sucrose-predictive cue (**Fig. 2h**), and neurons inhibited by photoidentified BLA→PL neurons (network-inhibited cells) showed a trend toward increased excitatory responding to the reward-associated cue or inhibition to the shock-predictive cue. Although the sample sizes for the inhibitory CCs and network-inhibited neurons were admittedly small, these data lead us to speculate that a competing reward-related network exists and is suppressed locally within the BLA[2,31].

### Anatomical implications

Several subtle effects from our experiments prompted us to speculate about the possible interactions between BLA and PL neurons. In our phototagging experiment (**Fig. 4**), we observed network-inhibited neurons in the BLA that were inhibited upon photostimulation of BLA→PL neurons. We speculate that BLA→PL neurons have collaterals that may synapse locally onto BLA interneurons that inhibit these network-inhibited cells, though it is possible that they collateralize to distal GABAergic neurons that have long-range projections back to the BLA. Though we are not aware of any direct evidence that the BLA contains GABAergic neurons that project to the PL, our experiments do not allow us to exclude this possibility.

Although in our optogenetic manipulations (**Figs. 6** and **7**) we aimed our optical fiber at the PL region of the mPFC, it is possible that we also targeted BLA terminals in surrounding areas. We took care to photoinhibit BLA terminals in mPFC only during the 20-s cue presentation, as we wanted to avoid paradoxical vesicle release associated with prolonged illumination of ArchT-expressing axon terminals[32]. Even so, we observed a minority of neurons in the PL (4%; **Supplementary Fig. 9h**) that showed an increase in activity upon photoinhibition of BLA terminals, which may result from network disinhibition. It may also be noteworthy that our optogenetic manipulations produced rather subtle behavioral changes (**Figs. 6** and **7**). The relatively small effect sizes may reflect either redundancy in the circuitry involved in this task or technical challenges related to using rats as opposed to mice (including greater volume of illumination required or lower relative expression levels achieved).

We found similar proportions of correlated BLA/PL cells during all task events, and a substantial proportion of cell pairs exhibited correlated activity during more than one event. This suggests that there are consistent anatomical relationships between the BLA and PL that are selectively modulated depending on the memory that is being retrieved. While we found evidence supporting bidirectional flow of information during reward-seeking epochs, the flow of information became biased toward the BLA→PL direction during fear epochs. This biased flow of information was not due to increased responsiveness to the shock-predictive cue compared to the sucrose-predictive cue in the BLA as a whole. More specific hypotheses of the underlying change in effective connectivity might include the possibility that BLA neurons that signal fear memory are more likely to connect functionally in a leading manner with PL. In addition, while BLA neurons that encode the same cue value may be more likely to facilitate each other than neurons that encode the opposite cue value, there is debate as to whether such populations are anatomically intermingled or segregated, and as to how they interact[7,8,31,33]. This suggests that statistical interrelationships are unlikely to remain completely independent across reward and fear retrieval. Despite this, we observed dynamic changes in the functional relationship between the BLA and PL that differentiated reward versus fear memory retrieval, with the BLA driving PL activity more strongly during the retrieval of fear than reward. A possible explanation for this could be that another structure mediates the changing relationship between the BLA and PL. One potential candidate is the ventral hippocampus, which is required for the expression of conditioned fear responses[22] and preferentially modulates activity in both the BLA and PL during states of elevated fear and anxiety[34,35].

### Could another BLA→mPFC pathway preferentially guide reward-seeking behavior?

Other mPFC subregions, such as the infralimbic cortex (IL), have different functions than PL in the regulation of reward-seeking and fear responses. In the reward domain, while PL activity is required for the initial acquisition of goal-directed reward-seeking behavior, IL activity is required for habitual reward-seeking behavior in over-trained animals[36–38]. Furthermore, IL shows stronger increases in activity than PL during reward-seeking tasks[18]. In addition, IL activity has also been correlated with food enticement[39], contextually driven reward-seeking responses[13] and Pavlovian-to-instrumental transfer of reward-seeking behavior[40]. In the fear domain, while PL activity is crucial for fear expression[11,21,41], IL activity is crucial for fear extinction and the inhibition of fear responses later on[19]. The ability of IL to inhibit fear could reliably allow reward-related signals to emerge without conflicting with fear signals, thus allowing reward-seeking behavior to occur. Future studies could focus on determining the function of the BLA→IL pathway during reward–fear discrimination and test the hypothesis that IL may be a reward-biased pathway between the BLA and the mPFC.

### Potential implications for impact of emotion on cognition

While we found evidence for both 'bottom-up' (BLA→PL) and 'top-down' (PL→BLA) interactions, overall, BLA→PL regulation dominated over the reciprocal PL→BLA regulation during fear retrieval. This finding is consistent with other models that predict transfer of information from the BLA to PL during fear learning[11,12,24,25,42]. Furthermore, recent studies that examined neural oscillations in the theta and gamma frequencies of local field potentials report synchronized activity between the BLA and PL[43–45]. However, these oscillations do not clearly reflect preferential bottom-up BLA→PL regulation during fear retrieval. In contrast, top-down PL→BLA regulation has been reported to dominate during the presentation of 'safety' cues (for example, cues that do not predict electrical shocks)[43,44] or during anesthesia in untrained animals[46]. Thus, it appears that bottom-up BLA→PL regulation dominates during high-fear states, whereas top-down PL→BLA regulation dominates during low-fear states. Nonetheless, we did not observe stronger top-down PL→BLA regulation during reward-seeking behavior, which is a low-fear state. Perhaps some bottom-up BLA→PL regulation might have occurred during reward-seeking that countered the opposite, top-down PL→BLA regulation during this low-fear, reward-seeking state.

After being trained using only neural activity during the individual fear- and reward-associated cues, machine learning algorithms were able to decode subject behavior using neural activity from competition trials (**Fig. 5**). The ability to predict behavior in the face of conflicting cues suggests that limbic representations of singular motivational states are nested within the representation of these states in conflict. Indeed, the representation of emotional conflict in the BLA is not only associated with the cues that trigger positive or negative emotional states, but also the behavioral expression of those states[2]. Despite variability across or even within animals, behavior on competition trials was decisive within individual trials, suggesting that emotional conflict is inherently unstable and quickly pivots toward simpler, singular motivational states. Our findings support the notion that the process of conflict resolution or state stabilization has, to some extent, already occurred in the information communicated by the BLA to the PL[47–50].

In summary, the present study establishes a new model and identifies new vistas for exploration regarding the distal networks and microcircuitry involved in the neural mechanisms guiding action selection in situations of conflict.

## METHODS

Methods, including statements of data availability and any associated accession codes and references, are available in the online version of the paper.

*Note: Any Supplementary Information and Source Data files are available in the online version of the paper.*


### ACKNOWLEDGMENTS

The authors thank S. Sorooshyari for discussion and assistance on Matlab programming, as well as C. Wildes, and the entire Tye laboratory for discussion and support on this project. A.B.-R. was supported by the Brain and Behavior Research Foundation (NARSAD Young Investigator Award) and NIMH (Research Supplement to Promote Diversity in Health-Related Sciences). E.Y.K. was supported by the Collaborative Clinical Neuroscience Fellowship and the American Brain Foundation Clinical Research Training Fellowship. W.A.R.-G. and P.A.P.-R. were supported by the MIT Summer Research Program, which received support from the Center for Brains, Minds and Machines (CBMM), NSF (STC Award CCF-1231216) and NIH (Endure Award 1R25-MH092912-01). E.H.N. was supported by the National Science Foundation Graduate Research Fellowship (NSF GRFP), the Integrative Neuronal Systems Training Fellowship (T32 GM007484) and the Training Program in the Neurobiology of Learning and Memory. A.C.F.-O. was supported by an institutional NRSA training grant (5T32GM007484-38). P.N. was supported by the Singleton, Leventhal and Whitaker fellowships. C.A.L. was supported by an NSF Graduate Research Fellowship, an Integrative Neuronal Systems Fellowship and the James R. Killian Fellowship. M.J.P., K.N.P. and M.A. were supported by the MIT Undergraduate Research Opportunities Program. K.K.A. was supported by the MIT Research Assistantship Program. K.M.T. is a New York Stem Cell Foundation - Robertson Investigator and McKnight Scholar, and this work was supported by funding from the JPB Foundation, PIIF, PNDRF, JFDP, Whitehall Foundation, Klingenstein Foundation, NARSAD Young Investigator Award, Alfred P Sloan Foundation, New York Stem Cell Foundation, McKnight Foundation, NIH R01-MH102441-01 (NIMH), R01-AA023305-01 (NIAAA) and NIH Director's New Innovator Award DP2-DK-102256-01 (NIDDK).


### AUTHOR CONTRIBUTIONS

A.B.-R. and K.M.T. conceived and designed experiments. A.B.-R. and K.N.P. designed and constructed electrodes and optrodes for neural recordings. A.B.-R. performed surgeries to chronically implant electrodes and performed single-unit recordings. A.B.-R., C.A.L. and K.N.P. sorted extracellular waveforms. A.B.-R. and E.Y.K. analyzed electrophysiology data. E.Y.K. wrote the Matlab scripts for the support vector machine learning algorithms. E.M.I., M.J.P., K.N.P., K.K.A., P.A.P.-R. and M.A. built optical fibers. A.B.-R., E.M.I., M.J.P., W.A.R.-G., K.N.P. and M.A. performed animal training and analyzed behaviors from videos. A.B.-R., E.M.I., M.J.P., W.A.R.-G., A.C.F.-O., K.N.P., K.K.A. and M.A. performed histological assessment. E.H.N. assisted with programing of the neural recording workstation and wrote the Matlab script for quantification of animal movement. P.N. assisted with Med-PC programming for behavioral studies and wrote the Matlab scripts to analyze port entry data and waveform properties. A.B. performed *ex vivo* whole-cell patch-clamp electrophysiological recordings. A.B. and A.C.F.-O. assisted with figures. A.B.-R., E.Y.K. and K.M.T. made figures and wrote the manuscript. All authors contributed to the editing and revision of the final version of the manuscript.

### COMPETING FINANCIAL INTERESTS

The authors declare no competing financial interests.




1. Maren, S. & Quirk, G.J. Neuronal signalling of fear memory. *Nat. Rev. Neurosci.* **5**, 844–852 (2004).
2. Janak, P.H. & Tye, K.M. From circuits to behaviour in the amygdala. *Nature* **517**, 284–292 (2015).
3. Rogan, M.T., Stäubli, U.V. & LeDoux, J.E. Fear conditioning induces associative long-term potentiation in the amygdala. *Nature* **390**, 604–607 (1997).
4. Paton, J.J., Belova, M.A., Morrison, S.E. & Salzman, C.D. The primate amygdala represents the positive and negative value of visual stimuli during learning. *Nature* **439**, 865–870 (2006).
5. Tye, K.M., Stuber, G.D., de Ridder, B., Bonci, A. & Janak, P.H. Rapid strengthening of thalamo-amygdala synapses mediates cue-reward learning. *Nature* **453**, 1253–1257 (2008).

6. Shabel, S.J. & Janak, P.H. Substantial similarity in amygdala neuronal activity during conditioned appetitive and aversive emotional arousal. *Proc. Natl. Acad. Sci. USA* **106**, 15031–15036 (2009).
7. Namburi, P. *et al.* A circuit mechanism for differentiating positive and negative associations. *Nature* **520**, 675–678 (2015).
8. Beyeler, A. *et al.* Divergent routing of positive and negative information from the amygdala during memory retrieval. *Neuron* **90**, 348–361 (2016).
9. Choi, J.-S. & Kim, J.J. Amygdala regulates risk of predation in rats foraging in a dynamic fear environment. *Proc. Natl. Acad. Sci. USA* **107**, 21773–21777 (2010).
10. Amir, A., Lee, S.-C., Headley, D.B., Herzallah, M.M. & Pare, D. Amygdala signaling during foraging in a hazardous environment. *J. Neurosci.* **35**, 12994–13005 (2015).
11. Burgos-Robles, A., Vidal-Gonzalez, I. & Quirk, G.J. Sustained conditioned responses in prelimbic prefrontal neurons are correlated with fear expression and extinction failure. *J. Neurosci.* **29**, 8474–8482 (2009).
12. Senn, V. *et al.* Long-range connectivity defines behavioral specificity of amygdala neurons. *Neuron* **81**, 428–437 (2014).
13. Moorman, D.E. & Aston-Jones, G. Prefrontal neurons encode context-based response execution and inhibition in reward seeking and extinction. *Proc. Natl. Acad. Sci. USA* **112**, 9472–9477 (2015).
14. McGarry, L.M. & Carter, A.G. Inhibitory gating of basolateral amygdala inputs to the prefrontal cortex. *J. Neurosci.* **36**, 9391–9406 (2016).
15. Dilgen, J., Tejeda, H.A. & O'Donnell, P. Amygdala inputs drive feedforward inhibition in the medial prefrontal cortex. *J. Neurophysiol.* **110**, 221–229 (2013).
16. Gabbott, P.L.A., Warner, T.A., Jays, P.R.L., Salway, P. & Busby, S.J. Prefrontal cortex in the rat: projections to subcortical autonomic, motor, and limbic centers. *J. Comp. Neurol.* **492**, 145–177 (2005).
17. Ishikawa, A., Ambroggi, F., Nicola, S.M. & Fields, H.L. Contributions of the amygdala and medial prefrontal cortex to incentive cue responding. *Neuroscience* **155**, 573–584 (2008).
18. Burgos-Robles, A., Bravo-Rivera, H. & Quirk, G.J. Prelimbic and infralimbic neurons signal distinct aspects of appetitive instrumental behavior. *PLoS One* **8**, e57575 (2013).
19. Burgos-Robles, A., Vidal-Gonzalez, I., Santini, E. & Quirk, G.J. Consolidation of fear extinction requires NMDA receptor-dependent bursting in the ventromedial prefrontal cortex. *Neuron* **53**, 871–880 (2007).
20. Sotres-Bayon, F. & Quirk, G.J. Prefrontal control of fear: more than just extinction. *Curr. Opin. Neurobiol.* **20**, 231–235 (2010).
21. Courtin, J. *et al.* Prefrontal parvalbumin interneurons shape neuronal activity to drive fear expression. *Nature* **505**, 92–96 (2014).
22. Sierra-Mercado, D., Padilla-Coreano, N. & Quirk, G.J. Dissociable roles of prelimbic and infralimbic cortices, ventral hippocampus, and basolateral amygdala in the expression and extinction of conditioned fear. *Neuropsychopharmacology* **36**, 529–538 (2011).
23. Sangha, S., Robinson, P.D., Greba, Q., Davies, D.A. & Howland, J.G. Alterations in reward, fear and safety cue discrimination after inactivation of the rat prelimbic and infralimbic cortices. *Neuropsychopharmacology* **39**, 2405–2413 (2014).
24. Laviolette, S.R., Lipski, W.J. & Grace, A.A. A subpopulation of neurons in the medial prefrontal cortex encodes emotional learning with burst and frequency codes through a dopamine D4 receptor-dependent basolateral amygdala input. *J. Neurosci.* **25**, 6066–6075 (2005).
25. Sotres-Bayon, F., Sierra-Mercado, D., Pardilla-Delgado, E. & Quirk, G.J. Gating of fear in prelimbic cortex by hippocampal and amygdala inputs. *Neuron* **76**, 804–812 (2012).
26. Nieh, E.H. *et al.* Decoding neural circuits that control compulsive sucrose seeking. *Cell* **160**, 528–541 (2015).
27. Tye, K.M. *et al.* Amygdala circuitry mediating reversible and bidirectional control of anxiety. *Nature* **471**, 358–362 (2011).
28. Chow, B.Y. *et al.* High-performance genetically targetable optical neural silencing by light-driven proton pumps. *Nature* **463**, 98–102 (2010).
29. Mattis, J. *et al.* Principles for applying optogenetic tools derived from direct comparative analysis of microbial opsins. *Nat. Methods* **9**, 159–172 (2011).
30. Armbruster, B.N., Li, X., Pausch, M.H., Herlitze, S. & Roth, B.L. Evolving the lock to fit the key to create a family of G protein-coupled receptors potently activated by an inert ligand. *Proc. Natl. Acad. Sci. USA* **104**, 5163–5168 (2007).
31. Kim, J., Pignatelli, M., Xu, S., Itohara, S. & Tonegawa, S. Antagonistic negative and positive neurons of the basolateral amygdala. *Nat. Neurosci.* **19**, 1636–1646 (2016).
32. Mahn, M., Prigge, M., Ron, S., Levy, R. & Yizhar, O. Biophysical constraints of optogenetic inhibition at presynaptic terminals. *Nat. Neurosci.* **19**, 554–556 (2016).
33. Zhang, W. *et al.* Functional circuits and anatomical distribution of response properties in the primate amygdala. *J. Neurosci.* **33**, 722–733 (2013).
34. Adhikari, A., Topiwala, M.A. & Gordon, J.A. Single units in the medial prefrontal cortex with anxiety-related firing patterns are preferentially influenced by ventral hippocampal activity. *Neuron* **71**, 898–910 (2011).
35. Jin, J. & Maren, S. Fear renewal preferentially activates ventral hippocampal neurons projecting to both amygdala and prefrontal cortex in rats. *Sci. Rep.* **5**, 8388 (2015).
36. Killcross, S. & Coutureau, E. Coordination of actions and habits in the medial prefrontal cortex of rats. *Cereb. Cortex* **13**, 400–408 (2003).
37. Balleine, B.W. & O'Doherty, J.P. Human and rodent homologies in action control: corticostriatal determinants of goal-directed and habitual action. *Neuropsychopharmacology* **35**, 48–69 (2010).
38. Smith, K.S., Virkud, A., Deisseroth, K. & Graybiel, A.M. Reversible online control of habitual behavior by optogenetic perturbation of medial prefrontal cortex. *Proc. Natl. Acad. Sci. USA* **109**, 18932–18937 (2012).
39. Valdés, J.L., Maldonado, P., Recabarren, M., Fuentes, R. & Torrealba, F. The infralimbic cortical area commands the behavioral and vegetative arousal during appetitive behavior in the rat. *Eur. J. Neurosci.* **23**, 1352–1364 (2006).
40. Keistler, C., Barker, J.M. & Taylor, J.R. Infralimbic prefrontal cortex interacts with nucleus accumbens shell to unmask expression of outcome-selective Pavlovian-to-instrumental transfer. *Learn. Mem.* **22**, 509–513 (2015).
41. Corcoran, K.A. & Quirk, G.J. Activity in prelimbic cortex is necessary for the expression of learned, but not innate, fears. *J. Neurosci.* **27**, 840–844 (2007).
42. Klavir, O., Genud-Gabai, R. & Paz, R. Functional connectivity between amygdala and cingulate cortex for adaptive aversive learning. *Neuron* **80**, 1290–1300 (2013).
43. Likhtik, E., Stujenske, J.M., Topiwala, M.A., Harris, A.Z. & Gordon, J.A. Prefrontal entrainment of amygdala activity signals safety in learned fear and innate anxiety. *Nat. Neurosci.* **17**, 106–113 (2014).
44. Stujenske, J.M., Likhtik, E., Topiwala, M.A. & Gordon, J.A. Fear and safety engage competing patterns of theta-gamma coupling in the basolateral amygdala. *Neuron* **83**, 919–933 (2014).
45. Karalis, N. *et al.* 4-Hz oscillations synchronize prefrontal-amygdala circuits during fear behavior. *Nat. Neurosci.* **19**, 605–612 (2016).
46. Likhtik, E., Pelletier, J.G., Paz, R. & Paré, D. Prefrontal control of the amygdala. *J. Neurosci.* **25**, 7429–7437 (2005).
47. Etkin, A., Egner, T., Peraza, D.M., Kandel, E.R. & Hirsch, J. Resolving emotional conflict: a role for the rostral anterior cingulate cortex in modulating activity in the amygdala. *Neuron* **51**, 871–882 (2006).
48. Comte, M. *et al.* Dissociating bottom-up and top-down mechanisms in the cortico-limbic system during emotion processing. *Cereb. Cortex* **26**, 144–155 (2016).
49. Rohr, C.S. *et al.* The neural networks of subjectively evaluated emotional conflicts. *Hum. Brain Mapp.* **37**, 2234–2246 (2016).
50. Kanske, P. & Kotz, S.A. Emotion speeds up conflict resolution: a new role for the ventral anterior cingulate cortex? *Cereb. Cortex* **21**, 911–919 (2011).

## ONLINE METHODS

**Animals.** All procedures were approved by the Committee on Animal Care of the Massachusetts Institute of Technology and the Animal Care and Use Review Office of the USAMRMC, in compliance with the PHS Policy on Humane Care and Use of Laboratory Animals (Public Law 99–158). Adult male Long-Evans rats weighing ~275–300 g (3 months old) were acquired from a commercial supplier (Taconic Biosciences) and were housed individually in Plexiglas home cages in a vivarium with controlled temperature, humidity and pressure. Rats were maintained on a regular 12-h light/dark cycle and all experiments were performed during the light phase. Water was available *ad libitum*. Standard rat chow was restricted to 20 g/d.

**Surgeries.** Rats were anesthetized using isoflurane gas (~2.0%), and surgeries were performed using stereotaxic apparatuses (Kopf Instruments). Midline incisions were made down the scalp using surgical blades and craniotomies were opened using a dental drill. Coordinates to target the BLA were −2.60 to −2.80 mm anterior–posterior (AP), ±4.80 to ±5.00 mm medial–lateral (ML) and −8.50 to −8.80 mm dorsal–ventral (DV). Coordinates to target PL were +3.00 to +2.90 mm AP, ±0.50 to ±0.75 mm ML and −3.75 to −4.00 mm DV. All coordinates are relative to bregma. Implants were secured to the skull using stainless steel self-tapping screws (3.18 mm; Small Parts), adhesive cement (C&B Metabond, Parkell) and dental acrylic (Ortho-Jet, Lang Dental). Incisions were sutured and postoperative care and analgesia (5 mg/kg ketoprofen or 1.5 mg/kg meloxicam) were provided for 4 d. Rats were allowed to fully recover from surgery for 2 weeks.

**Optogenetic manipulations.** Viral vectors were infused during a surgical procedure that occurred at least 12–16 weeks before implanting optical fibers. All viral aliquots were obtained from the University of North Carolina Vector Core, unless otherwise specified. DNA sequences for viral constructs can be found online (http://www.optogenetics.org/). A 10-µL microsyringe with a 33-Ga needle (Nanofil, WPI) was used to deliver viral vectors into the targets at a rate of 0.1 µL/min, using a microsyringe pump (UMP3/Micro4; WPI). Viral volumes of ~700–1,000 nL were infused per target. Needles were kept at the infusion site for an extra 10 min to allow viral diffusion. Needles were slowly withdrawn at an approximate rate of 1 mm/min.

For optogenetic stimulation, the BLA was unilaterally transduced with a serotype-5 adeno-associated viral vector ($AAV_5$) encoding the blue-light-sensitive cation pump *Chlamydomonas reinhardtii* channelrhodopsin-2 (ChR2), which was fused to enhanced yellow fluorescent protein (eYFP) and expressed under the calcium/calmodulin-dependent protein kinase II alpha (*Camk2a*) promoter ($AAV_5$-CaMKIIα-ChR2(H134R)-eYFP). Animals in the control group received a viral vector that encoded only eYFP ($AAV_5$-CaMKIIα-eYFP). For optogenetic inhibition, the BLA was bilaterally transduced with a viral vector encoding the yellow-light-sensitive outward proton pump *Halorubrum sodomense* TP009 archaerhodopsin (ArchT), which was fused to green fluorescent protein (GFP) and expressed under the *Camk2a* promoter ($AAV_9$-CaMKIIα-ArchT-GFP). Animals in the control group received a viral vector that encoded only GFP ($AAV_8$-CaMKIIα-GFP).

Optical fibers were chronically implanted in the dorsal portion of PL to either stimulate or inhibit BLA inputs. These implants consisted of a Ø400-µm-core multimode fiber (NA = 0.48; Thorlabs) that was held in a stainless steel ferrule (Precision Fiber Products). Optical fibers were cut at ~5–8 mm from the bottom of the ferrules to reach PL. Fibers were polished until reaching an ~85–95% light transmission efficiency. During behavioral testing, optical fibers were connected to patch cords (Doric), which were in turn connected to blue or yellow light lasers (OEM Laser Systems) using FC/PC adapters located above the operant chambers. Laser output was controlled with a Master-8 pulse stimulator (A.M.P.I.). For photostimulation, 473-nm DPSS lasers (100 mW) were used to deliver 5-ms pulses of blue light at a frequency of 20 Hz, with a power of ~10 mW at the tip of the optical fibers (~80 mW/mm$^2$). For photoinhibition, 589-nm DPSS lasers (100 mW) were used to deliver constant yellow light at a power of ~8 mW at the tip of the optical fibers (~64 mW/mm$^2$). The blue laser was activated 500 ms before CS onset and deactivated 500 ms after CS offset, whereas the yellow laser was activated 1,000 ms before CS onset and deactivated 1,000 ms after CS offset.

**Pharmacology experiment.** Optogenetic and pharmacology approaches were combined to rule out the possibility of stimulation of fibers of passage. After unilaterally transducing the BLA with ChR2, a 20-Ga stainless steel cannula was chronically implanted above PL (stereotaxic coordinates: 2.95 mm anterior, 0.60 mm lateral and 3.00 mm ventral from bregma). A 24-Ga dummy was inserted to prevent clogging of the cannula, and 24-Ga injectors extending 1 mm from the tip of the cannula were used to infuse drugs into PL. A 10-µL microsyringe (Nanofil, WPI) was used to infuse drugs at a rate of 0.1 µL/min, using a microsyringe pump (UMP3/Micro4; WPI).

Drugs were delivered into PL before the insertion of optical fibers and behavioral testing. Animals were tested on two days in a counterbalanced fashion shortly after infusion of either artificial cerebrospinal fluid (ACSF) or the AMPA and NMDA antagonists NBQX (22 mM (ref. 51); 2,3-dihydroxy-6-nitro-7-sulfamoyl-benzo[f]quinoxaline-2,3-dione; Tocris) and AP5 (38 mM (ref. 51); (2*R*)-amino-5-phosphonovaleric acid; Tocris). A total volume of 500 nL of ACSF or NBQX + AP5 (250 nL each) was infused into PL. Injectors were kept at the infusion site for an extra 5 min to allow drug diffusion. After drug infusion (~10 min), Ø400-µm-core optical fibers, which were mounted on stainless steel ferrules and glued to nylon dust caps, were inserted and attached to the cannulas. Optical fibers extended ~250–500 µm beyond the cannula tips. Animals were then transferred to operant chambers and connected to patch cords for testing.

**Chemogenetic silencing.** Viral vectors were used to express either the control fluorophore mCherry or the $G_i$-coupled receptor hM4D(Gi), which silences neural activity upon activation with a designer drug. mCherry or hM4D(Gi) were selectively expressed in the BLA cells terminating in PL using a Cre-dependent dual-virus strategy in which the BLA was infused with a virus containing mCherry or hM4D(Gi) in a double-floxed inverted open reading cassette ($AAV_5$-hSyn-DIO-mCherry or $AAV_5$-hSyn-DIO-hM4D(Gi)-mCherry), whereas PL was infused with a retrograde canine virus type-2 encoding Cre recombinase (CAV2-Cre (ref. 52); Institute of Molecular Genetics of Montpellier). Viral volumes of ~700–1,000 nL were infused per site at a rate of 0.1 µL/min. Viral expression was allowed for ~12–16 weeks before behavioral testing. hM4D(Gi) was activated with the designer drug clozapine-*N*-oxide (CNO; Sigma-Aldrich), which was diluted in a solution of 5% DMSO and 0.9% saline. Systemic injections (i.p.) were performed ~15–20 min before behavioral testing at a dose of 10 mg/kg to inhibit neuronal activity. Behavioral testing was also performed after multiple vehicle injections (5% DMSO in 0.9% saline).

**Behavioral tasks.** Rats were trained in standard operant chambers (23 × 30 × 40 cm; Med Associates) located inside sound-attenuating cubicles. Each chamber was equipped with a red house light, light cues, speakers for the delivery of tone or white noise cues, a syringe pump to deliver sucrose, a sucrose port that was equipped with an infrared beam for the detection of entries and exits, and a grid floor for the delivery of electrical shocks. A customized digital-relay circuit was added between the shock generator and grid floor to minimize electrical artifacts. Chambers were scrubbed with 70% isopropyl alcohol after testing each animal.

All training phases occurred in the context. The first phase of training consisted of the acquisition of a Pavlovian reward association in which rats learned to associate a conditioned stimulus with sucrose (that is, CS-Suc). To facilitate reward acquisition, rats were pre-exposed multiple times to sucrose in the home cage as well as in the training chambers. Reward conditioning consisted of the presentation of either a light cue or a sine wave tone cue (5 kHz, 80 dB) that lasted for 20 s and predicted the delivery of a 30% sucrose solution (120 µL/trial). Sucrose was delivered over 10 s during the cue presentation (5–15 s, relative to CS onset). Rats underwent three reward sessions (one per day), each consisting of a total of 25 trials delivered over ~35 min. The ITI was variable, with an average of 1 min. Sucrose was removed by vacuum immediately after cue offset if rats did not retrieve it during the CS.

The second phase of training consisted of the discrimination of conditioned stimuli that predicted sucrose reward (CS-Suc), aversive shocks (CS-Shock) or no outcome (CS–). The light and tone cues were counterbalanced across rats for the CS-Suc and CS-Shock associations. The white noise cue was always used for the CS–. The aversive shocks (0.40 mA) lasted for 0.5 s and co-terminated with the CS (19.5–20 s, relative to CS onset). CS-Suc, CS-Shock and CS– trials occurred in a pseudorandom manner. Rats underwent at least three discrimination sessions (one per day), each consisting of a total of 60 trials delivered over ~83 min. The ITI was variable, with an average of 1 min.

The third phase of training tested the direct competition of reward- and fear-related behaviors. In addition to individual CS-Suc and CS-Shock trials, this phase of training included competition trials, in which the CS-Suc and CS-Shock associations were co-presented to induce conflicting motivational drives and the potential for competition between reward- and fear-associated behaviors. CS-Suc, CS-Shock and competition trials occurred in a pseudorandom manner. A total of 60 trials were delivered over ~83 min during these competition sessions (variable ITI, with an average of 1 min).

**Reward and fear behaviors.** Entries into the sucrose port provided a readout of reward-related behavior. Timestamps for port entries and exits were sampled from beam breaks (Med-PC IV, Med Associates). These timestamps were used to quantify the amount of time that animals spent in the port. Freezing responses, which are defined as the lack of all movement except for respiration[53], provided a readout of fear-related behavior. Videos were sampled using infrared cameras at 30 fps, and freezing was quantified using an automated custom Matlab script that quantified frame-by-frame changes in total pixel intensity as approximations for animal motion. Frame-by-frame motion values were then converted into freezing scores using a binary method relative to a motion threshold (that is, motion levels above a certain threshold were classified as no freezing, whereas motion levels below a certain threshold were classified as freezing). The time that animals spent in the port was subtracted from the freezing quantification, as animals showed little motion while collecting sucrose.

***In vivo* single-unit electrophysiology.** Extracellular single-unit recordings were performed using in-house-built multichannel electrodes. An electrode consisted of a 10 × 2 pin connector (Mill-Max Manufacturing Corp) that accommodated 16 microwires for single-unit recordings, an extra microwire for analog reference and a low-resistance 200-µm silver wire to provide ground (A-M Systems). A 22.9-µm HML-insulated nichrome microwire was used (Stablohm 675, California Fine Wire). A 26-Ga stainless steel cannula was attached to one of the electrode pins to insert the microwire bundle. Microwires were secured to the connector pins using a silver print coating (GC Electronics). After testing for short circuits, all connections were secured using dental acrylic. Final cutting of the microwire tips was performed using serrated fine scissors (Fine Science Tools). The microwire tips were gold-plated to reduce impedance and improve the signal-to-noise ratio[54]. Gold plating was achieved by submerging the electrode tips in a solution containing equal parts of a non-cyanide gold solution (SIFCO Selective Plating) and a 1 mg/mL polyethylene glycol solution (Sigma-Aldrich). A cathodal electric current of 1 µA was then applied until the impedance of each channel was reduced to ~200–300 kΩ.

Extracellular waveforms exceeding a voltage threshold were band-pass filtered (500–5,000 Hz) and digitized at 25 kHz using a multichannel extracellular recording workstation (Tucker-Davis Technologies). Rats were habituated to the recording tethers before experiments by connecting them multiple times (~30 min/d) while the experimenters adjusted the voltage thresholds to isolate stable single units. During this procedure, rats also were habituated to the operant chambers. Neural activity was monitored during behavioral assessment, and the recorded waveforms were sorted offline using commercial software (Offline Sorter, Plexon Inc.). Principal components and peak–valley voltage values were assessed for each waveform and then plotted in three-dimensional feature space to define clusters formed by single units.

***In vivo* photoidentification of the BLA→PL population.** The activity of BLA cells terminating in PL (the BLA→PL population) was monitored using a combination of single-unit recordings and optogenetic tools. First, ChR2 was selectively expressed in the BLA→PL population using the Cre-dependent dual-virus strategy, in which the BLA was infused with a virus containing ChR2 in a DIO cassette ($AAV_5$-EF1α-DIO-ChR2(H134R)-eYFP) whereas PL was infused with the retrograde CAV2-Cre virus. Viral volumes of 1 µL were infused in each target using 33-Ga needles. Viral expression was allowed for ~6 months before chronically implanting an optrode (electrode containing an optical fiber for light delivery) into the BLA and a wire-bundle electrode into PL. In contrast to wire bundles, optrodes were constructed by attaching microwires around an optical fiber (Ø 300 µm, NA = 0.37; Thorlabs) that was in turn attached to the electrode connector. Microwires extended ~500 µm from the tip of the optical fiber. Photoidentification of BLA→PL cells was achieved by delivering pulses of 473-nm blue light with a power of ~25–30 mW at the tip of the optical fibers (~17–20 mW/mm$^2$ at the tip of the recording microwires). Two stimulation patterns were used: (i) 5-ms pulses at 1 Hz and (ii) 1-s pulses of constant light. These stimulation patterns were delivered in a pseudorandomly dispersed fashion with at least 20 iterations of each and with an average inter-stimulus interval of 10 s. This photoidentification procedure was conducted shortly after the recording session in which animals underwent behavioral testing.

***Ex vivo* slice electrophysiology.** *Brain tissue preparation.* BLA slices from 7 animals were examined. Approximately 6 months after transduction of the BLA with the $AAV_5$-EF1α-DIO-ChR2-eYFP viral vector and transduction of PL with the retrograde CAV2-Cre virus, rats were anesthetized with 90 mg/kg pentobarbital and perfused transcardially with 50 mL of cold (~4 °C), modified artificial cerebrospinal fluid (ACSF) containing (in mM) 75 sucrose, 87 NaCl, 2.5 KCl, 1.3 $NaH_2PO_4$, 7 $MgCl_2$, 0.5 $CaCl_2$, 25 $NaHCO_3$ and 5 ascorbic acid. The brain was then extracted and glued (Roti coll 1; Carl Roth GmbH) to the platform of a semiautomatic vibrating blade microtome (VT1200; Leica). The platform was placed in the slicing chamber containing modified ACSF at 4 °C. 300-µm coronal sections containing the BLA were collected in a holding chamber filled with ACSF saturated with 95% $O_2$ and 5% $CO_2$, containing (in mM) 126 NaCl, 2.5 KCl, 1.25 $NaH_2PO_4$, 1.0 $MgCl_2$, 2.4 $CaCl_2$, 26.0 $NaHCO_3$ and 10 glucose. Recordings were started 1 h after slicing, and the temperature was maintained at approximately 31 °C both in the holding chamber and during the recordings.

*Whole-cell patch-clamp recordings.* Recordings were made on visually identified neurons expressing eYFP. Oxygenated ACSF was perfused onto the slice with a peristaltic pump (Minipuls3; Gilson) at ~3 mL/min. Recorded cells were filled with Alexa Fluor 350 and biocytin. Voltage- and current-clamp recordings were conducted using glass microelectrodes (4–7 MΩ) molded with a horizontal puller (P-1000) and filled with a solution containing (in mM) 125 potassium gluconate, 20 HEPES, 10 NaCl, 3 Mg-ATP, 8 biocytin and 2 Alexa Fluor 350 (pH 7.33; 287 mOsm). Recorded signals were amplified using a MultiClamp 700B amplifier (Molecular Devices). Analog signals were digitized at 10 kHz using Digidata 1440 and recorded using the pClamp10 software (Molecular Devices).

After opening the cell membrane, neurons were confirmed to express ChR2 if they showed a constant inward current in voltage clamp in response to a 1-s constant blue light pulse, with a light power density of 84 mW/mm$^2$ (20 mW with a 40× objective) delivered via a 470-nm LED light source. From the 30 recorded neurons, 6 were confirmed to express ChR2. The remaining 24 neurons were confirmed to not express ChR2 nor to receive inputs from nearby ChR2 neurons, as they did not respond to the light stimulus. Cell bodies for the 24 neighboring cells were located at least 150 µm from the cell bodies of ChR2-expressing neurons.

After categorizing the cells as ChR2-expressing or nonexpressing, we recorded the photoresponse of the expressing neurons in current clamp. The six ChR2$^+$ neurons received 5-ms single pulses delivered every 10 s and 20-s trains of 5-ms pulses at 1 Hz at increasing light power density until a maximum of 84 mW/mm$^2$ (20 mW with a 40× objective). The location within the BLA of all recorded neurons was confirmed after the recording. Colocalization of Alexa Fluor 350 and eYFP was confirmed for the six ChR2$^+$ neurons.

*Latency of photoresponses.* Offline analysis was performed using Clampfit software (Molecular Devices). Light-evoked latencies of action potentials were measured during 40 light stimulations delivered at 1 Hz (5-ms pulses; two individual 20-pulse trains). Latencies were measured from the onset of the light pulse to the peak of the action potential.

**Histology.** Rats were euthanized with sodium pentobarbital (150 mg/kg) and microlesions were produced at the recording sites by passing an anodal electrical current (20 s at ~25–35 µA on at least four channels). Rats were transcardially perfused with ice-cold phosphate buffer saline (PBS) and 4% paraformaldehyde (PFA, pH 7.3). Brains were collected and fixed in 4% PFA for 24 h and equilibrated in 30% sucrose for 48 h. Coronal sections were cut at 60 µm using a microtome (HM430, Thermo Fisher Scientific).

Brain sections containing the BLA and PL were incubated for 30 min in a DNA-specific fluorescent probe (DAPI: 4′,6-diamidino-2-phenylindole; 1:50,000 dilution). After four washes in PBS (10 min each), sections were mounted on microscope slides using fluorescence-compatible PVD-DABCO medium. Confocal images were acquired with an Olympus FV1000 confocal laser-scanning microscope, using a 10×, 0.40 NA or 40×, 1.30 NA oil immersion objective.




doi:10.1038/nn.4553

Image stitches and serial *z*-stacks were assembled with commercial imaging software (Fluoview, Olympus). Expression of eYFP and DAPI was examined in sections containing various anterior–posterior coronal levels of the BLA and PL. Microlesions were examined on confocal images and reconstructed onto coronal drawings adapted from a rat brain atlas[55].

**Statistical analyses.** All statistical analyses were based on two-tailed comparisons and were performed using GraphPad Prism (GraphPad Software, Inc.), unless otherwise specified. Although no statistical tests were used to predetermine sample sizes, our sample sizes are consistent with previous publications[56–58]. All data met the assumptions of every statistical tests used. The Kolmogorov–Smirnov normality test was used to determine whether data sets required parametric or non-parametric statistical tests.

*Randomization and blinding.* For behavioral training, the counterbalanced auditory and visual CSs were randomly assigned to animals. Pseudorandom trial sequences were generated to deliver CS-Suc, CS-Shock, CS–, competition, laser-off and laser-on trials. All animals received the same trial and laser sequences in any given experiment. Viral treatments for optogenetic and chemogenetic experiments were randomly assigned to animals. For the pharmacology experiment, the vehicle and drug treatments were randomly assign during the initial test session, whereas they were counterbalanced during the second test session. Although blinding was not performed, behavioral testing was controlled by software and data analyses were performed using customized automated methods whenever possible. In addition, all experiments were designed with appropriate internal controls (for example, within-subject comparisons of laser-off versus laser-on trials, within-subject comparisons of CS-Suc versus CS-Shock trials, etc.).

*Exclusion of animals, cells or data points.* Several animals were excluded from this study due to either electrode misplacement ($n$ = 2 animals), lack of viral expression ($n$ = 5 animals), viral leakage ($n$ = 2 animals) or breakage or misplacement of optical fibers ($n$ = 3 animals). Several cells were also excluded from this study (BLA: $n$ = 22 cells, PL: $n$ = 23 cells) due to repetitions across channels. In addition, for cross-correlation analyses, we excluded cells that fired at low frequencies (<0.1 Hz), which typically produce unpopulated correlograms with spurious peaks and troughs. One data point was excluded from the decoding analysis as it was detected by the Grubbs' test as a statistically significant outlier.

*Behavioral data.* Pearson's correlation test was used on a subset of freezing data to determine whether our automated quantification method provided reliable values compared to hand-scoring (d.f. = 58; $R$ = 0.989; $P$ < 0.0001; $n$ = 60 trials including CS-Suc, CS-Shock and competition; $n$ = 3 animals). For the initial behavioral experiments, within-subject comparisons of port and freezing data across distinct CSs were performed using either paired $t$-test (in the case of two conditions) or one-way analysis of variance (ANOVA) with repeated-measures and Bonferroni *post hoc* tests (in the case of three or more conditions). For optogenetic and chemogenetic experiments, normalizations were performed to port entry and freezing data by calculating the difference between experimental conditions (% time values were used for the subtractions). For instance, the percentage of time that animals spent performing either of the behaviors during laser-off trials was subtracted from laser-on trials (that is, laser-on minus laser-off). Similarly, values obtained during the first test session in the chemogenetic experiment were subtracted from values obtained during subsequent sessions (for example, CNO minus Veh1). Statistical comparisons between groups were performed using two-way ANOVA with repeated measures and Bonferroni *post hoc* tests.

*Quality of cluster sorting.* Single units were considered for analysis if clusters met two sorting quality statistical parameters: (i) multivariate analysis of variance (MANOVA; probability threshold for significance was set to $P$ < 0.01), which indicated that each cluster was positioned at a statistically different feature space location at any given feature space; and (ii) the non-parametric J3 statistic, which measured the ratio of between-cluster to within-cluster scatter. These cluster statistics were examined using Offline Sorter (Plexon Inc.). To avoid duplicates across channels, autocorrelograms and cross-correlograms of simultaneously recorded units were inspected using Neuroexplorer (NEX Technologies).

*Putative principal cells and interneurons.* Using a hierarchical clustering method, BLA and PL cells were separated into putative principal neurons versus interneurons based on spike width and firing frequency[59,60]. Three parameters were used: (i) duration of the depolarization phase at half amplitude, (ii) duration of the hyperpolarization phase at half amplitude and (iii) the average firing frequency during the entire recording session.

*Cross-correlations.* Cross-correlations (CCs) were assessed to examine whether BLA and PL cells exhibited different patterns of functional interactions during distinct task epochs. Analyses for CCs were performed using a combination of tools in Neuroexplorer (NEX Technologies), Matlab (MathWorks) and R (R Core Team; https://www.R-project.org/). CCs were examined during various task epochs: (i) ITI, (ii) CS-Suc, (iii) CS-Shock, (iv) CS– and (v) competition. The ITI epochs were pseudorandomly generated such that they matched the number of CS epochs in any given recording session and such that the ITI epochs were at least 5 s away from any CS epoch. To generate CCs, the BLA spikes were used as the reference events and the PL spikes were used as the target events. CCs were generated for a window of ±1,000 ms relative to the reference spikes, using bin widths of 25 ms (ref. 61).

Two correction methods were applied to control for apparent correlations that might be due to CS-elicited covariation or nonstationary firing rates: (i) a trial-shift predictor, in which spike trains from the reference and target neurons were compared during shifted trials (19 trial shifts were applied per neural pair); and (ii) a spike-shuffle predictor, in which the spike trains of the reference neurons were repeatedly shuffled over time (100 random spike shuffles per trial were applied). The trial-shift predictor and spike-shuffle predictor correlograms were individually subtracted from the raw correlograms, and neural pairs were deemed significantly correlated if peaks or troughs reached statistical significance after application of both correction methods. The statistical significance of peaks and troughs was determined by $z$-score transformations of the corrected correlograms, relative to the average s.d. of the correlograms generated for each predictor. Significant peaks and troughs were evaluated within an experimental window of ±100 ms relative to the reference spikes, using a $z$-score criterion that was based on a two-tailed significance level of $P$ < 0.01 and that was Bonferroni-corrected for multiple comparisons (that is, eight 25-ms bins within the ±100 ms window; actual $P$ = 0.01/8 = 0.00125). The significance $P$-value of 0.00125 corresponded to $z$-score thresholds of $z$ > 3.23 for excitatory CCs or $z$ < −3.23 for inhibitory CCs. CCs had to meet these significance thresholds for both predictor corrections (trial-shifting and spike-shuffling) to be considered for further analyses.

Since 25-ms bins were too broad to detect coincident firing, zero-lag 'common-input' correlations[62] were examined from 5-ms binned correlograms with the central bin centered at zero (that is, ±2.5 ms). If the 5-ms binned correlograms exhibited peaks or troughs centered at zero, correlations were considered to be due to common input and were excluded from analyses.

The timing of peaks and troughs in the 25-ms-binned correlograms was examined to determine putative lead and lag. Excluding zero-lag cell pairs, correlations were considered to be led by BLA if peaks or troughs occurred after the BLA reference spikes (that is, within +2.5 to +100 ms in the correlograms), whereas correlations were considered to be led by PL if peaks or troughs occurred before the BLA reference spikes (that is, within −100 to −2.5 ms in the correlograms). Proportions of significantly correlated cell pairs were compared across task epochs using Bonferroni-corrected chi-square tests. Results obtained with the 25-ms-binned correlograms were confirmed using 10-ms-binned correlograms[63]. However, the narrower bins in the setting of cells with low firing rates led to highly sparse correlograms with increased variability and the potential for false positive and false negative correlations. In addition, the narrower bins failed to detect many inhibitory correlations that were detected with the wider bins, due to increased variability and floor effects, especially in the low-firing-rate cell pairs.

*CS-evoked responses.* The response of individual cells to CSs was examined using a combination of the non-parametric Wilcoxon signed-rank test (as primary) and a $z$-score test (as secondary). Given the existence of cells in both the BLA and PL that typically show either transient or prolonged responses to CSs[64–68], two signed-rank tests with 1,000 bootstraps and Bonferroni corrections were performed per CS. For transient responses, neural activity was binned in 25-ms intervals, and comparisons were made between a baseline window ranging from −1 to 0 s and an experimental window ranging from 0 to 300 ms, relative to CS onset. For prolonged responses, activity was binned in 50-ms intervals, and comparisons were made between a baseline window ranging from −2 to 0 s and an experimental window ranging from 0 to 1.5 s, relative to CS onset. The $z$-score test confirmed that the peak responses reached a certain significance threshold of either $z$ > 2.58 for excitatory responses (corresponding to $P$ < 0.01) or $z$ < −1.96 for inhibitory responses (corresponding to $P$ < 0.05). Cells that met both the Wilcoxon and $z$-score criteria were then considered CS-responsive cells. Proportions of CS-responsive populations were compared using chi-square tests with Bonferroni corrections for multiple comparisons.

*Machine learning to decode neuronal activity and predict behavior.* A machine-learning algorithm[69,70] was used to determine whether behavioral responses during competition trials could be predicted based on how individual cells responded during CS-Suc and CS-Shock trials. Neural data for individual cells was extracted for the entire 20 s of each trial (20 trials for the CS-Suc, 20 trials for the CS-Shock and 20 trials for competition). These data were then preprocessed by binning neural activity within each individual trial into 50-ms bins. Spike density estimates for each trial were then generated by convolving the binned rasters with a Gaussian kernel (s.d. of 200 ms). The dimensionality of each cell's data was further reduced using principal component analysis across all trial types[71], retaining the first four principal component scores for each trial. This procedure reduced the data from 400 data points per cell per trial (50-ms bins over 20 s) to only four data points per cell per trial. The same preprocessing steps were used for pairs of BLA and PL cells, except that the spike trains of each cell were concatenated before principal component analysis, and eight principal components were selected in total for each pair of cells. Each pair of cells was separately preprocessed using all possible combinations of simultaneously recorded cells.

The reduced, preprocessed data was then used to train a support vector machine (SVM) classifier[72,73]. The SVM classifier was trained using linear kernels (fitcsvm.m, Matlab R2015b) to determine the optimal hyperplane that separated neural activity during the CS-Suc and CS-Shock trials. The identified separating hyperplane was then used to predict behavioral responses during competition trials by classifying neuronal activity as 'more CS-Suc-like' or 'more CS-Shock-like' on a trial-by-trial basis. Cross-validation was not necessary, as data from the competition trials were never used to train the classifier but only used to test it. The predicted classification was compared to the actual behavioral output of the animal to determine whether the prediction was correct or incorrect. The decoding accuracy for a given cell or cell pair was calculated as the percentage of competition trials in which the predicted behavioral response matched the actual response of the animal. The statistical significance of the calculated decoding accuracies were empirically determined using permutation tests, which compared the decoding accuracy for real training data to decoding accuracies obtained after scrambling the identity of the CS-Suc and CS-Shock trials 1,000 times, each time generating a permuted separating hyperplane that was used to classify the actual neural data from competition trials[74]. The decoding accuracy obtained using the hyperplane derived from the actual CS-Suc and CS-Shock neural data was compared to the permuted distribution only once; therefore, there was no need to correct for multiple comparisons. For between-population comparisons of the decoding accuracies, we used one-way ANOVA with Bonferroni *post hoc* tests. For within-population comparisons against scrambled data, we used Bonferroni-corrected paired *t*-tests.

A **Supplementary Methods Checklist** is available.

**Data and code availability.** All relevant data and code supporting the findings of this study are available from the corresponding author upon reasonable request.


51. Felix-Ortiz, A.C. *et al.* BLA to vHPC inputs modulate anxiety-related behaviors. *Neuron* **79**, 658–664 (2013).
52. Kremer, E.J., Boutin, S., Chillon, M. & Danos, O. Canine adenovirus vectors: an alternative for adenovirus-mediated gene transfer. *J. Virol.* **74**, 505–512 (2000).
53. Blanchard, R.J., Flannelly, K.J. & Blanchard, D.C. Defensive behavior of laboratory and wild *Rattus norvegicus*. *J. Comp. Psychol.* **100**, 101–107 (1986).
54. Ferguson, J.E., Boldt, C. & Redish, A.D. Creating low-impedance tetrodes by electroplating with additives. *Sens. Actuators A Phys.* **156**, 388–393 (2009).
55. Paxinos, G. & Watson, C. *The Rat Brain in Stereotaxic Coordinates* (Academic, 1998).
56. Meyer, R.M., Burgos-Robles, A., Liu, E., Correia, S.S. & Goosens, K.A. A ghrelin–growth hormone axis drives stress-induced vulnerability to enhanced fear. *Mol. Psychiatry* **19**, 1284–1294 (2014).
57. Do-Monte, F.H., Quiñones-Laracuente, K. & Quirk, G.J. A temporal shift in the circuits mediating retrieval of fear memory. *Nature* **519**, 460–463 (2015).
58. Felix-Ortiz, A.C., Burgos-Robles, A., Bhagat, N.D., Leppla, C.A. & Tye, K.M. Bidirectional modulation of anxiety-related and social behaviors by amygdala projections to the medial prefrontal cortex. *Neuroscience* **321**, 197–209 (2016).
59. Barthó, P. *et al.* Characterization of neocortical principal cells and interneurons by network interactions and extracellular features. *J. Neurophysiol.* **92**, 600–608 (2004).
60. Likhtik, E., Pelletier, J.G., Popescu, A.T. & Paré, D. Identification of basolateral amygdala projection cells and interneurons using extracellular recordings. *J. Neurophysiol.* **96**, 3257–3265 (2006).
61. Livneh, U. & Paz, R. Amygdala-prefrontal synchronization underlies resistance to extinction of aversive memories. *Neuron* **75**, 133–142 (2012).
62. Abeles, M. & Gerstein, G.L. Detecting spatiotemporal firing patterns among simultaneously recorded single neurons. *J. Neurophysiol.* **60**, 909–924 (1988).
63. Paz, R., Bauer, E.P. & Paré, D. Measuring correlations and interactions among four simultaneously recorded brain regions during learning. *J. Neurophysiol.* **101**, 2507–2515 (2009).
64. Tye, K.M. & Janak, P.H. Amygdala neurons differentially encode motivation and reinforcement. *J. Neurosci.* **27**, 3937–3945 (2007).
65. Herry, C. *et al.* Switching on and off fear by distinct neuronal circuits. *Nature* **454**, 600–606 (2008).
66. Johansen, J.P., Tarpley, J.W., LeDoux, J.E. & Blair, H.T. Neural substrates for expectation-modulated fear learning in the amygdala and periaqueductal gray. *Nat. Neurosci.* **13**, 979–986 (2010).
67. Amano, T., Duvarci, S., Popa, D. & Paré, D. The fear circuit revisited: contributions of the basal amygdala nuclei to conditioned fear. *J. Neurosci.* **31**, 15481–15489 (2011).
68. Pendyam, S. *et al.* Fear signaling in the prelimbic-amygdala circuit: a computational modeling and recording study. *J. Neurophysiol.* **110**, 844–861 (2013).
69. Hastie, T., Tibshirani, R. & Friedman, J. *The Elements of Statistical Learning: Data Mining, Inference, and Prediction* 2nd edn. (Springer, 2011).
70. Narayanan, N.S. & Laubach, M. Methods for studying functional interactions among neuronal populations. *Methods Mol. Biol.* **489**, 135–165 (2009).
71. Richmond, B.J. & Optican, L.M. Temporal encoding of two-dimensional patterns by single units in primate inferior temporal cortex. II. Quantification of response waveform. *J. Neurophysiol.* **57**, 147–161 (1987).
72. Cristianini, N. & Shawe-Taylor, J. *An Introduction to Support Vector Machines and Other Kernel-based Learning Methods* (Cambridge Univ. Press, 2000).
73. Schlkopf, B. & Smola, A.J. *Learning with Kernels: Support Vector Machines, Regularization, Optimization, and Beyond* (MIT Press, 2001).
74. Good, P.I. *Permutation, Parametric, and Bootstrap Tests of Hypotheses* (Springer, 2005).





doi:10.1038/nn.4553

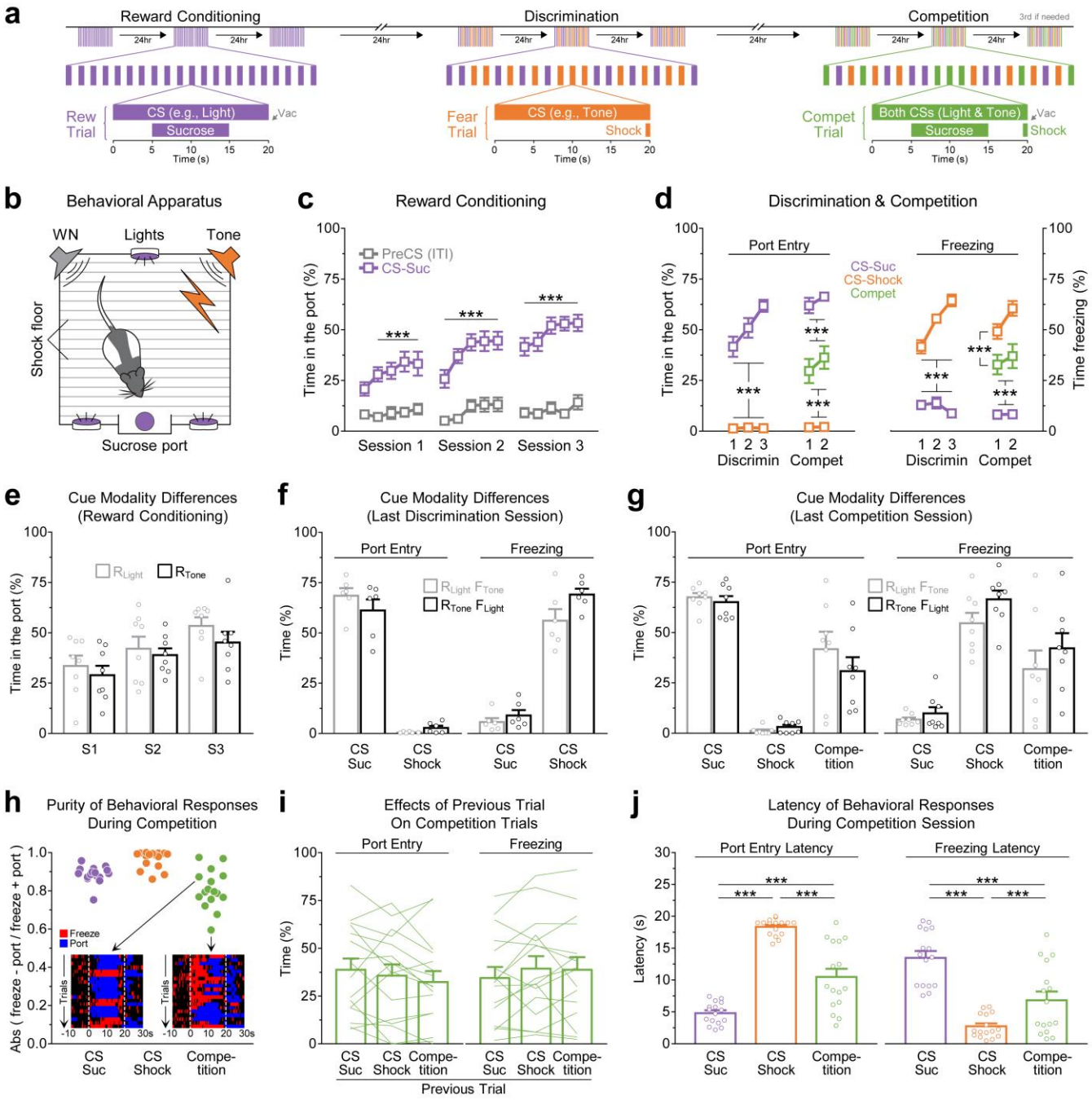


**Supplementary Figure 1**

**Progression of port entry and freezing responses across training.**

Related to Figure 1. **(a-b)** Training timeline and behavioral apparatus. Sensory modalities for the sucrose- and shock-predictive cues (conditioned stimuli, CSs) were counterbalanced across animals. During competition trials, the CS-Suc and CS-Shock associations were co-presented to induce conflicting motivational drives and competition between the reward- and fear-related behaviors. **(c)** Progression of port entry responses during reward conditioning, plotted in blocks of five trials (repeated measures two-way ANOVA with Bonferroni post-hoc tests, epoch x trial-block interaction, $F_{14,448} = 5.36$, $P < 0.001$; $t_{14} > 4.16$, ***$P < 0.001$). **(d)** Progression of port entry and freezing responses during the discrimination and competition sessions, plotted as session-blocks (trial-type x training-session interactions; port entry during discrimination, $F_{2,60} = 21.4$, $P < 0.001$; freezing during discrimination, $F_{2,60} = 23.4$, $P < 0.001$; port entry during competition, $F_{1,30} = 1.68$, $P = 0.20$; freezing during competition, $F_{1,30} = 7.37$, $P = 0.011$; Bonferroni post-hoc tests, $t_{14} > 3.89$, ***$P$

< 0.001). **(e-g)** Effects of cue modality on behavioral performance. Superimposed dots represent individual subjects. No significant statistical differences were detected between animals that were trained with the light cue for the reward association and the tone cue for the fear association ($R_{Light}$ $F_{Tone}$: $n$ = 8 animals), or vice versa ($R_{Tone}$ $F_{Light}$: $n$ = 8 animals) (Reward Conditioning: two-way repeated measures ANOVA, group x training-session interaction, $F_{2,28}$ = 0.57, $P$ = 0.57) (Discrimination Session: Bonferroni-corrected unpaired T-Tests, all $t_{14}$ < 1.71, all $P$ > 0.11) (Competition Session: Bonferroni-corrected unpaired T-Tests, all $t_{14}$ < 1.61, all $P$ > 0.13). **(h)** Purity of behavioral responses across trial types during the last competition session. Dots represent individual animals. Values closer to "1" indicate that animals tended to solely perform a behavioral response type (either port entry or freezing) during each trial (*see inset heatmap on the left*). Values away from "1" indicate that animals tended to perform behavioral transitions (from freezing to port entry, or vice versa) within single trials (*see inset heatmap on the right*). **(i)** Effects of previous trial on behavioral output during competition trials. Connecting lines represent individual subjects. No significant differences were detected (repeated measures one-way ANOVA: port entries, $F_{2,15}$ = 1.81, $P$ = 0.18; freezing, $F_{2,15}$ = 1.56, $P$ = 0.23). **(j)** Latency of port entry and freezing responses during competition. Superimposed dots represent latencies for individual subjects. Latencies were capped at 20 s, which was the maximum trial length. Significant differences were detected across trial types for port entry latencies (repeated measures one-way ANOVA with Bonferroni post-hoc tests, $F_{2,47}$ = 99.7, $P$ < 0.001; all $t_{15}$ > 5.89, all ***$P$ < 0.001) and freezing latencies ($F_{2,47}$ = 64.6, $P$ < 0.001; all $t_{15}$ > 4.29, all ***$P$ < 0.001). In all data panels, error bars represent s.e.m.

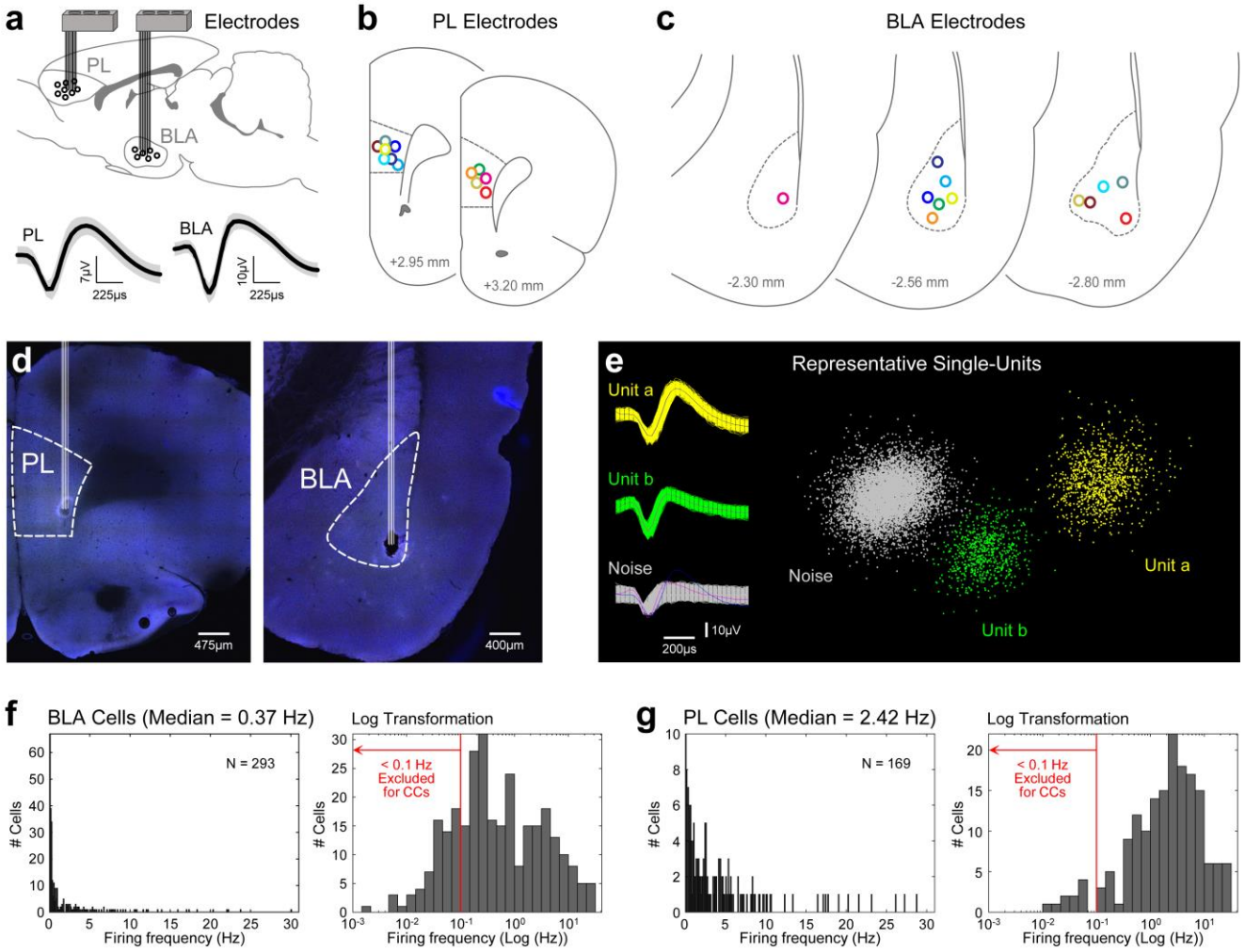


**Supplementary Figure 2**

**Histological reconstruction of neural recording sites in the BLA and PL.**

Related to Figures 2, 3, 4, and 5. **(a-c)** Electrodes were chronically implanted in both the BLA and PL for simultaneous single-unit recordings. Error bands for the representative waveforms represent s.d. Circles of matching colors in the coronal drawings correspond to the same animal. **(d)** Representative confocal images show the recording sites for one animal. **(e)** Representative waveforms and clusters from well-isolated cells. Waveforms are illustrated in a superimposed manner for each cluster. Clusters are shown in three-dimensional principal component space. **(f-g)** Distribution of firing frequencies for the BLA and PL cells. Red lines indicate the cutoffs used to exclude low firing rate cells (<0.1 Hz) from the cross-correlation analyses, as cells with such firing rates typically produce unpopulated correlograms with spurious peaks that may result on false positive correlations.

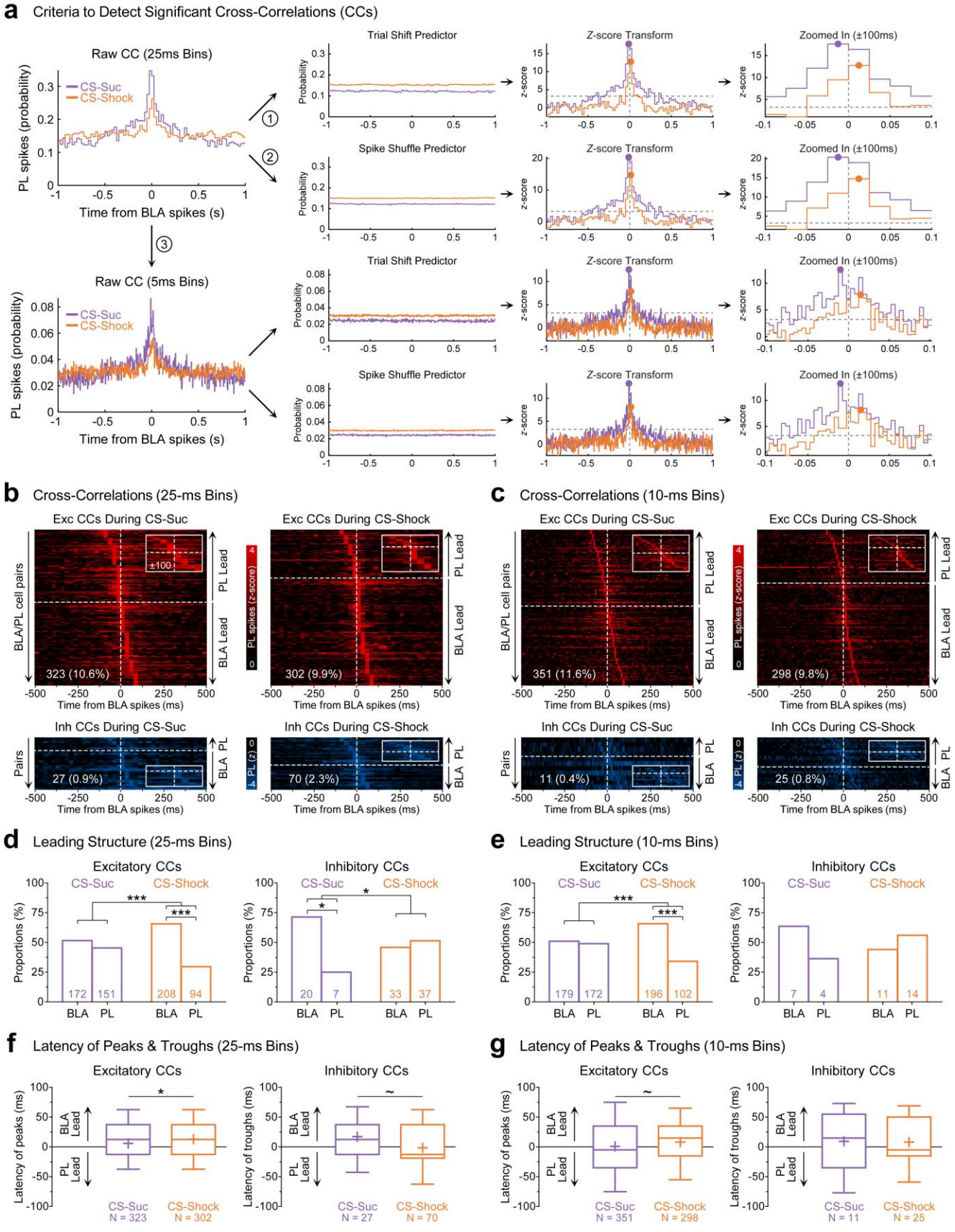


Nature Neuroscience: doi:10.1038/nn.4553

**Supplementary Figure 3**

**Criteria used for the detection of significant correlations between the BLA and PL cells, and side-by-side results with multiple time bin sizes.**

Related to Figure 2. **(a)** Cross-correlograms were calculated using 25-ms time bins, they were then corrected using two different predictor methods (trial shifting and spike shuffling) to eliminate confounds produced by CS-elicited changes in firing frequency, and they were then *z*-score transformed to detect significant peaks or troughs. **(a1)** Correction by shifting trials (repeated 19 times per trial type). **(a2)** Correction by shuffling spike trains (repeated 100 times per trial type). **(a3)** Repetition of the analysis using 5-ms time bins to detect and exclude "zero-lag correlations" (i.e., peaks or troughs that are centered at zero, ±2.5 ms), which typically result from common input-induced comodulation. The resulting correlograms from the shift and shuffle predictors (second column) were subtracted from the raw correlograms (first column), and the difference was *z*-score transformed (third column; zoomed in on the fourth column) to detect significant peaks or troughs within the time window of interest (±100 ms). Peaks or troughs were required to reach a *z*-value threshold (indicated by dashed horizontal lines) that was calculated based on a *P*-level of <0.01 (corrected for two-tail comparisons and Bonferroni-corrected for multiple comparisons). Significant peaks in these representative correlograms are indicated with colored dots for each trial type. To classify neural pairs as significantly correlated, peaks or troughs were required to exceed the significance threshold after correcting with both predictor correctors (trial-shifting and spike shuffling), and do not show "zero-lag" latencies in the 5-ms binned correlograms. In addition, neural pairs were classified as either "BLA led" if peaks or troughs occurred within the range of +2.5 to +100 ms, or as "PL led" if peaks or troughs occurred within the range of -100 to -2.5 ms, relative to the BLA reference spikes. **(b-c)** Side-by-side cross-correlation results using either 25-ms or 10-ms bin widths. Numbers within the heatmaps represent the proportion of significantly correlated BLA/PL neural pairs during the CS-Suc and CS-Shock trials. Inset heatmaps show zoomed in views of the time window of interest (±100 ms). **(d-e)** Lead and lag results using either 25 ms or 10 ms bins. With both bin widths, excitatory correlations were likelier to be led by the BLA during the CS-Shock trials, whereas inhibitory correlations were likelier to be led by the BLA during the CS-Suc trials. Chi-square tests for the 25-ms binned excitatory CCs: $X^2 = 29.8$ and $^{***}P < 0.001$ (BLA vs PL during the CS-Shock), $X^2 = 16.0$ and $^{***}P < 0.001$ (CS-Suc vs CS-Shock ratios). Chi-square tests for the 25-ms binned inhibitory CCs: $X^2 = 5.99$ and $^{*}P = 0.014$ (BLA vs PL during the CS-Suc), $X^2 = 5.70$ and $^{*}P = 0.017$ (CS-Suc vs CS-Shock ratios). Chi-square tests for the 10-ms binned excitatory CCs: $X^2 = 21.0$ and $^{***}P < 0.001$ (BLA vs PL during the CS-Shock), $X^2 = 14.4$ and $^{***}P < 0.001$ (CS-Suc vs CS-Shock ratios). Chi-square tests for the 10-ms binned inhibitory CCs: $X^2 = 0.67$ and $P = 0.41$ (BLA vs PL during the CS-Suc), $X^2 = 1.18$ and $P = 0.28$ (CS-Suc vs CS-Shock ratios). **(f-g)** Mean latency of peaks and troughs. Boxes represent the median and the 25$^{th}$ to 75$^{th}$ percentiles, whiskers represent the 10$^{th}$ and 90$^{th}$ percentiles, and the plus signs (+) within the boxes represent the mean latencies per event. The mean latencies for the excitatory correlations with the 25-ms bins were as follow: CS-Suc, 5.9±2.5 ms; CS-Shock, 13.0±2.4 ms (unpaired T-test: $t_{623} = 2.05$, $^{*}P = 0.041$). The mean latencies for the inhibitory correlations with the 25-ms bins were as follow: CS-Suc, 17.1±7.6 ms; CS-Shock, -1.4±5.2 ms ($t_{95} = 1.95$, $^{\sim}P = 0.055$). The mean latencies for the excitatory correlations with the 10-ms bins were as follow: CS-Suc, 2.0±2.7 ms; CS-Shock, 8.1±2.5 ms ($t_{623} = 2.05$, $^{\sim}P = 0.064$). The mean latencies for the inhibitory correlations with the 10-ms bins were as follow: CS-Suc, 9.5±15.0 ms; CS-Shock, 8.2±8.9 ms ($t_{34} = 0.08$, $P = 0.94$).

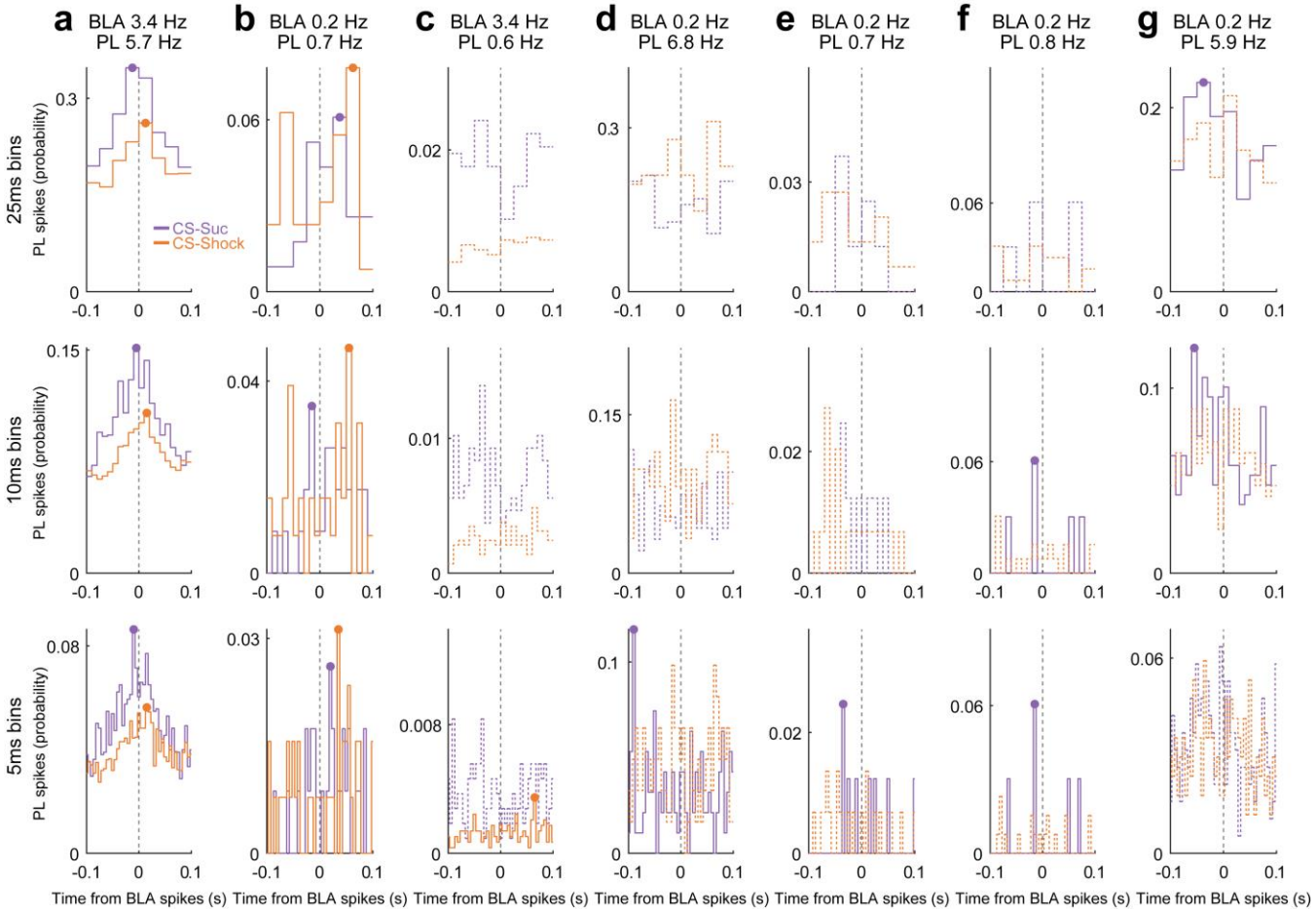


**Supplementary Figure 4**

**Representative raw cross-correlations demonstrating potential increased variability with smaller time bin widths.**

Related to Figure 2. Cross-correlations for each neural pair (individual columns) are represented in triplicate using three different bin widths: 25 ms (top row), 10 ms (middle row), and 5 ms (bottom row). Significant correlations are displayed as solid lines, and non-significant correlations are displayed as dotted lines. Significant peaks are indicated by colored dots. While these examples illustrate the y-axes as PL spike probability, the significance of each correlation was assessed using our compound criteria based on *z*-score thresholds after correcting with the trial-shifting and spike-shuffling predictors (as in **Supplementary Fig. S3a**). **(a)** Correlograms between representative BLA and PL cells with moderate firing frequencies that showed consistent peaks and lead/lag timings across all three bin widths. **(b)** Correlograms between representative BLA and PL cells with relatively low firing frequencies that showed peaks and lead/lag timings that were somewhat inconsistent across the distinct bin widths. **(c-d)** Example correlograms between representative BLA and PL cells with either low or moderate firing frequencies that exhibited spurious significant peaks when using the narrowest 5-ms bin widths, raising concerns for false positives due to the increased variability obtained with the small bins. **(e-f)** Example correlograms between representative BLA and PL cells both with relatively low firing frequencies that also showed spurious significant peaks with the smaller bin widths. These examples also raised concerns for false positives when using small bin widths due to sparse firing. **(g)** Example correlograms that represent the potential for false negatives with the 5-ms bins, which may be due to splitting of the peaks among adjacent bins, or due to the more stringent *z*-score criteria, which required additional corrections for multiple comparison in the case of the 5-ms bins compared to the wider bin widths. In summary, our dataset provided more reliable cross-correlation results when using the relatively wider bin widths (25 ms).

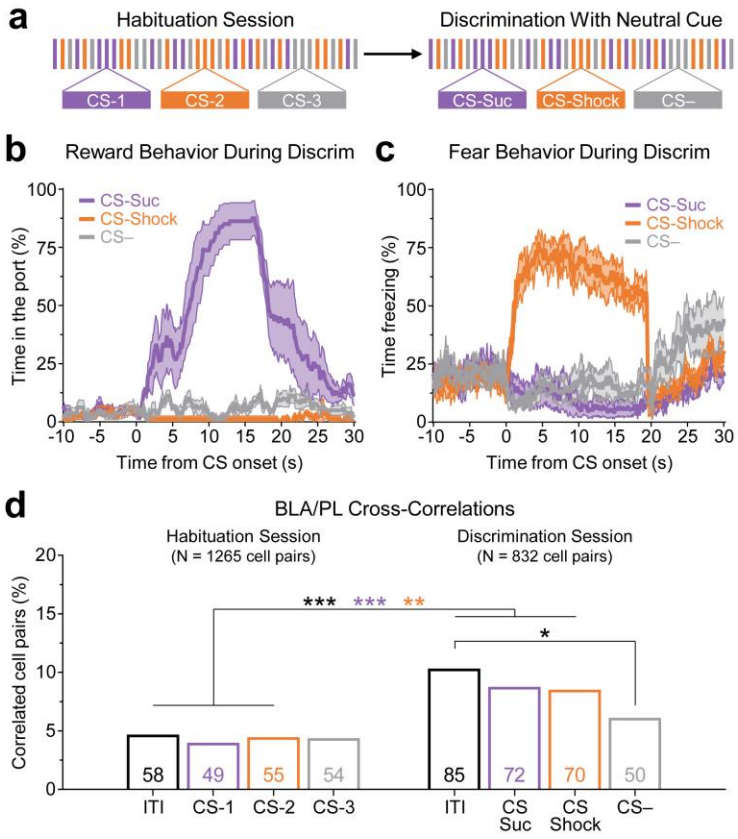


**Supplementary Figure 5**

**BLA and PL exhibited less correlated activity during a habituation session prior to the acquisition of the reward and fear memories, as well as during a neutral cue after acquiring the memories.**

Related to Figure 2. **(a)** On a subset of animals ($n$ = 4), BLA/PL recordings were performed during an initial habituation session in which three cues (light, tone, and white noise) were presented without any outcome. These cues were then paired with either sucrose, shock, or no outcome to become the CS-Suc, CS-Shock, and neutral CS–, respectively. Recordings were then performed during a discrimination session after animals acquired these associations. **(b-c)** Behavioral responses during the discrimination session. While animals showed selective port entry and freezing responses to the CS-Suc and CS-Shock, respectively, they did not display any of these behaviors during the neutral CS–. Error bands represent s.e.m. **(d)** Proportion of BLA/PL neural pairs that exhibited significantly correlated activity during either the habituation or discrimination session. Significantly higher proportions of BLA/PL neural pairs exhibited correlated activity during the discrimination session than the habituation session during all epochs, except the CS– (Bonferroni-corrected chi-square tests comparing habituation versus discrimination: ITI, $X^2$ = 21.6, ***$P$ < 0.001; CS-Suc, $X^2$ = 18.6, ***$P$ < 0.001; CS-Shock, $X^2$ = 13.0, **$P$ = 0.0012; CS–, $X^2$ = 2.91, $P$ = 0.36). In addition, during the discrimination session there were fewer correlated neural pairs during the CS– than during the other epochs (Bonferroni-corrected chi-square tests: CS– vs ITI, $X^2$ = 8.40, *$P$ = 0.015; CS– vs CS-Suc, $X^2$ = 3.7, $P$ = 0.22; CS– vs CS-Shock, $X^2$ = 3.11, $P$ = 0.31). These findings support the hypothesis that BLA/PL correlations strengthened with learning.

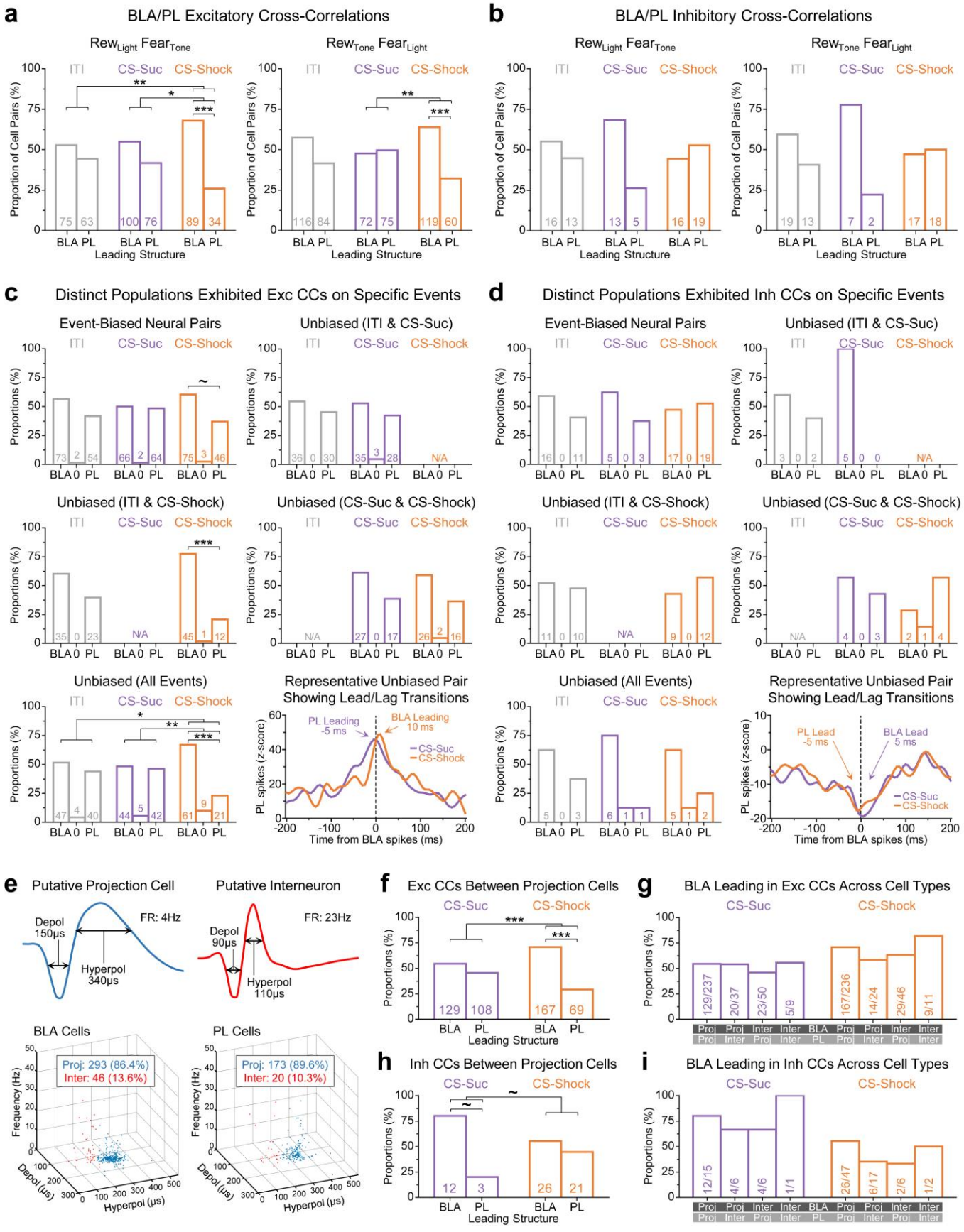


Nature Neuroscience: doi:10.1038/nn.4553

**Supplementary Figure 6**

**Variations on cross-correlation lead/lag across counterbalanced cue conditions, event-biased populations, and putative projection neurons and interneurons.**

Related to Figure 2. **(a-b)** Lead/lag comparisons between animals that received the light cue for the rewarding CS-Suc association and the tone cue for the fearful CS-Shock association ("$Rew_{Light}$ $Fear_{Tone}$", $n$ = 6 subjects), or vice versa ("$Rew_{Tone}$ $Fear_{Light}$", $n$ = 6 subjects). On both counterbalanced combinations, the BLA was still likelier to lead the excitatory correlations during the CS-Shock (Bonferroni-corrected chi-square tests: $Rew_{Light}$ $Fear_{Tone}$; BLA vs PL during CS-Shock, $X^2$ = 16.8, ***$P$ < 0.001; CS-Shock vs ITI, $X^2$ = 9.03, **$P$ = 0.008; CS-Shock vs CS-Suc, $X^2$ = 7.52, *$P$ = 0.018; $Rew_{Tone}$ $Fear_{Light}$; BLA vs PL during CS-Shock, $X^2$ = 13.1, ***$P$ < 0.001; CS-Shock vs ITI, $X^2$ = 2.88, $P$ = 0.27; CS-Shock vs CS-Suc, $X^2$ = 10.2, **$P$ = 0.004). In addition, the BLA was still likelier to lead the inhibitory correlations during the CS-Suc on both cue combinations. However, statistical comparisons for the inhibitory correlations were unreliable due to the overall low numbers. **(c-d)** Lead/lag on distinct BLA/PL pairwise populations that exhibited correlations during either specific task events ("event-biased populations") or during various task events ("unbiased populations"). While zero-lag "common-input" correlations were included in this analysis (represented in the bars as "0"), they were not considered for statistical comparisons due to the overall low numbers (Event-Biased BLA vs PL: $X^2$ = 4.66, ~$P$ = 0.087; Unbiased to ITI & CS-Shock BLA vs PL: $X^2$ = 13.2, ***$P$ < 0.001; Unbiased to All Events BLA vs PL: $X^2$ = 13.4, ***$P$ < 0.001; Unbiased to All Events CS-Shock vs ITI: $X^2$ = 7.59, *$P$ = 0.018; Unbiased to All Events CS-Shock vs CS-Suc: $X^2$ = 9.66, **$P$ = 0.006). Representative correlations in the line plots were constructed using 5-ms bins and were smoothed using a Gaussian distribution for illustration purposes. **(e-i)** Lead/lag comparisons across putative projection cells and interneurons. **(e)** BLA and PL cells were classified as putative projection cells or interneurons based on three properties: depolarization half-width, hyperpolarization half-width, and mean firing frequency. A hierarchical clustering method was used to separate cells into two populations: wide spike-width (putative projection cells; *blue dots*) or narrow spike-widths (putative interneurons; *red dots*). **(f)** Lead/lag results for the excitatory correlations after excluding putative interneurons. The BLA was still likelier to lead excitatory correlations during the CS-Shock, but not during the CS-Suc (BLA vs PL during CS-Shock: $X^2$ = 27.7, ***$P$ < 0.001; CS-Shock vs CS-Suc: $X^2$ = 13.5, ***$P$ < 0.001). **(g)** Proportion of BLA-led excitatory correlations across multiple combinations between the putative projection cells and interneurons. **(h)** Lead/lag results for the inhibitory correlations after excluding putative interneurons. The BLA was still likelier to lead more of the inhibitory correlations during the CS-Suc, but not during the CS-Shock (BLA vs PL during CS-Suc: $X^2$ = 3.75, ~$P$ = 0.053; CS-Shock vs CS-Suc: $X^2$ = 2.92, ~$P$ = 0.087). **(i)** Proportion of BLA-led inhibitory correlations across multiple combinations between the putative projection cells and interneurons.

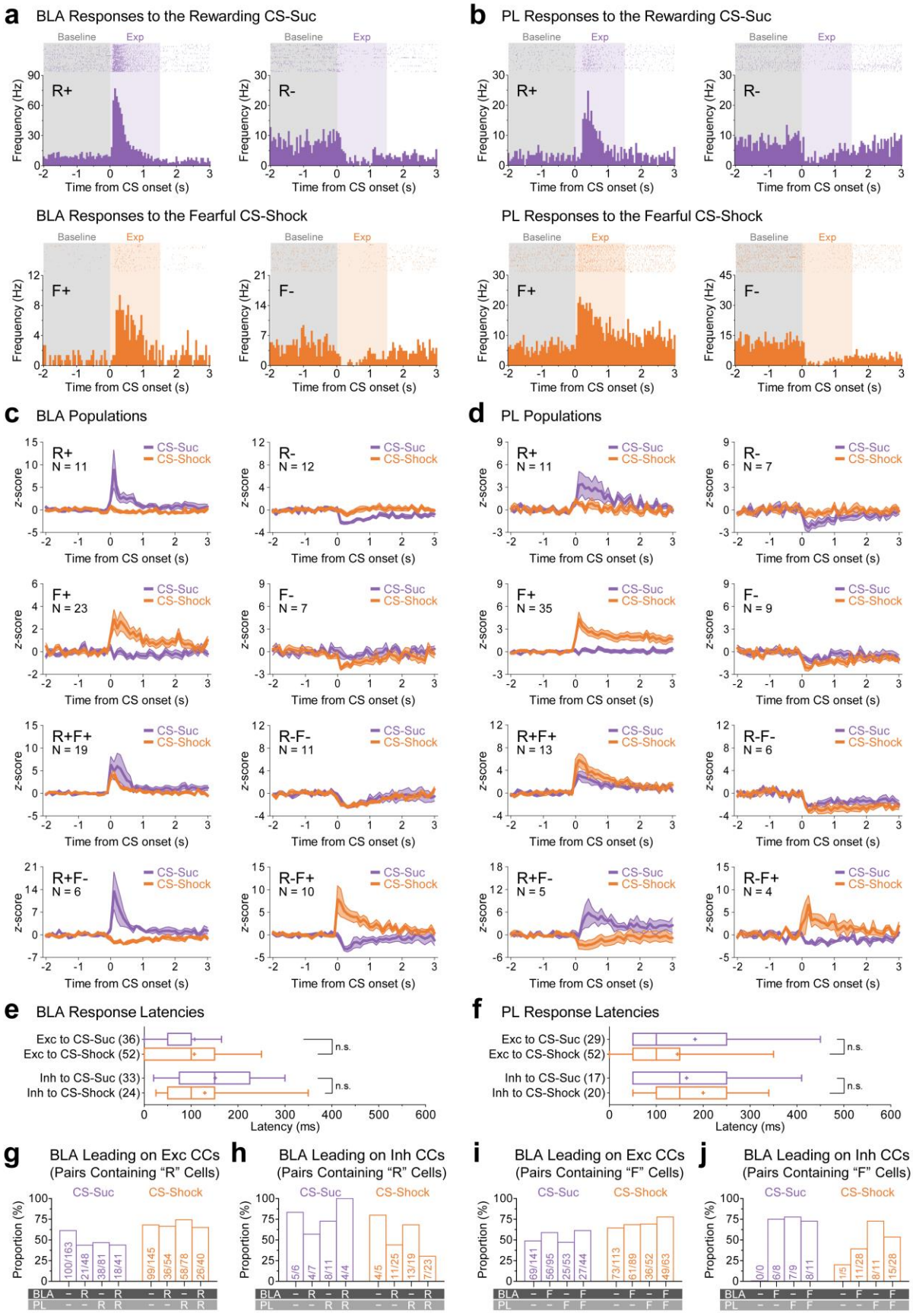


Nature Neuroscience: doi:10.1038/nn.4553

**Supplementary Figure 7**

**CS-responsive populations in the BLA and PL, and cross-correlations across responsive and nonresponsive cells during reward–fear discrimination.**

Related to Figure 3. **(a-b)** Representative BLA and PL cells exhibiting significant changes in activity during the reward- or fear-related CSs. Cells were deemed as either "R+", "R-", "F+", or "F-", respectively, if they exhibited a selective increase or decrease in activity to either of the CSs. Cells that exhibited significant responses to CSs were deemed as "R+F+", "R-F-", "R+F-", or "R-F+", respectively. **(c-d)** Mean response for each CS-responsive population in the BLA and PL. Error bands represent s.e.m. **(e-f)** Response latencies per CS. Numbers within parentheses indicate the overall number of cells that responded to each CS, with either excitation ("Exc"; increased activity) or inhibition ("Inh"; decreased activity). Boxes represent the median and the $25^{th}$ to $75^{th}$ percentiles, whiskers represent the $10^{th}$ and $90^{th}$ percentiles, and the plus signs (+) within the boxes represent the mean response latencies, using 50-ms time bins. The mean latencies obtained for the BLA cells were as follow: excitation to the CS-Suc, 108±32; excitation to the CS-Shock, 107±21; inhibition to the CS-Suc, 152±18; inhibition to the CS-Shock, 129±24. The mean latencies obtained for the PL cells were as follow: excitation to the CS-Suc, 183±32; excitation to the CS-Shock, 145±23; inhibition to the CS-Suc, 165±31; inhibition to the CS-Shock, 200±42. No significant differences were detected with the Dunn's post-hoc tests between the response latencies for the CS-Suc and CS-Shock. **(g-j)** Cross-correlation lead/lag comparisons among populations of BLA and PL cells that exhibited significant responses to the reward-related cue ("R cells") or the fear-related cue ("F cells").

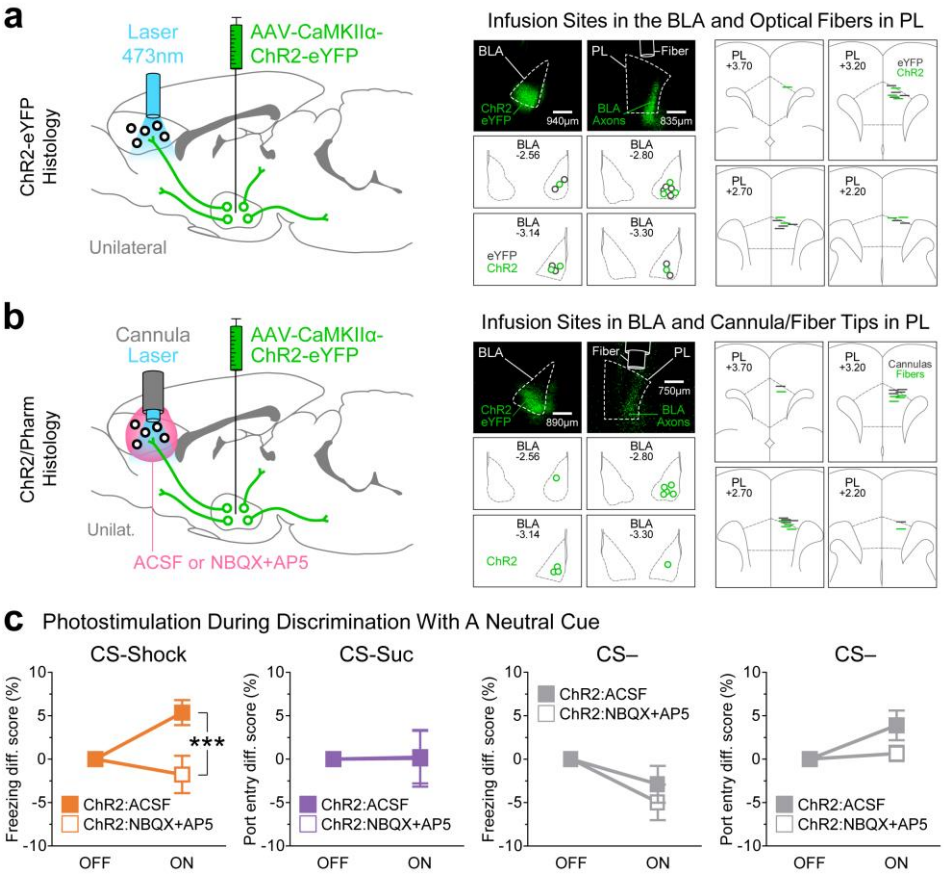


**Supplementary Figure 8**

**Histological assessment for the BLA→PL stimulation experiments and behavioral effects during a discrimination session with a neutral cue.**

Related to Figure 6. **(a)** Histological reconstruction of viral infusions and location of optical fibers (eYFP: $n$ = 10 animals; ChR2: $n$ = 8 animals). Circles in the BLA drawings represent the center of viral infusions. Dashes in the PL drawings represent the optical fiber tips. **(b)** Histology for the pharmacology experiment ($n$ = 10 animals). Dashes in the PL drawings represent the position of cannulas and optical fibers. **(c)** Photostimulation during the discrimination of a CS-Suc, CS-Shock, and a neutral cue (CS–). Animals were tested over two days shortly after infusion of either ACSF or NBQX+AP5. Difference scores are plotted relative to laser-OFF trials. A significant interaction between the drug and laser treatments was detected for freezing responses during CS-Shock trials (repeated measures two-way ANOVA with Bonferroni post-hoc tests: $F_{1,18}$ = 7.57, $P$ = 0.013; $t_{18}$ = 3.89, ***$P$ < 0.001). No significant interaction effects were detected for port entries during CS-Suc trials ($F_{1,18}$ = 0.01, $P$ = 0.97). No significant interaction effects were detected for either behavior during the CS– (freezing, $F_{1,18}$ = 0.50, $P$ = 0.49; port entry, $F_{1,18}$ = 2.84, $P$ = 0.11). Error bars represent s.e.m.

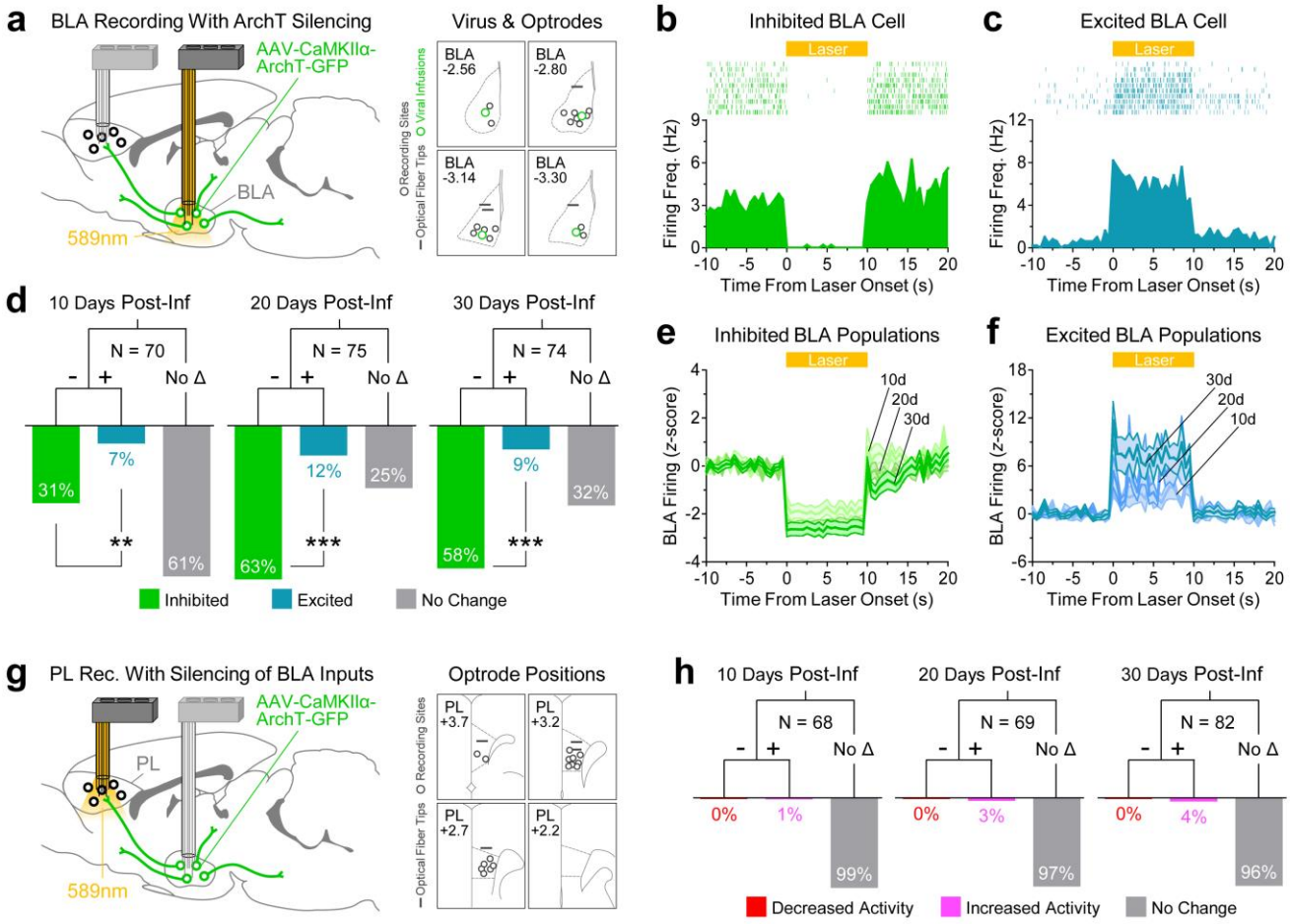


**Supplementary Figure 9**

**Validation of the ArchT viral construct and effects of optogenetically mediated inhibition of BLA inputs on the spontaneous firing of PL neurons.**

Related to Figure 7. **(a)** Single-unit activity was monitored in the BLA at several time points after viral infusion to determine whether the ArchT construct produced reliable silencing. In the coronal drawings, four recording sites are illustrated per animal ($n$ = 4 subjects), as microlesions were performed on four representative channels along the circumference of the optical fiber. **(b-c)** BLA units exhibiting ArchT-induced inhibition or excitation. **(d)** Quantification of the BLA cells that exhibited significant inhibition ("-"), excitation ("+"), or no change ("No Δ"). ArchT-induced inhibition predominated at all recording time points (chi-square tests comparing inhibited and excited populations: 10 days, $X^2$ = 9.07, $^{**}P$ = 0.003; 20 days, $X^2$ = 19.4, $^{***}P$ < 0.001; 30 days, $X^2$ = 20.0, $^{***}P$ < 0.001). **(e-f)** Population histograms for the inhibited and excited BLA cells. **(g)** Assessment of spontaneous activity in PL upon local ArchT-induced inhibition of BLA inputs. Coronal drawings show the recording sites in PL. **(h)** Quantification of the PL cells that exhibited significant changes in activity during inhibition of BLA inputs. Inhibition of BLA inputs produced sparse effects on the spontaneous activity of PL neurons (Fisher exact probability tests: 10 days, $P$ = 1.00; 20 days, $P$ = 0.50; 30 days, $P$ = 0.25). Error bands represent s.e.m.

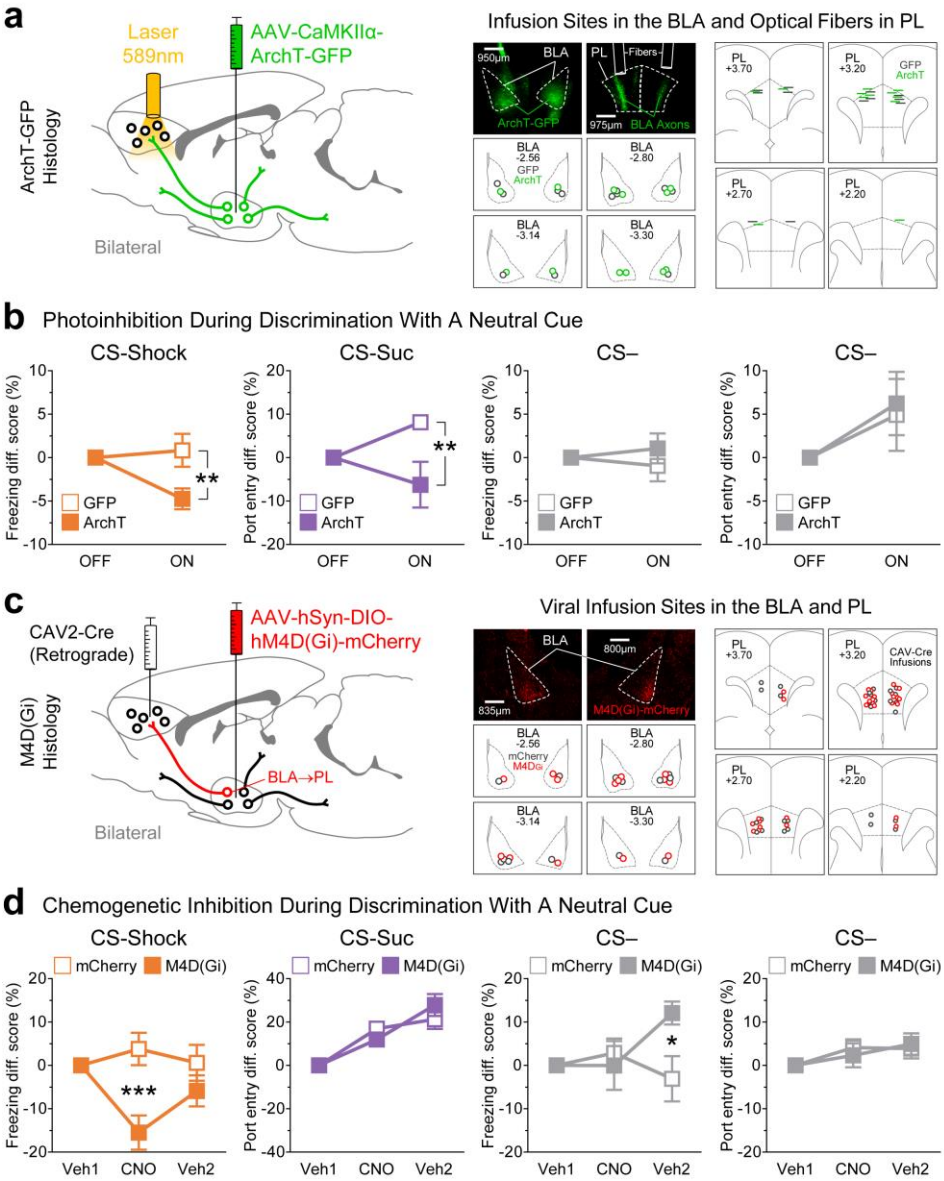


**Supplementary Figure 10**

**Histological assessment for the BLA→PL inhibition experiments and behavioral effects during discrimination sessions with a neutral cue.**

Related to Figure 7. **(a)** Histology for the optogenetic inhibition experiments (GFP: *n* = 6 animals; ArchT: *n* = 6 animals). **(b)** ArchT-mediated photoinhibition during the discrimination of a CS-Suc, CS-Shock, and a neutral cue (CS–). Difference scores are plotted relative to laser-OFF trials. A significant group x laser treatment interaction was detected for freezing responses during CS-Shock trials (repeated measures two-way ANOVA with Bonferroni post-hoc tests: $F_{1,10}$ = 6.17, $P$ = 0.032; $t_{10}$ = 3.51, **$P$ = 0.006). Significant interaction effects were also detected for port entries during CS-Suc trials ($F_{1,10}$ = 6.86, $P$ = 0.026; $t_{10}$ = 3.70, **$P$ = 0.004). No significant effects were detected for either behavior during the CS– (freezing, $F_{1,10}$ = 0.65, $P$ = 0.44; port entry, $F_{1,10}$ = 0.06, $P$ = 0.82). **(c)** Histology for the chemogenetic inhibition experiments (mCherry: *n* = 7 animals; M4D(Gi): *n* = 7 animals). CAV2-Cre infusions in PL were determined from needle tracks, and two infusion sites are illustrated per animal as the CAV2-Cre virus was infused into two dorsal-ventral PL locations to maximize tissue coverage. **(d)** Chemogenetic inhibition during the discrimination of a CS-Suc, CS-Shock, and CS–. Animals were tested over three days after systemic injections of either CNO or vehicle. Difference scores are plotted relative to the first vehicle session. A significant group x drug treatment interaction was detected for freezing during the CS-Shock ($F_{2,24}$ = 6.22, $P$ = 0.007; $t_{12}$ = 4.32, ***$P$ = 0.001). No significant interaction effects were detected for port entries during the CS-Suc ($F_{2,24}$ = 2.25, $P$ = 0.13). While a significant interaction effect was detected for freezing during the CS– ($F_{2,24}$ = 4.95, $P$ = 0.016; $t_{12}$ = 3.00, *$P$ = 0.011),

this effect was not related to the CNO treatment (group difference during CNO, $P = 0.58$). Port entry responses during the CS– were also unaffected ($F_{2,24} = 0.42$, $P = 0.66$). Error bars represent s.e.m.

nature neuroscience

Corresponding Author: Kay M. Tye

Manuscript Number: NN-A54538

Manuscript Type: Article

# Main Figures: 7

# Supplementary Figures: 10

# Supplementary Tables: 0

# Supplementary Videos: 0

# Reporting Checklist for Nature Neuroscience

This checklist is used to ensure good reporting standards and to improve the reproducibility of published results. For more information, please read Reporting Life Sciences Research.

**Please note that in the event of publication, it is mandatory that authors include all relevant methodological and statistical information in the manuscript.**

## Statistics reporting, by figure

- Please specify the following information for each panel reporting quantitative data, and where each item is reported (section, e.g. Results, & paragraph number).
- Each figure legend should ideally contain an exact sample size (n) for each experimental group/condition, where n is an exact number and not a range, a clear definition of how n is defined (for example x cells from x slices from x animals from x litters, collected over x days), a description of the statistical test used, the results of the tests, any descriptive statistics and clearly defined error bars if applicable.
- For any experiments using custom statistics, please indicate the test used and stats obtained for each experiment.
- Each figure legend should include a statement of how many times the experiment shown was replicated in the lab; the details of sample collection should be sufficiently clear so that the replicability of the experiment is obvious to the reader.
- For experiments reported in the text but not in the figures, please use the paragraph number instead of the figure number.

Note: Mean and standard deviation are not appropriate on small samples, and plotting independent data points is usually more informative. When technical replicates are reported, error and significance measures reflect the experimental variability and not the variability of the biological process; it is misleading not to state this clearly.

| | | TEST USED | | n | | | DESCRIPTIVE STATS (AVERAGE, VARIANCE) | | P VALUE | | DEGREES OF FREEDOM & F/t/z/R/ETC VALUE | |
|---|---|---|---|---|---|---|---|---|---|---|---|---|
| | FIGURE NUMBER | WHICH TEST? | SECTION & PARAGRAPH # | EXACT VALUE | DEFINED? | SECTION & PARAGRAPH # | REPORTED? | SECTION & PARAGRAPH # | EXACT VALUE | SECTION & PARAGRAPH # | VALUE | SECTION & PARAGRAPH # |
| example | 1a | one-way ANOVA | Fig. legend | 9, 9, 10, 15 | mice from at least 3 litters/group | Methods para 8 | error bars are mean +/- SEM | Fig. legend | p = 0.044 | Fig. legend | F(3, 36) = 2.97 | Fig. legend |
| example | results, para 6 | unpaired t-test | Results para 6 | 15 | slices from 10 mice | Results para 6 | error bars are mean +/- SEM | Results para 6 | p = 0.0006 | Results para 6 | t(28) = 2.808 | Results para 6 |
| + - | | | | | | | | | | | | |



Nature Neuroscience: doi:10.1038/nn.4553

| | TEST USED | | n | | | DESCRIPTIVE STATS (AVERAGE, VARIANCE) | | P VALUE | | DEGREES OF FREEDOM & F/t/z/R/ETC VALUE | |
|---|---|---|---|---|---|---|---|---|---|---|---|
| | FIGURE NUMBER | WHICH TEST? | SECTION & PARAGRAPH # | EXACT VALUE | DEFINED? | SECTION & PARAGRAPH # | REPORTED? | SECTION & PARAGRAPH # | EXACT VALUE | SECTION & PARAGRAPH # | VALUE | SECTION & PARAGRAPH # |
| + - | fig1 | paired t-test | fig1 legend | 16 | rats from 1 group | fig1 legend | error bars are mean +/- sem | fig1 legend | p<0.001 | fig1 legend | t15=20.3 | fig1 legend |
| + - | fig1 | paired t-test | fig1 legend | 16 | rats from 1 group | fig1 legend | error bars are mean +/- sem | fig1 legend | p<0.001 | fig1 legend | t15=20.6 | fig1 legend |
| + - | fig1 | repeated measures ANOVA | fig1 legend | 16 | rats from 1 group | fig1 legend | error bars are mean +/- sem | fig1 legend | p<0.001 | fig1 legend | f2,30=107.6 | fig1 legend |
| + - | fig1 | repeated measures ANOVA | fig1 legend | 16 | rats from 1 group | fig1 legend | error bars are mean +/- sem | fig1 legend | p<0.001 | fig1 legend | f2,30=89.0 | fig1 legend |
| + - | fig2 | Bonferroni-corrected chi-square test | fig2 legend | 344 | pairs of neurons | fig2g | fractions | fig2g | p=0.14 | fig2 legend | X2 = 3.83 | fig2 legend |
| + - | fig2 | Bonferroni-corrected chi-square test | fig2 legend | 333 | pairs of neurons | fig2g | fractions | fig2g | p=0.71 | fig2 legend | X2 = 0.91 | fig2 legend |
| + - | fig2 | Bonferroni-corrected chi-square test | fig2 legend | 317 | pairs of neurons | fig2g | fractions | fig2g | p<0.001 | fig2 legend | X2 = 29.2 | fig2 legend |
| + - | fig2 | Bonferroni-corrected chi-square test | fig2 legend | 344+333 | pairs of neurons | fig2g | fractions | fig2g | p=0.78 | fig2 legend | X2 = 0.71 | fig2 legend |
| + - | fig2 | Bonferroni-corrected chi-square test | fig2 legend | 344+317 | pairs of neurons | fig2g | fractions | fig2g | p=0.004 | fig2 legend | X2 = 10.4 | fig2 legend |
| + - | fig2 | Bonferroni-corrected chi-square test | fig2 legend | 333+317 | pairs of neurons | fig2g | fractions | fig2g | p<0.001 | fig2 legend | X2 = 16.0 | fig2 legend |
| + - | fig2 | Bonferroni-corrected chi-square test | fig2 legend | 61 | pairs of neurons | fig2h | fractions | fig2h | p=0.72 | fig2 legend | X2 = 0.89 | fig2 legend |
| + - | fig2 | Bonferroni-corrected chi-square test | fig2 legend | 28 | pairs of neurons | fig2h | fractions | fig2h | p=0.11 | fig2 legend | X2 = 4.28 | fig2 legend |
| + - | fig2 | Bonferroni-corrected chi-square test | fig2 legend | 72 | pairs of neurons | fig2h | fractions | fig2h | p=0.97 | fig2 legend | X2 = 0.15 | fig2 legend |
| + - | fig2 | Bonferroni-corrected chi-square test | fig2 legend | 61+28 | pairs of neurons | fig2h | fractions | fig2h | p=0.35 | fig2 legend | X2 = 2.33 | fig2 legend |
| + - | fig2 | Bonferroni-corrected chi-square test | fig2 legend | 61+72 | pairs of neurons | fig2h | fractions | fig2h | p=0.56 | fig2 legend | X2 = 1.37 | fig2 legend |





Nature Neuroscience: doi:10.1038/nn.4553

| | | | | | | | | | | | | |
|---|---|---|---|---|---|---|---|---|---|---|---|---|
| + - | fig2 | Bonferroni-corrected chi-square test | fig2 legend | 28+72 | pairs of neurons | fig2h | fractions | fig2h | p=0.05 | fig2 legend | X2 = 5.70 | fig2 legend |
| + - | fig3 | Bonferroni-corrected chi-square test | fig3 legend | 293 | neurons | fig3a | percents | fig3a | p>0.056 | fig3 legend | X2 < 9.50 | fig3 legend |
| + - | fig3 | paired t-test | fig3 legend | 12 | rats | fig3 legend | error bars are mean +/- sem | fig3c | p=0.56 | fig3 legend | t11=0.61 | fig3 legend |
| + - | fig3 | repeated measures 2-way ANOVA | fig3 legend | 12 | rats | fig3a | error bars are mean +/- sem | fig3d | p=0.91 | fig3 legend | F1,22=0.01 | fig3 legend |
| + - | fig3 | repeated measures 2-way ANOVA | fig3 legend | 12 | rats | fig3a | error bars are mean +/- sem | fig3d | p=0.24 | fig3 legend | F1,22=1.48 | fig3 legend |
| + - | fig3 | repeated measures 2-way ANOVA | fig3 legend | 12 | rats | fig3a | error bars are mean +/- sem | fig3d | p=0.85 | fig3 legend | F1,22=0.04 | fig3 legend |
| + - | fig3 | Bonferroni-corrected chi-square test | fig3 legend | 12 | rats | fig3 legend | percents | fig3 legend | p<0.024 | fig3 legend | X2 < 11.06 | fig3 legend |
| + - | fig3 | Bonferroni-corrected chi-square test | fig3 legend | 12 | rats | fig3 legend | percents | fig3 legend | p=0.079 | fig3 legend | X2 = 8.86 | fig3 legend |
| + - | fig3 | paired t-test | fig3 legend | 12 | rats | fig3 legend | error bars are mean +/- sem | fig3 legend | p=0.011 | fig3 legend | t11=3.03 | fig3 legend |
| + - | fig3 | repeated measures 2-way ANOVA | fig3 legend | 12 | rats | fig3a | error bars are mean +/- sem | fig3h | p=0.0013 | fig3 legend | F1,22=13.5 | fig3 legend |
| + - | fig3 | repeated measures 2-way ANOVA | fig3 legend | 12 | rats | fig3a | error bars are mean +/- sem | fig3h | p=0.069 | fig3 legend | F1,22=3.66 | fig3 legend |
| + - | fig3 | repeated measures 2-way ANOVA | fig3 legend | 12 | rats | fig3a | error bars are mean +/- sem | fig3h | p=0.28 | fig3 legend | F1,22=1.23 | fig3 legend |
| + - | fig3 | Bonferroni post-hoc test | fig3 legend | 12 | rats | fig3 legend | error bars are mean +/- sem | fig3 legend | p=0.0026 | fig3 legend | t11=3.32 | fig3 legend |
| + - | fig3 | Bonferroni post-hoc test | fig3 legend | 12 | rats | fig3 legend | error bars are mean +/- sem | fig3 legend | p<0.001 | fig3 legend | t11=3.73 | fig3 legend |
| + - | fig5 | paired t-test | fig5 legend | 8 | neurons | fig5 legend | error bars are mean +/- sem | fig5e | p=0.013 | fig5 legend | t7=3.31 | fig5 legend |
| + - | fig5 | paired t-test | fig5 legend | 8 | neurons | fig5 legend | error bars are mean +/- sem | fig5e | p=0.007 | fig5 legend | t7=3.74 | fig5 legend |
| + - | fig5 | paired t-test | fig5 legend | 41 | neurons | fig5 legend | error bars are mean +/- sem | fig5e | p=0.028 | fig5 legend | t40=2.29 | fig5 legend |
| + - | fig5 | one-way ANOVA | fig5 legend | 57 | neurons | fig5 legend | error bars are mean +/- sem | fig5e | p=0.042 | fig5 legend | F2,54=3.36 | fig5 legend |
| + - | fig5 | Bonferroni post-hoc test | fig5 legend | 8+41 | neurons | fig5 legend | error bars are mean +/- sem | fig5e | p=0.017 | fig5 legend | t47=2.47 | fig5 legend |
| + - | fig5 | Bonferroni post-hoc test | fig5 legend | 8+41 | neurons | fig5 legend | error bars are mean +/- sem | fig5e | p=0.23 | fig5 legend | t47=1.22 | fig5 legend |
| + - | fig5 | paired t-test | fig5 legend | 39 | pairs of neurons | fig5f | error bars are mean +/- sem | fig5f | p=0.006 | fig5 legend | t38=2.91 | fig5 legend |
| + - | fig5 | paired t-test | fig5 legend | 39 | pairs of neurons | fig5f | error bars are mean +/- sem | fig5f | p<0.001 | fig5 legend | t38=6.76 | fig5 legend |
| + - | fig5 | paired t-test | fig5 legend | 33 | pairs of neurons | fig5f | error bars are mean +/- sem | fig5f | p<0.001 | fig5 legend | t32=5.87 | fig5 legend |







Nature Neuroscience: doi:10.1038/nn.4553

| | | | | | | | | | | | | |
|---|---|---|---|---|---|---|---|---|---|---|---|---|
| + - | fig5 | paired t-test | fig5 legend | 69 | pairs of neurons | fig5f | error bars are mean +/- sem | fig5f | p<0.001 | fig5 legend | t68=10.5 | fig5 legend |
| + - | fig5 | paired t-test | fig5 legend | 285 | pairs of neurons | fig5f | error bars are mean +/- sem | fig5f | p<0.001 | fig5 legend | t284=8.36 | fig5 legend |
| + - | fig5 | paired t-test | fig5 legend | 125 | pairs of neurons | fig5f | error bars are mean +/- sem | fig5f | p<0.001 | fig5 legend | t124=4.24 | fig5 legend |
| + - | fig5 | one-way ANOVA | fig5 legend | 590 | pairs of neurons | fig5 legend | error bars are mean +/- sem | fig5f | p<0.001 | fig5 legend | F5,584=11.1 | fig5 legend |
| + - | fig5 | Bonferroni post-hoc test | fig5 legend | 39+39 | pairs of neurons | fig5 legend | error bars are mean +/- sem | fig5f | p=0.011 | fig5 legend | t76=2.64 | fig5 legend |
| + - | fig5 | Bonferroni post-hoc test | fig5 legend | 33+69 | pairs of neurons | fig5 legend | error bars are mean +/- sem | fig5f | p=0.50 | fig5 legend | t100=0.68 | fig5 legend |
| + - | fig5 | Bonferroni post-hoc test | fig5 legend | 285+125 | pairs of neurons | fig5 legend | error bars are mean +/- sem | fig5f | p=0.24 | fig5 legend | t408=1.18 | fig5 legend |
| + - | fig6 | repeated measures 2-way ANOVA | fig6 legend | 10+8 | rats | fig6 legend | error bars are mean +/- sem | fig6c | p=0.004 | fig6 legend | F1,16=11.4 | fig6 legend |
| + - | fig6 | repeated measures 2-way ANOVA | fig6 legend | 10+8 | rats | fig6 legend | error bars are mean +/- sem | fig6c | p=0.11 | fig6 legend | F1,16=2.88 | fig6 legend |
| + - | fig6 | repeated measures 2-way ANOVA | fig6 legend | 10+8 | rats | fig6 legend | error bars are mean +/- sem | fig6c | p=0.004 | fig6 legend | F1,16=11.4 | fig6 legend |
| + - | fig6 | ANOVA post-hoc test | fig6 legend | 10+8 | rats | fig6 legend | error bars are mean +/- sem | fig6c | p=0.0002 | fig6 legend | t16=4.78 | fig6 legend |
| + - | fig6 | repeated measures 2-way ANOVA | fig6 legend | 10+8 | rats | fig6 legend | error bars are mean +/- sem | fig6d | p=0.34 | fig6 legend | F1,16=0.95 | fig6 legend |
| + - | fig6 | repeated measures 2-way ANOVA | fig6 legend | 10+8 | rats | fig6 legend | error bars are mean +/- sem | fig6d | p=0.72 | fig6 legend | F1,16=0.13 | fig6 legend |
| + - | fig6 | repeated measures 2-way ANOVA | fig6 legend | 10+8 | rats | fig6 legend | error bars are mean +/- sem | fig6d | p=0.34 | fig6 legend | F1,16=0.95 | fig6 legend |
| + - | fig6 | repeated measures 2-way ANOVA | fig6 legend | 8 | rats | fig6 legend | error bars are mean +/- sem | fig6g | p=0.044 | fig6 legend | F1,14=4.88 | fig6 legend |
| + - | fig6 | repeated measures 2-way ANOVA | fig6 legend | 8 | rats | fig6 legend | error bars are mean +/- sem | fig6g | p=0.015 | fig6 legend | F1,14=7.64 | fig6 legend |
| + - | fig6 | repeated measures 2-way ANOVA | fig6 legend | 8 | rats | fig6 legend | error bars are mean +/- sem | fig6g | p=0.044 | fig6 legend | F1,14=4.88 | fig6 legend |
| + - | fig6 | Bonferroni post-hoc test | fig6 legend | 8 | rats | fig6 legend | error bars are mean +/- sem | fig6g | p=0.0075 | fig6 legend | t7=3.12 | fig6 legend |
| + - | fig6 | repeated measures 2-way ANOVA | fig6 legend | 8 | rats | fig6 legend | error bars are mean +/- sem | fig6h | p=0.28 | fig6 legend | F1,14=1.27 | fig6 legend |
| + - | fig6 | repeated measures 2-way ANOVA | fig6 legend | 8 | rats | fig6 legend | error bars are mean +/- sem | fig6h | p=0.0504 | fig6 legend | F1,14=4.58 | fig6 legend |
| + - | fig6 | repeated measures 2-way ANOVA | fig6 legend | 8 | rats | fig6 legend | error bars are mean +/- sem | fig6h | p=0.28 | fig6 legend | F1,14=1.27 | fig6 legend |
| + - | fig6 | repeated measures 2-way ANOVA | fig6 legend | 8 | rats | fig6 legend | error bars are mean +/- sem | fig6i | p=0.02 | fig6 legend | F1,14=6.79 | fig6 legend |







Nature Neuroscience: doi:10.1038/nn.4553

| | | | | | | | | | | | | |
|---|---|---|---|---|---|---|---|---|---|---|---|---|
| + - | fig6 | repeated measures 2-way ANOVA | fig6 legend | 8 | rats | fig6 legend | error bars are mean +/- sem | fig6i | p=0.19 | fig6 legend | F1,14=1.89 | fig6 legend |
| + - | fig6 | repeated measures 2-way ANOVA | fig6 legend | 8 | rats | fig6 legend | error bars are mean +/- sem | fig6i | p=0.02 | fig6 legend | F1,14=6.79 | fig6 legend |
| + - | fig6 | Bonferroni post-hoc test | fig6 legend | 8 | rats | fig6 legend | error bars are mean +/- sem | fig6i | p=0.0024 | fig6 legend | t7=3.69 | fig6 legend |
| + - | fig6 | repeated measures 2-way ANOVA | fig6 legend | 8 | rats | fig6 legend | error bars are mean +/- sem | fig6j | p=0.16 | fig6 legend | F1,14=2.18 | fig6 legend |
| + - | fig6 | repeated measures 2-way ANOVA | fig6 legend | 8 | rats | fig6 legend | error bars are mean +/- sem | fig6j | p=0.20 | fig6 legend | F1,14=1.83 | fig6 legend |
| + - | fig6 | repeated measures 2-way ANOVA | fig6 legend | 8 | rats | fig6 legend | error bars are mean +/- sem | fig6j | p=0.16 | fig6 legend | F1,14=2.18 | fig6 legend |
| + - | fig6 | Bonferroni post-hoc test | fig6 legend | 8 | rats | fig6 legend | error bars are mean +/- sem | fig6j | p=0.056 | fig6 legend | t7=2.09 | fig6 legend |
| + - | fig7 | repeated measures 2-way ANOVA | fig7 legend | 6+6 | rats | fig7 legend | error bars are mean +/- sem | fig7c | p=0.039 | fig7 legend | F1,10=5.64 | fig7 legend |
| + - | fig7 | repeated measures 2-way ANOVA | fig7 legend | 6+6 | rats | fig7 legend | error bars are mean +/- sem | fig7c | p=0.14 | fig7 legend | F1,10=2.75 | fig7 legend |
| + - | fig7 | repeated measures 2-way ANOVA | fig7 legend | 6+6 | rats | fig7 legend | error bars are mean +/- sem | fig7c | p=0.039 | fig7 legend | F1,10=5.64 | fig7 legend |
| + - | fig7 | Bonferroni post-hoc test | fig7 legend | 6+6 | rats | fig7 legend | error bars are mean +/- sem | fig7c | p=0.0072 | fig7 legend | t10=3.36 | fig7 legend |
| + - | fig7 | repeated measures 2-way ANOVA | fig7 legend | 6+6 | rats | fig7 legend | error bars are mean +/- sem | fig7d | p=0.14 | fig7 legend | F1,10=2.53 | fig7 legend |
| + - | fig7 | repeated measures 2-way ANOVA | fig7 legend | 6+6 | rats | fig7 legend | error bars are mean +/- sem | fig7d | p=0.22 | fig7 legend | F1,10=1.70 | fig7 legend |
| + - | fig7 | repeated measures 2-way ANOVA | fig7 legend | 6+6 | rats | fig7 legend | error bars are mean +/- sem | fig7d | p=0.14 | fig7 legend | F1,10=2.53 | fig7 legend |
| + - | fig7 | repeated measures 2-way ANOVA | fig7 legend | 6+6 | rats | fig7 legend | error bars are mean +/- sem | fig7e | p=0.046 | fig7 legend | F1,10=5.20 | fig7 legend |
| + - | fig7 | repeated measures 2-way ANOVA | fig7 legend | 6+6 | rats | fig7 legend | error bars are mean +/- sem | fig7e | p=0.063 | fig7 legend | F1,10=4.37 | fig7 legend |
| + - | fig7 | repeated measures 2-way ANOVA | fig7 legend | 6+6 | rats | fig7 legend | error bars are mean +/- sem | fig7e | p=0.046 | fig7 legend | F1,10=5.20 | fig7 legend |
| + - | fig7 | Bonferroni post-hoc test | fig7 legend | 6+6 | rats | fig7 legend | error bars are mean +/- sem | fig7e | p=0.0091 | fig7 legend | t10=3.23 | fig7 legend |
| + - | fig7 | repeated measures 2-way ANOVA | fig7 legend | 6+6 | rats | fig7 legend | error bars are mean +/- sem | fig7f | p=0.009 | fig7 legend | F1,10=10.5 | fig7 legend |
| + - | fig7 | repeated measures 2-way ANOVA | fig7 legend | 6+6 | rats | fig7 legend | error bars are mean +/- sem | fig7f | p=0.011 | fig7 legend | F1,10=9.73 | fig7 legend |
| + - | fig7 | repeated measures 2-way ANOVA | fig7 legend | 6+6 | rats | fig7 legend | error bars are mean +/- sem | fig7f | p=0.009 | fig7 legend | F1,10=10.5 | fig7 legend |







Nature Neuroscience: doi:10.1038/nn.4553

| | | | | | | | | | | | | |
|---|---|---|---|---|---|---|---|---|---|---|---|---|
| + - | fig7 | Bonferroni post-hoc test | fig7 legend | 6+6 | rats | fig7 legend | error bars are mean +/- sem | fig7f | p=0.001 | fig7 legend | t10=4.58 | fig7 legend |
| + - | fig7 | repeated measures 2-way ANOVA | fig7 legend | 7+7 | rats | fig7 legend | error bars are mean +/- sem | fig7i | p=0.09 | fig7 legend | F1,12=3.41 | fig7 legend |
| + - | fig7 | repeated measures 2-way ANOVA | fig7 legend | 7+7 | rats | fig7 legend | error bars are mean +/- sem | fig7i | p=0.0022 | fig7 legend | F2,24=7.96 | fig7 legend |
| + - | fig7 | repeated measures 2-way ANOVA | fig7 legend | 7+7 | rats | fig7 legend | error bars are mean +/- sem | fig7i | p=0.006 | fig7 legend | F2,24=6.31 | fig7 legend |
| + - | fig7 | Bonferroni post-hoc test | fig7 legend | 7+7 | rats | fig7 legend | error bars are mean +/- sem | fig7i | p=0.0033 | fig7 legend | t12=3.66 | fig7 legend |
| + - | fig7 | repeated measures 2-way ANOVA | fig7 legend | 7+7 | rats | fig7 legend | error bars are mean +/- sem | fig7j | p=0.72 | fig7 legend | F1,12=0.13 | fig7 legend |
| + - | fig7 | repeated measures 2-way ANOVA | fig7 legend | 7+7 | rats | fig7 legend | error bars are mean +/- sem | fig7j | p=0.51 | fig7 legend | F2,24=0.69 | fig7 legend |
| + - | fig7 | repeated measures 2-way ANOVA | fig7 legend | 7+7 | rats | fig7 legend | error bars are mean +/- sem | fig7j | p=0.58 | fig7 legend | F2,24=0.57 | fig7 legend |
| + - | fig7 | repeated measures 2-way ANOVA | fig7 legend | 7+7 | rats | fig7 legend | error bars are mean +/- sem | fig7k | p=0.25 | fig7 legend | F1,12=1.45 | fig7 legend |
| + - | fig7 | repeated measures 2-way ANOVA | fig7 legend | 7+7 | rats | fig7 legend | error bars are mean +/- sem | fig7k | p=0.91 | fig7 legend | F2,24=0.09 | fig7 legend |
| + - | fig7 | repeated measures 2-way ANOVA | fig7 legend | 7+7 | rats | fig7 legend | error bars are mean +/- sem | fig7k | p=0.09 | fig7 legend | F2,24=2.67 | fig7 legend |
| + - | fig7 | repeated measures 2-way ANOVA | fig7 legend | 7+7 | rats | fig7 legend | error bars are mean +/- sem | fig7l | p=0.72 | fig7 legend | F1,12=0.13 | fig7 legend |
| + - | fig7 | repeated measures 2-way ANOVA | fig7 legend | 7+7 | rats | fig7 legend | error bars are mean +/- sem | fig7l | p=0.55 | fig7 legend | F2,24=0.60 | fig7 legend |
| + - | fig7 | repeated measures 2-way ANOVA | fig7 legend | 7+7 | rats | fig7 legend | error bars are mean +/- sem | fig7l | p=0.84 | fig7 legend | F2,24=0.17 | fig7 legend |
| + - | fig s1 | repeated measures ANOVA | fig s1 legend | 16 | rats from 1 group | figS1 legend | error bars are mean +/- sem | figS1c | p<0.001 | fig s1 legend | F14,448=5.36 | fig s1 legend |
| + - | fig s1 | Bonferroni post-hoc test | fig s1 legend | 16 | rats from 1 group | figS1 legend | error bars are mean +/- sem | figS1c | p<0.001 | fig s1 legend | F2,60=21.4 | fig s1 legend |
| + - | fig s1 | repeated measures ANOVA | fig s1 legend | 16 | rats from 1 group | figS1 legend | error bars are mean +/- sem | figS1c | p<0.001 | fig s1 legend | F2,60=23.4 | fig s1 legend |
| + - | fig s1 | repeated measures ANOVA | fig s1 legend | 16 | rats from 1 group | figS1 legend | error bars are mean +/- sem | figS1d | p=0.20 | fig s1 legend | F1,30=1.68 | fig s1 legend |
| + - | fig s1 | repeated measures ANOVA | fig s1 legend | 16 | rats from 1 group | figS1 legend | error bars are mean +/- sem | figS1d | p=0.011 | fig s1 legend | F1,30=7.37 | fig s1 legend |
| + - | fig s1 | repeated measures ANOVA | fig s1 legend | 8+8 | rats | figS1 legend | error bars are mean +/- sem | figS1 legend | P=0.57 | fig s1 legend | F2,28-0.57 | fig s1 legend |
| + - | fig s1 | repeated measures ANOVA | fig s1 legend | 16 | rats from 1 group | figS1 legend | error bars are mean +/- sem | figS1 legend | P=0.18 | fig s1 legend | F2,15=1.81 | fig s1 legend |







Nature Neuroscience: doi:10.1038/nn.4553

| | | | | | | | | | | | | |
|---|---|---|---|---|---|---|---|---|---|---|---|---|
| + - | fig s1 | repeated measures ANOVA | fig s1 legend | 16 | rats from 1 group | figS1 legend | error bars are mean +/- sem | figS1 legend | P=0.23 | fig s1 legend | F2,15=1.56 | fig s1 legend |
| + - | fig s1 | repeated measures ANOVA | fig s1 legend | 16 | rats from 1 group | figS1 legend | error bars are mean +/- sem | figS1 legend | p<0.001 | fig s1 legend | F2,47=99.7 | fig s1 legend |
| + - | fig s1 | repeated measures ANOVA | fig s1 legend | 16 | rats from 1 group | figS1 legend | error bars are mean +/- sem | figS1 legend | p<0.001 | fig s1 legend | F2,47=64.6 | fig s1 legend |
| + - | FIG S5 | Bonferroni-corrected chi-square test | fig s5d legend | 58+85 49+72 55+70 54+50 | cell pairs | fig s5d | ITI fractions CS-Suc fractions CS-Shock fractions CS- fractions | fig s5 legend | ITI p<0.001 Suc p<0.001 Shck p=0.0012 CS- p=0.36 | fig s5 legend | ITI X2=21.6 Suc X2=18.6 Shck X2=13.0 CS- X2=2.91 | fig s5 legend |
| + - | FIG S5 | Bonferroni-corrected chi-square test | fig s5 legend | 85+50 | cell pairs | fig s5 legend | fractions ITI vs CS- | fig s5 legend | p=0.015 | fig s5 legend | X2=8.40 | fig s5 legend |
| + - | fig s6 | Bonferroni-corrected chi-square test | fig s6 legend | 89+34 | cell pairs | fig s6 legend | fractions | fig s6 legend | p<0.001 | fig s6 legend | X2=16.8 | fig s6 legend |
| + - | fig s6 | Bonferroni-corrected chi-square test | fig s6 legend | 89+34 vs 100+76 | cell pairs | fig s6 legend | fractions | fig s6 legend | p=0.018 | fig s6 legend | X2=7.52 | fig s6 legend |
| + - | fig s6 | Bonferroni-corrected chi-square test | fig s6 legend | 89+34 vs 75+63 | cell pairs | fig s6 legend | fractions | fig s6 legend | p=0.008 | fig s6 legend | X2=9.03 | fig s6 legend |
| + - | fig s8 | repeated measures ANOVA | fig s8 legend | 10+8 | rats | fig s8 legend | error bars are mean +/- sem | fig s10 legend | p=0.013 | fig s8 legend | F1,18=7.57 | fig s8 legend |
| + - | fig s8 | repeated measures ANOVA | fig s8 legend | 10+8 | rats | fig s8 legend | error bars are mean +/- sem | fig s10 legend | p=0.97 | fig s8 legend | F1,18=0.01 | fig s8 legend |
| + - | fig s8 | repeated measures ANOVA | fig s8 legend | 10+8 | rats | fig s8 legend | error bars are mean +/- sem | fig s10 legend | p=0.49 | fig s8 legend | F1,18=0.50 | fig s8 legend |
| + - | fig s8 | repeated measures ANOVA | fig s8 legend | 10+8 | rats | fig s8 legend | error bars are mean +/- sem | fig s10 legend | p=0.11 | fig s8 legend | F1,18=2.84 | fig s8 legend |
| + - | fig s10 | repeated measures ANOVA | fig s10 legend | 6+6 | rats | fig s10 legend | error bars are mean +/- sem | fig s10 legend | p=0.032 | fig s10 legend | F1,10=6.17 | fig s10 legend |
| + - | fig s10 | repeated measures ANOVA | fig s10 legend | 6+6 | rats | fig s10 legend | error bars are mean +/- sem | fig s10 legend | p=0.026 | fig s10 legend | F1,10=6.86 | fig s10 legend |
| + - | fig s10 | repeated measures ANOVA | fig s10 legend | 6+6 | rats | fig s10 legend | error bars are mean +/- sem | fig s10 legend | p=0.044 | fig s10 legend | F1,10=0.65 | fig s10 legend |
| + - | fig s10 | repeated measures ANOVA | fig s10 legend | 6+6 | rats | fig s10 legend | error bars are mean +/- sem | fig s10 legend | p=0.82 | fig s10 legend | F1,10=0.06 | fig s10 legend |
| + - | fig s10 | repeated measures ANOVA | fig s10 legend | 6+6 | rats | fig s10 legend | error bars are mean +/- sem | fig s10 legend | p=0.007 | fig s10 legend | F2,24=6.22 | fig s10 legend |
| + - | fig s10 | repeated measures ANOVA | fig s10 legend | 6+6 | rats | fig s10 legend | error bars are mean +/- sem | fig s10 legend | p=0.13 | fig s10 legend | F2,24=2.25 | fig s10 legend |
| + - | fig s10 | repeated measures ANOVA | fig s10 legend | 6+6 | rats | fig s10 legend | error bars are mean +/- sem | fig s10 legend | p=0.016 | fig s10 legend | F2,24=4.95 | fig s10 legend |
| + - | fig s10 | repeated measures ANOVA | fig s10 legend | 6+6 | rats | fig s10 legend | error bars are mean +/- sem | fig s10 legend | p=0.66 | fig s10 legend | F2,24=0.42 | fig s10 legend |





Nature Neuroscience: doi:10.1038/nn.4553

| | | | | | | | | | | | | |
|---|---|---|---|---|---|---|---|---|---|---|---|---|
| + - | fig s1 | Bonferroni post-hoc test | figS1 legend | 16 | rats from 1 group | figS1 legend | error bars are mean +/- sem | figS1 legend | p<0.001 | figS1 legend | t45>3.89 | figS1 legend |
| + - | fig s1 | Bonferroni corrected unpaired T-test | figS1 legend | 8+8 | rats | figS1 legend | error bars are mean +/- sem | figS1 legend | p>0.11 | figS1 legend | t14<1.71 | figS1 legend |
| + - | fig s1 | Bonferroni corrected unpaired T-test | figS1 legend | 8+8 | rats | figS1 legend | error bars are mean +/- sem | figS1 legend | p>0.13 | figS1 legend | t14<1.61 | figS1 legend |
| + - | fig s1 | repeated measures ANOVA | figS1 legend | 16 | rats from 1 group | figS1 legend | error bars are mean +/- sem | figS1 legend | p<0.001 | figS1 legend | t14>5.89 | figS1 legend |
| + - | fig s1 | repeated measures ANOVA | figS1 legend | 16 | rats from 1 group | figS1 legend | error bars are mean +/- sem | figS1 legend | p<0.001 | figS1 legend | t14>4.29 | figS1 legend |
| + - | fig 7 | Bonferroni post-hoc test | fig7 legend | 7+7 | rats | fig7 legend | error bars are mean +/- sem | fig7 legend | p=0.025 | fig7 legend | t12=2.56 | fig7 legend |
| + - | FigS3 | Chi-Square Test | FigS3 Legend | 208+94 | Pairs of Neurons | FigS3 legend | Fractions | FigS3 legend | p<0.001 | FigS3 legend | X2=29.8 | FigS3 legend |
| + - | FigS3 | Chi-Square Test | FigS3 Legend | 323+302 | Pairs of Neurons | FigS3 legend | Fractions | FigS3 legend | p<0.001 | FigS3 legend | X2=16.0 | FigS3 legend |
| + - | FigS3 | Chi-Square Test | FigS3 Legend | 20+7 | Pairs of Neurons | FigS3 legend | Fractions | FigS3 legend | p=0.014 | FigS3 legend | X2=5.99 | FigS3 legend |
| + - | FigS3 | Chi-Square Test | FigS3 Legend | 27+67 | Pairs of Neurons | FigS3 legend | Fractions | FigS3 legend | p=0.017 | FigS3 legend | X2=5.70 | FigS3 legend |
| + - | FigS3 | Chi-Square Test | FigS3 Legend | 196+102 | Pairs of Neurons | FigS3 legend | Fractions | FigS3 legend | p<0.001 | FigS3 legend | X2=21.0 | FigS3 legend |
| + - | FigS3 | Chi-Square Test | FigS3 Legend | 351+298 | Pairs of Neurons | FigS3 legend | Fractions | FigS3 legend | p<0.001 | FigS3 legend | X2=14.4 | FigS3 legend |
| + - | FigS3 | Chi-Square Test | FigS3 legend | 7+4 | Pairs of Neurons | FigS3 legend | Fractions | FigS3 legend | p=0.41 | FigS3 legend | X2=0.67 | FigS3 legend |
| + - | FigS3 | Chi-Square Test | FigS3 legend | 11+25 | Pairs of Neurons | FigS3 legend | Fractions | FigS3 legend | p=0.28 | FigS3 legend | X2=1.18 | FigS3 legend |
| + - | FigS3 | Unpaired T-test | FigS3f legend | 323+302 | Cell Pairs | FigS3f legend | Fractions | FigS3 legend | p=0.041 | FigS3f legend | t623=2.05 | FigS3f legend |
| + - | FigS3 | Unpaired T-test | FigS3f legend | 27+70 | Cell Pairs | FigS3f legend | Fractions | FigS3 legend | p=0.055 | FigS3f legend | t95=1.95 | FigS3f legend |
| + - | FigS3 | Unpaired T-test | FigS3g legend | 351+298 | Cell Pairs | FigS3f legend | Fractions | FigS3 legend | p=0.064 | FigS3g legend | t647=1.86 | FigS3g legend |
| + - | FigS3 | Unpaired T-test | FigS3g legend | 11+25 | Cell Pairs | FigS3f legend | Fractions | FigS3 legend | p=0.94 | FigS3g legend | t34=0.08 | FigS3g legend |
| + - | FigS6 | Bonferroni-corrected chi-square test | FigS6a legend | 119+60 | Pairs of Cells | FigS6a legend | Fractions | FigS6a legend | p<0.001 | FigS6a legend | X2=13.1 | FigS6a legend |
| + - | FigS6 | Bonferroni-corrected chi-square test | FigS6a legend | 119+60 vs 116+84 | Pairs of Cells | FigS6a legend | Fractions | FigS6a legend | p=0.27 | FigS6a legend | X2=2.88 | FigS6a legend |
| + - | FigS6 | Bonferroni-corrected chi-square test | FigS6a legend | 119+60 vs 72+75 | Pairs of Cells | FigS6a legend | Fractions | FigS6a legend | p=0.004 | FigS6a legend | X2=10.2 | FigS6a legend |
| + - | FigS6 | Bonferroni-corrected chi-square test | FigS6c legend | 75+46 | Pairs of Cells | FigS6c legend | Fractions | FigS6c legend | p=0.087 | FigS6c legend | X2=4.66 | FigS6c legend |
| + - | FigS6 | Bonferroni-corrected chi-square test | FigS6c legend | 45+12 | Pairs of Cells | FigS6c legend | Fractions | FigS6c legend | p<0.001 | FigS6c legend | X2=13.2 | FigS6c legend |





Nature Neuroscience: doi:10.1038/nn.4553

| | | | | | | | | | | | | |
|---|---|---|---|---|---|---|---|---|---|---|---|---|
| + - | FigS6 | Bonferroni-corrected chi-square test | FigS6c legend | 61+21 | Pairs of Cells | FigS6c legend | Fractions | FigS6c legend | p<0.001 | FigS6c legend | X2=13.4 | FigS6c legend |
| + - | FigS6 | Bonferroni-corrected chi-square test | FigS6c legend | 61+21 vs 47+40 | Pairs of Cells | FigS6c legend | Fractions | FigS6c legend | p=0.018 | FigS6c legend | X2=7.59 | FigS6c legend |
| + - | FigS6 | Bonferroni-corrected chi-square test | FigS6c legend | 61+21 vs 45+42 | Pairs of Cells | FigS6c legend | Fractions | FigS6c legend | p=0.006 | FigS6c legend | X2=9.66 | FigS6c legend |
| + - | FigS6 | Chi-Square Test | FigS6f legend | 167+69 | Pairs of Cells | FigS6f legend | Fractions | FigS6f legend | p<0.001 | FigS6f legend | X2=27.7 | FigS6f legend |
| + - | FigS6 | Chi-Square Test | FigS6f legend | 167+69 vs 129+108 | Pairs of Cells | FigS6f legend | Fractions | FigS6f legend | p<0.001 | FigS6f legend | X2=13.5 | FigS6f legend |
| + - | FigS6 | Chi-Square Test | FigS6f legend | 12+3 | Pairs of Cells | FigS6f legend | Fractions | FigS6f legend | p=0.053 | FigS6f legend | X2=3.75 | FigS6f legend |
| + - | FigS6 | Chi-Square Test | FigS6f legend | 12+3 vs 26+21 | Pairs of Cells | FigS6f legend | Fractions | FigS6f legend | p=0.087 | FigS6f legend | X2=2.92 | FigS6f legend |
| + - | Fig S9 | Chi-Square Test | FigS9d legend | 22+5 | Cells (10d) | FigS9d legend | Proportions | FigS9d legend | p=0.003 | FigS9d legend | X2=9.07 | FigS9d legend |
| + - | Fig S9 | Chi-Square Test | FigS9d legend | 47+9 | Cells (20d) | FigS9d legend | Proportions | FigS9d legend | p<0.001 | FigS9d legend | X2=19.4 | FigS9d legend |
| + - | Fig S9 | Chi-Square Test | FigS9d legend | 43+7 | Cells (30d) | FigS9d legend | Proportions | FigS9d legend | p<0.001 | FigS9d legend | X2=20.0 | FigS9d legend |
| + - | Fig S9 | Fisher's exact test | FigS9h legend | 0/68 vs 1/68 | Cells (10d) | FigS9h legend | Proportions | FigS9h legend | p=1.00 | FigS9h legend | n/a | n/a |
| + - | Fig S9 | Fisher's exact test | FigS9h legend | 0/69 vs 2/69 | Cells (20d) | FigS9h legend | Proportions | FigS9h legend | p=0.50 | FigS9h legend | n/a | n/a |
| + - | Fig S9 | Fisher's exact test | FigS9h legend | 0/82 vs 3/82 | Cells (30d) | FigS9h legend | Proportions | FigS9h legend | p=0.25 | FigS9h legend | ----- | FigS9h legend |
| + - | Methods | Pearson correlation test | Methods | 60 | Trials | Methods | Average scores per trial (20s each) | Methods | p<0.0001 | Methods | R=0.989 | Methods |
| + - | Fig S10 | Bonferroni post-hoc test | Fig S10b legend | 6+6 | animals | Fig S10b legend | error bars are mean +/- sem | Fig S10b legend | p=0.006 | Fig S10b legend | t10=3.51 | Fig S10b legend |
| + - | Fig S10 | Bonferroni post-hoc test | Fig S10b legend | 6+6 | animals | Fig S10b legend | error bars are mean +/- sem | Fig S10b legend | p=0.004 | Fig S10b legend | t10=3.70 | Fig S10b legend |
| + - | Fig S10 | Bonferroni post-hoc test | Fig S10d legend | 7+7 | animals | Fig S10d legend | error bars are mean +/- sem | Fig S10d legend | p=0.001 | Fig S10d legend | t12=4.32 | Fig S10d legend |
| + - | Fig S10 | Bonferroni post-hoc test | Fig S10d legend | 7+7 | animals | Fig S10d legend | error bars are mean +/- sem | Fig S10d legend | p=0.011 | Fig S10d legend | t12=3.00 | Fig S10d legend |
| + - | | | | | | | | | | | | |
| + - | | | | | | | | | | | | |
| + - | | | | | | | | | | | | |
| + - | | | | | | | | | | | | |







Nature Neuroscience: doi:10.1038/nn.4553

## Representative figures

1. Are any representative images shown (including Western blots and immunohistochemistry/staining) in the paper?

   If so, what figure(s)?

Fig 2ab Sample cross corr
Fig 4 Sample phototagging response
Fig 5 Sample competition behavior and sample neural decoding
Fig 6a & e: Sample histology
Fig 7 a & g: Sample histology
SFig 1h: Competition behavior
SFig 2: Sample electrophysiology histology & neural waveforms
SFig 3: Sample cross correlations
SFig4: Sample cross correlations
SFig6: Sample cross correlations & waveforms
SFig7: Sample neural responses
SFig8: Sample Histology
SFig9: Sample neural responses to optogenetic manipulation
SFig10: Sample Histology

2. For each representative image, is there a clear statement of how many times this experiment was successfully repeated and a discussion of any limitations in repeatability?

   If so, where is this reported (section, paragraph #)?

All samples are representative examples of pooled data noted in the same figures

## Statistics and general methods

1. Is there a justification of the sample size?

   If so, how was it justified?

   Where (section, paragraph #)?

   Even if no sample size calculation was performed, authors should report why the sample size is adequate to measure their effect size.

No. As stated in the Methods (section on "Statistical Analyses"), no statistical tests were used to pre-determine sample sizes, but our sample sizes are consistent with previous publications.

2. Are statistical tests justified as appropriate for every figure?

   Where (section, paragraph #)?

Yes. Methods under the "Statistical Analyses" section.

   a. If there is a section summarizing the statistical methods in the methods, is the statistical test for each experiment clearly defined?

Yes. Section on "Statistical Analyses".

   b. Do the data meet the assumptions of the specific statistical test you chose (e.g. normality for a parametric test)?

      Where is this described (section, paragraph #)?

Yes. As stated in the Methods (section on "Statistical Analyses"), the Kolmogorov-Smirnov normality test was used to determine if data sets required parametric or non-parametric statistical tests.

   c. Is there any estimate of variance within each group of data?

      Is the variance similar between groups that are being statistically compared?

      Where is this described (section, paragraph #)?

Yes. As stated in the Methods (section on "Statistical Analyses"), all data met the assumptions of every statistical tests used.





Nature Neuroscience: doi:10.1038/nn.4553

| | |
|---|---|
| d. Are tests specified as one- or two-sided? | Yes. As stated in the Methods (section on "Statistical Analyses"), all statistical analyses were based on two-tailed comparisons. |
| e. Are there adjustments for multiple comparisons? | Yes. This is stated in the Methods (section on "Statistical Analyses"), as well as throughout the figure legends for all relevant statistical tests, which were corrected using the Bonferroni method. |
| 3. To promote transparency, *Nature Neuroscience* has stopped allowing bar graphs to report statistics in the papers it publishes. If you have bar graphs in your paper, please make sure to switch them to dot-plots (with central and dispersion statistics displayed) or to box-and-whisker plots to show data distributions. | All bar graphs are displayed along with superimposed data distributions (individual data points), or displayed as box plots with details for the median, mean, box limits and whisker limits provided in the figure legends. |
| 4. Are criteria for excluding data points reported?<br>Was this criterion established prior to data collection?<br>Where is this described (section, paragraph #)? | Yes. There is a section in the Methods on "Exclusion of Animals, Cells, or Data Points". Criteria stated in this section was established prior to completion of all datasets. |
| 5. Define the method of randomization used to assign subjects (or samples) to the experimental groups and to collect and process data.<br>If no randomization was used, state so.<br>Where does this appear (section, paragraph #)? | Methods include a section on "Randomization and Blinding". As stated in this section, randomization was performed for viral and drug treatments, pseudo-random trial sequences were produced for behavioral testing, and all experiments were designed with appropriate internal controls to allow within-subject comparisons (e.g., laser-OFF versus laser-ON trials; counterbalanced drug vs vehicle treatments, etc.). |
| 6. Is a statement of the extent to which investigator knew the group allocation during the experiment and in assessing outcome included?<br>If no blinding was done, state so.<br>Where (section, paragraph #)? | As stated in the Methods (sub-sections on "Randomization and Blinding" and "Behavioral Data"), blinding was not performed, but behavioral testing was controlled by software and data analyses were performed using customized automated methods whenever possible. For instance, port entry responses were sampled by software from beam breaks (Med-PC; Med Associates), whereas freezing responses were assessed by a customized Matlab-based method that quantified animal motion from videos. |
| 7. For experiments in live vertebrates, is a statement of compliance with ethical guidelines/regulations included?<br>Where (section, paragraph #)? | The Methods (section on "Animals"; paragraph #1) state the following: "All procedures were approved by the Committee on Animal Care of the Massachusetts Institute of Technology and the Animal Care and Use Review Office of the USAMRMC, in compliance with the PHS Policy on Humane Care and Use of Laboratory Animals (Public Law 99–158)." |
| 8. Is the species of the animals used reported?<br>Where (section, paragraph #)? | Yes. Methods under "Animals" section (paragraph #1). Rats were used in the study. |
| 9. Is the strain of the animals (including background strains of KO/ transgenic animals used) reported?<br>Where (section, paragraph #)? | Yes. Methods under "Animals" section (paragraph #1). Long-Evans rats were used in the study. |
| 10. Is the sex of the animals/subjects used reported?<br>Where (section, paragraph #)? | Yes. Methods under "Animals" section (paragraph #1). Animals used were males for all experiments. |





Nature Neuroscience: doi:10.1038/nn.4553

| | |
|---|---|
| 11. Is the age of the animals/subjects reported?<br>Where (section, paragraph #)? | Yes. Methods under "Animals" section (paragraph #1). Animals were approximately 275-300 g (3-months-old) upon arrival to the vivarium from the commercial vendor. |
| 12. For animals housed in a vivarium, is the light/dark cycle reported?<br>Where (section, paragraph #)? | Yes. Methods under "Animals" section (paragraph #1). Animals were maintained on a regular 12-hr light/dark cycle. |
| 13. For animals housed in a vivarium, is the housing group (i.e. number of animals per cage) reported?<br>Where (section, paragraph #)? | Yes. Methods under "Animals" section (paragraph #1). Animals were individually housed. |
| 14. For behavioral experiments, is the time of day reported (e.g. light or dark cycle)?<br>Where (section, paragraph #)? | Yes. Methods under "Animals" section (paragraph #1). All experiments were performed during the light phase. |
| 15. Is the previous history of the animals/subjects (e.g. prior drug administration, surgery, behavioral testing) reported?<br>Where (section, paragraph #)? | n/a |
| a. If multiple behavioral tests were conducted in the same group of animals, is this reported?<br>Where (section, paragraph #)? | Yes. Methods under the "Behavioral Tasks" section. |
| 16. If any animals/subjects were excluded from analysis, is this reported?<br>Where (section, paragraph #)? | Yes. Methods ("Exclusion of Animals" under the "Statistical Analyses" section). |
| a. How were the criteria for exclusion defined?<br>Where is this described (section, paragraph #)? | Animals were excluded due to either electrode misplacement (n = 2), lack of viral expression (n = 5), viral leakage (n = 2), or breakage or misplacement of optical fibers (n = 3). |
| b. Specify reasons for any discrepancy between the number of animals at the beginning and end of the study.<br>Where is this described (section, paragraph #)? | Numbers reported in the manuscript consistently reflect all animals present at the end of the study. |

## Reagents

| | |
|---|---|
| 1. Have antibodies been validated for use in the system under study (assay and species)? | n/a |
| a. Is antibody catalog number given?<br>Where does this appear (section, paragraph #)? | n/a |





Nature Neuroscience: doi:10.1038/nn.4553

b. Where were the validation data reported (citation, supplementary information, Antibodypedia)?

Where does this appear (section, paragraph #)?

n/a

2. Cell line identity

a. Are any cell lines used in this paper listed in the database of commonly misidentified cell lines maintained by ICLAC and NCBI Biosample?

Where (section, paragraph #)?

n/a

b. If yes, include in the Methods section a scientific justification of their use--indicate here in which section and paragraph the justification can be found.

n/a

c. For each cell line, include in the Methods section a statement that specifies:

- the source of the cell lines
- have the cell lines been authenticated? If so, by which method?
- have the cell lines been tested for mycoplasma contamination?

Where (section, paragraph #)?

n/a





Nature Neuroscience: doi:10.1038/nn.4553

## Data availability

Provide a Data availability statement in the Methods section under "Data availability", which should include, where applicable:

- Accession codes for deposited data
- Other unique identifiers (such as DOIs and hyperlinks for any other datasets)
- At a minimum, a statement confirming that all relevant data are available from the authors
- Formal citations of datasets that are assigned DOIs
- A statement regarding data available in the manuscript as source data
- A statement regarding data available with restrictions

See our data availability and data citations policy page for more information.

Data deposition in a public repository is mandatory for:

a. Protein, DNA and RNA sequences
b. Macromolecular structures
c. Crystallographic data for small molecules
d. Microarray data

Deposition is strongly recommended for many other datasets for which structured public repositories exist; more details on our data policy are available here. We encourage the provision of other source data in supplementary information or in unstructured repositories such as Figshare and Dryad.

We encourage publication of Data Descriptors (see Scientific Data) to maximize data reuse.

Where is the Data Availability statement provided (section, paragraph #)?

Methods: "Data and Code Availability"

All relevant data and code supporting the findings of this study are available from the corresponding author upon reasonable request.

## Computer code/software

Any custom algorithm/software that is central to the methods must be supplied by the authors in a usable and readable form for readers at the time of publication. However, referees may ask for this information at any time during the review process.

1. Identify all custom software or scripts that were required to conduct the study and where in the procedures each was used.

1. Methods (section on "Reward and Fear Behaviors"): Freezing was quantified using an automated custom MATLAB script that quantified frame-by-frame changes in total pixel intensity, as approximations for animal motion.
2. Methods (sections on "Cross-Correlations" and "Machine Learning"): Analyses were performed using a combination of tools in Neuroexplorer (NEX Technologies), Matlab (MathWorks), and R (R Core Team; https://www.R-project.org/).

2. If computer code was used to generate results that are central to the paper's conclusions, include a statement in the Methods section under "**Code availability**" to indicate whether and how the code can be accessed. Include version information as necessary and any restrictions on availability.

Methods: "Data and Code Availability"

All relevant data and code supporting the findings of this study are available from the corresponding author upon reasonable request.





Nature Neuroscience: doi:10.1038/nn.4553

## Human subjects

| | |
|---|---|
| 1. Which IRB approved the protocol?<br>Where is this stated (section, paragraph #)? | n/a |
| 2. Is demographic information on all subjects provided?<br>Where (section, paragraph #)? | n/a |
| 3. Is the number of human subjects, their age and sex clearly defined?<br>Where (section, paragraph #)? | n/a |
| 4. Are the inclusion and exclusion criteria (if any) clearly specified?<br>Where (section, paragraph #)? | n/a |
| 5. How well were the groups matched?<br>Where is this information described (section, paragraph #)? | n/a |
| 6. Is a statement included confirming that informed consent was obtained from all subjects?<br>Where (section, paragraph #)? | n/a |
| 7. For publication of patient photos, is a statement included confirming that consent to publish was obtained?<br>Where (section, paragraph #)? | n/a |

## fMRI studies

For papers reporting functional imaging (fMRI) results please ensure that these minimal reporting guidelines are met and that all this information is clearly provided in the methods:

| | |
|---|---|
| 1. Were any subjects scanned but then rejected for the analysis after the data was collected? | n/a |
| a. If yes, is the number rejected and reasons for rejection described?<br>Where (section, paragraph #)? | n/a |
| 2. Is the number of blocks, trials or experimental units per session and/or subjects specified?<br>Where (section, paragraph #)? | n/a |
| 3. Is the length of each trial and interval between trials specified? | n/a |





Nature Neuroscience: doi:10.1038/nn.4553

| | |
|---|---|
| 4. Is a blocked, event-related, or mixed design being used? If applicable, please specify the block length or how the event-related or mixed design was optimized. | n/a |
| 5. Is the task design clearly described?<br>Where (section, paragraph #)? | n/a |
| 6. How was behavioral performance measured? | n/a |
| 7. Is an ANOVA or factorial design being used? | n/a |
| 8. For data acquisition, is a whole brain scan used?<br>If not, state area of acquisition. | n/a |
| a. How was this region determined? | n/a |
| 9. Is the field strength (in Tesla) of the MRI system stated? | n/a |
| a. Is the pulse sequence type (gradient/spin echo, EPI/spiral) stated? | n/a |
| b. Are the field-of-view, matrix size, slice thickness, and TE/TR/ flip angle clearly stated? | n/a |
| 10. Are the software and specific parameters (model/functions, smoothing kernel size if applicable, etc.) used for data processing and pre-processing clearly stated? | n/a |
| 11. Is the coordinate space for the anatomical/functional imaging data clearly defined as subject/native space or standardized stereotaxic space, e.g., original Talairach, MNI305, ICBM152, etc? Where (section, paragraph #)? | n/a |
| 12. If there was data normalization/standardization to a specific space template, are the type of transformation (linear vs. nonlinear) used and image types being transformed clearly described? Where (section, paragraph #)? | n/a |
| 13. How were anatomical locations determined, e.g., via an automated labeling algorithm (AAL), standardized coordinate database (Talairach daemon), probabilistic atlases, etc.? | n/a |
| 14. Were any additional regressors (behavioral covariates, motion etc) used? | n/a |
| 15. Is the contrast construction clearly defined? | n/a |
| 16. Is a mixed/random effects or fixed inference used? | n/a |





Nature Neuroscience: doi:10.1038/nn.4553

| | |
|---|---|
| a. If fixed effects inference used, is this justified? | n/a |
| 17. Were repeated measures used (multiple measurements per subject)? | n/a |
| a. If so, are the method to account for within subject correlation and the assumptions made about variance clearly stated? | n/a |
| 18. If the threshold used for inference and visualization in figures varies, is this clearly stated? | n/a |
| 19. Are statistical inferences corrected for multiple comparisons? | n/a |
| a. If not, is this labeled as uncorrected? | n/a |
| 20. Are the results based on an ROI (region of interest) analysis? | n/a |
| a. If so, is the rationale clearly described? | n/a |
| b. How were the ROI's defined (functional vs anatomical localization)? | n/a |
| 21. Is there correction for multiple comparisons within each voxel? | n/a |
| 22. For cluster-wise significance, is the cluster-defining threshold and the corrected significance level defined? | n/a |

## Additional comments

| | |
|---|---|
| Additional Comments | |





Nature Neuroscience: doi:10.1038/nn.4553